An integrated model of milling and flotation for the optimal recovery of sulphide ores at the Kansanshi mine

by

MARTIN LUSAMBO

Submitted in accordance with the requirements for

the degree of

MAGISTER TECHNOLOGIAE

in the subject

ENGINEERING: CHEMICAL

at the

UNIVERSITY OF SOUTH AFRICA

Supervisor: Prof. FRANCOIS MULENGA

November 2019

DECLARATION

Name: Martin Lusambo

Student number: 5544-002-9

Degree: Master of Technology – Engineering: Chemical

An integrated model of milling and flotation for the optimal recovery of sulphide ores at the Kansanshi mine

I declare that the above dissertation is my own work and that all the sources that I have used or quoted have been indicated and acknowledged by means of complete references.

I further declare that I submitted the dissertation to originality checking software and that it falls within the accepted requirements for originality.

I further declare that I have not previously submitted this work, or part of it, for examination at Unisa for another qualification or at any other higher education institution.

05/11/2019

SIGNATURE DATE

Dedication

I dedicate this research work to my wife Hellen and children Mulenga, Riba, Mwalimu, Natasha and Taizya. Thank you very much for your understanding and encouragement. The journey was indeed a very challenging one and could not have been accomplished without your encouraging and inspiring words when hope of successfully completing this work was almost lost. To my children thank you for understanding my long absence from home and not being around to help with your homework.

Acknowledgements

First and foremost, glory be to God for His grace. Indeed, all good things come from above.

Secondly, I would like to convey my heartfelt gratitude to Prof. Francois Mulenga for supervising my research work. It was a long a challenging journey which could not have come to fruition without your wise guidance, constructive criticism and patience. Thank you for helping me believe this could be done.

Abstract

Kansanshi mine sulphide ore circuit did not achieve target flotation recovery in 2016, hence it was deemed necessary to carry out a research aimed at optimizing this circuit. The objective of the research was to optimise the Kansanshi milling and flotation circuit processing a copper sulphide ore.

In line with this, samples were obtained around the circuit and processed in the laboratory for moisture content, slurry concentration, particle size distribution, and flotation response. This information was then used to build a computer-based model of the Kansanshi milling and flotation circuit. This was done in MODSIM®, a software package specialising in the design and simulation of mineral processing operations. After careful appraisal, appropriate models were selected for the semi autogenous grinding (SAG) and ball mills, SAG mill discharge screen, hydrocyclones, pebble crusher, and the flotation cells. The calibrated model was then used to simulate the effects of key operating parameters on flotation recovery.

Analysis using the attainable region technique revealed that the SAG mill feed-rate should be adjusted from 1719 tph to 2090 tph. This would lead to a better utilisation of the pebble crusher that can process 358 tph of pebbles from the current 198 tph. From the simulation work, it was established that rougher flotation recovery can be improved from the current 80.0 % to 82.3 %. The techno-economic benefits of the proposition are yet to be investigated.

Findings from the research concluded that the milling circuit optimum operating parameter; which generated a final product falling predominantly in the range -150 +38 µm were SAG and ball mills conditions of ball sizes 200 and 40mm respectively, ball mill ball filling 32% and rotational speed between 75 and 80% for both SAG and ball mills. The optimum hydrocyclone feed slurry concentration was found to be 62% solids. Additionally, the SAG mill discharge screen aperture size of 6 mm was the optimum. It must be noted that slurry concentration did not

show any impact on both the SAG and ball mills performance. The SAG mill ball filling did not show any significant improvement on performance.

Keywords: Milling, froth flotation, population balance framework, attainable region, process optimisation, MODSIM®

Publications

Lusambo, M., Mulenga, F.K., 2018. Empirical model of recovery response of copper sulphide circuit at Kansanshi mine. Journal of the Southern Africa Institute of Mining and Metallurgy, vol. 118, no.11, pp 1179 – 1184

Table of contents

Declaration ..... **ii**
Dedication ..... **iii**
Acknowledgements ..... **iv**
Abstract ..... **v**
Publications ..... **vii**
List of figures ..... **xi**
List of tables ..... **xiv**
Chapter 1 Introduction **1**
1.1 Background 1
1.2 Research problem 2
1.3 Research objectives 5
1.4 Scope of the research 6
1.5 Layout of the dissertation 8
Chapter 2 Literature review **9**
2.1 Introduction 9
2.2 Crushing equipment 9
2.3 Tumbling mills 10
2.3.1 Breakage mechanisms of tumbling mills 10
2.3.2 Autogenous and semi-autogenous mills 12
2.3.3 Ball milling 13
2.3.4 Material transport through tumbling mills 15
2.3.5 Operating parameters of tumbling mills 17
2.4 Size classification 19
2.4.1 Vibrating screens 19
2.4.2 Hydrocyclones 20
2.4.3 Partition curve of size classifiers 22
2.4.4 Empirical models of size classifiers 24
2.5 Froth flotation 25
2.5.1 Principle of froth flotation 26
2.5.1 Kinetics of batch flotation tests 26
2.6 Population balance framework 29
2.6.1 Application to comminution machines 30
2.6.2 Population balance model of ball milling 31
2.6.3 Population balance model of fully- and semi-autogenous mills 34
2.6.4 Population balance model of froth flotation 36
2.7 Optimisation of mineral processing circuits 37
2.7.1 Optimisation of classical SABC circuits 38
2.7.2 Optimisation of flotation circuits 41

2.7.3 Attainable region paradigm 42
2.7.4 Future outlook 44
2.8 Summary 45
Chapter 3 Laboratory testwork and plant survey programme 46
3.1 Introduction 46
3.2 Specifications of the Kansanshi sulphide ore circuit 47
3.3 Plant surveying campaign 52
3.4 Sample preparation 57
3.5 Particle size analysis 58
3.6 Challenges faced as part of the experimental work 62
Chapter 4 Reconciliation of surveyed industrial data 65
4.1 Introduction 65
4.2 Particle size distributions 65
4.3 Mass balancing and data reconciliation 71
4.4 Performance of the recycle pebble crusher 74
4.5 Performance of the ball mill 74
4.6 Performance of the nest of hydrocyclones 75
4.7 Summary 78
Chapter 5 Model building of the Kansanshi sulphide ore circuit 79
5.1 Introduction 79
5.2 Creating the project in MODSIM® 79
5.3 Semi-autogenous milling unit 83
5.4 Vibrating screen 84
5.5 Pebble crusher 85
5.6 Ball milling unit 85
5.7 Cluster of hydrocyclones 87
5.8 Model of the flotation section 88
5.9 Calibration of the Kansanshi simulation model 90
5.10 Limitations of the models 91
Chapter 6 Optimisation of the Kansanshi sulphide ore circuit 93
6.1 Introduction 93
6.2 Simulation of the performance of the Kansanshi circuit 93
6.2.1 Effects of SAG discharge screen on circuit performance 94
6.2.2 Effects of pebble crusher on circuit performance 96
6.2.3 Effects of SAG milling on circuit performance 98
6.2.4 Effects of ball milling on circuit performance 104
6.2.5 Effects of hydrocycloning on circuit performance 109
6.3 Integrated optimisation of the Kansanshi circuit 111
6.3.1 Definition of the state variables 113
6.3.2 Effects of the aperture size of the SAG mill discharge screen 113

6.3.3 Effects of the closed size setting of the pebble crusher 114
6.3.4 Effects of the ball filling of the SAG mill 115
6.3.5 Effects of ball size used in the SAG mill 117
6.3.6 Effects of the SAG mill speed 118
6.3.7 Effects of SAG mill throughput 119
6.3.8 Effects of the ball filling of the ball mill 121
6.3.9 Effects of ball size used in the ball mill 122
6.3.10 Effects of ball mill speed 123
6.3.11 Effects of the slurry concentration of the ball mill 124
6.3.12 Effects of the slurry concentration of the hydrocylone feed..... 125
6.4 Significance of the simulation results 127
6.5 Conclusion 128
Chapter 7 Conclusion and recommendations.....129
7.1 Introduction 129
7.2 Modelling the sections of the Kansanshi sulphide ore circuit 129
7.3 Attainable region analysis of the Kansanshi sulphide ore circuit 130
7.4 Recommendations for future work 130
References 133
Appendices 142

List of figures

Figure 1.1 Map of the Republic of Zambia showing the location of the Kansanshi mine (Modified after National Geographical Society, 2013) 2
Figure 2.1 Summary of the breakage mechanisms commonly found in comminution equipment (after Napier-Munn et al., 1996) 11
Figure 2.2 Charge motion in tumbling mills (Wills and Napier-Munn, 2006) 12
Figure 2.3 Example of tracer response of a full-scale mill of overflow discharge design (after Makokha et al., 2011) 16
Figure 2.4 Schematic representation of a vibrating screen (Will and Napier-Munn, 2006) 20
Figure 2.5 Key design parameters of a hydrocyclone (from Wikedzi, 2018) 21
Figure 2.6 Typical partition curve of a hydrocyclone 22
Figure 2.7 Simplified representation of the flotation mechanism (Hu, 2014) .. 27
Figure 2.8 Effect of the specific comminution energy E_{cs} on the breakage index t_{10} (after Napier-Munn et al., 1996) 35
Figure 2.9 Classical design of a Semi-Autogenous mill, Ball mill, and Crusher circuit also known as SABC design 38
Figure 2.10 Generic methodology for the optimisation of comminution circuits (after Napier-Munn et al., 1996) 39
Figure 2.11 Principle of mixing in the AR space (Mulenga and Bwalya, 2015) ... 43
Figure 3.1 Kansanshi sulphide ore circuit 49
Figure 3.2 On-stream analyser multiplexer sampler 55
Figure 3.3 Cyclone distributor poppet sampler 56
Figure 3.4 A belt cut sample of the SAG mill feed 57
Figure 3.5 Dry sample of the SAG mill feed 58
Figure 3.6 Stack of screens spanning from 125 mm down to 3.5 mm 59
Figure 3.7 Stack of screens spanning from 2500 µm down to 25 µm 61
Figure 4.1 Particle size distributions of the feed, overflow and underflow of the nest of hydrocylones 66
Figure 4.2 Tromp curves of the nest of hydrocyclones 69
Figure 4.3 Particle size distributions of the feed and the discharge of the ball mill 70
Figure 4.4 Particle size distributions of the feed and the discharge of the SAG mill 70
Figure 5.1 Flowsheet of the Kansanshi sulphide ore milling and flotation circuits in MODSIM® 81

Figure 5.2 MODSIM® systems data entry form with data for Kansanshi milling circuit 81
Figure 5.3 MODSIM® model data specification form with SAG mill data 81
Figure 5.4 Particle size distribution and flowrate of the feed 83
Figure 5.5 Comparison between MODSIM® predicted andsurveyed particle size distributions for the feed and discharge of the SAG mill 86
Figure 5.6 Comparison between MODSIM® predicted andsurveyed particle size distribution of the feed and discharge of the ball mill 87
Figure 5.7 Comparison between MODSIM® predicted and surveyed particle size distributions around the hydrocyclones.....88
Figure 5.8 Comparison between MODSIM® predicted and survey data.....91
Figure 6.1 Variation of the size and rate of pebbles produced with the aperture size of the SAG mill discharge screen 95
Figure 6.2 Particle size distributions of key milling streams for optimized SAG discharge screen. Legend: bc – base case, opt – optimized, cof – cyclone overflow, bmd – ball mill discharge, sagd – SAG mill discharge.....96
Figure 6.3 Simulated effects of the closed side setting of the pebble crusher .97
Figure 6.4 Performance of the Kansanshi milling circuit for the optimized pebble crusher 97
Figure 6.5 Simulated effects of the ball filling of the SAG mill 99
Figure 6.6 Simulated effects of ball size used in the SAG mill.....100
Figure 6.7 Performance of the Kansanshi milling circuit for optimized ball size of the SAG mill 100
Figure 6.8 Simulated effects of SAG mill speed.....101
Figure 6.9 Performance of the Kansanshi milling circuit for optimized SAG mill speed.....102
Figure 6.10 Simulated effects of SAG mill throughput 103
Figure 6.11 Performance of the Kansanshi milling circuit for optimized SAG mill throughput.....104
Figure 6.12 Simulated effects of the ball filling of the ball mill.....105
Figure 6.13 Performance of the Kansanshi milling circuit for the optimized ball filling of the ball mill 105
Figure 6.14 Simulated effects of the ball size used in the ball mill 106
Figure 6.15 Performance of the Kansanshi milling circuit for optimized ball size of the ball mill 107
Figure 6.16 Simulated effects of ball mill speed.....108
Figure 6.17 Performance of the milling circuit for optimized ball mill speed ...108
Figure 6.18 Simulated effects of the solid content of the hydrocyclone feed ..110

Figure 6.19 Performance of the milling circuit for optimized slurry concentration of the hydrocyclone feed 110
Figure 6.20 Variation of m1 and m2 with the aperture size of the SAG mill discharge screen 113
Figure 6.21 Effect of SAG mill discharge screen on flotation performance 114
Figure 6.22 Variation of m1 and m2 with the closed side setting of the pebble crusher 115
Figure 6.23 Effect of pebble crusher on flotation performance.....115
Figure 6.24 Variation of m1 and m2 with the ball filling of the SAG mill 116
Figure 6.25 Effect of the ball filling of the SAG mill on flotation performance .116
Figure 6.26 Variation of m1 and m2 with the ball size of the SAG mill 117
Figure 6.27 Effect of the ball size of the SAG mill on flotation performance....117
Figure 6.28 Variation of m1 and m2 with SAG mill speed 118
Figure 6.29 Effect of SAG mill speed on flotation performance 119
Figure 6.30 Variation of m1 and m2 with SAG mill throughput 120
Figure 6.31 Effect of SAG mill throughput on flotation performance 120
Figure 6.32 Variation of m1 and m2 with the ball filling of the ball mill 121
Figure 6.33 Effect of the ball filling of the ball mill on flotation performance ..122
Figure 6.34 Variation of m1 and m2 with the ball size of the ball mill.....122
Figure 6.35 Effect of the ball size of the ball mill on flotation performance.....123
Figure 6.36 Variation of m1 and m2 with ball mill speed.....124
Figure 6.37 Effect of ball mill speed on flotation performance.....124
Figure 6.38 Effect of solid content of the ball mill on flotation performance ..125
Figure 6.39 Variation of m1 and m2 with the solid content of the hydrocyclone feed 126
Figure 6.40 Effect of the solid content of the hydrocyclone feed on flotation .126

List of tables

Table 3.1 Specifications of the comminution and flotation equipment used in the sulphide ore circuit, Kansanshi 51
Table 3.2 Sampling points and associated resources 54
Table 4.1 Performance data of the cluster of hydrocyclones 67
Table 4.2 Computation of the Tromp curve data 68
Table 4.3 Operational and mass balanced streams around Kansanshi milling circuit (tonnage rates on dry basis) 72
Table 4.4 Performance indicators of the SAG mill and pebble crusher 73
Table 4.5 Performance indicators of the ball mill 74
Table 4.6 Efficiency indicators for the cluster of hydrocyclones.....75
Table 4.7 Factors for conversion of fraction passing in the overflow to the short-circuiting T_X (Metso Minerals, 2010) 76
Table 4.8 Categorisation of hydrocyclone efficiency based on imperfection I (Murthy and Basavaraj, 2012) 76
Table 4.9 General guide to evaluating hydrocyclone by-pass to underflow B_{pf} on performance (Napier-Munn et al., 1996) 77
Table 5.1 Values of the impact and abrasion resistance parameter values of Kansanshi sulphide ores (Bepswa et al., 2015).....84
Table 5.2 Flotation rate constants (Minerals Technology Int., 2012) 89
Table 6.1 Comparison between surveyed and MODSIM® predicted data 94
Table 6.2 Optimised simulation parameters of the Kansanshi circuit 112

Chapter 1 Introduction

1.1 Background

In recent years, there has been a significant increase in the demand for copper to sustain infrastructure developments and expansions in emerging economies like China (Hu, 2014). In most regions of the world, rich ore bodies have depleted and stiffer environmental regulations have been put in place to mitigate the impact of metal extraction processes on surrounding communities. This has triggered research into more efficient ways of recovering minerals from low grade ores. The Kansanshi mine has also experienced declining feed grades to the processing plant. This has resulted in challenges in attaining targeted concentrate grades and recoveries.

Kansanshi is the largest copper mine on the African continent with production capabilities of 340 000 tons of copper and 120000 ounces of gold per annum (Bepswa et al., 2015). It produced a total of 250 801 tons of copper in 2017 (Newall, 2017). The Kansanshi mine is 80 % owned by First Quantum Minerals Limited and 20 % by the government of the Republic of Zambia through the Zambian Consolidated Copper Mines Investments Holdings (ZCCM IH). The mine is located approximately 10 km north of Solwezi, the administrative headquarters of the North Western province and 18 km south of the border with the Democratic Republic of Congo as shown in Figure 1.1.

Figure 1.1 Map of the Republic of Zambia showing the location of the Kansanshi mine (Modified after National Geographical Society, 2013)

The copper in the Kansanshi ore deposit is hosted in a range of minerals including chalcopyrite, secondary copper sulphides, native copper, cuprite, malachite, azurite and chrysocolla (Kalichini, 2015). The ore consists of varying proportions of sulphide and oxide copper minerals, this has necessitated classification of the ore into three distinct categories: sulphide, mixed, and oxide ores. As such, three separate processing circuits are used for milling the ore down to a standard targeted grind size of 80 % passing 150 µm before froth flotation and leaching.

The sulphide ore circuit did not attain the target recovery in 2016 and 2017. This has prompted the implementation of various initiatives aimed at improving the recovery for the sulphide ore circuit.

1.2 Research problem

Ore grades have been declining at the Kansanshi concentrator over the past years. The average feed grade to the sulphide ore circuit was 0.77 % total copper metal (TCu) in 2017 (Mphanza, 2018) compared to 0.98 % TCu in 2015(Mphanza, 2016). This has resulted in challenges in achieving target concentrate grades and recoveries.

Various initiatives are being pursued at the Kansanshi concentrator in order to reduce operational costs and improve plant efficiency. Initiatives undertaken on the sulphide ore circuit included laboratory and plant trials of new flotation reagents and installation of Jameson cell and Proflote® technologies. The introduction of the two flotation technologies was aimed at improving the recovery of fines. It was hoped that this would curb the copper losses identified in the fine fractions of milled ore product. The grate at the discharge end of the semi-autogenous (SAG) mill has also been changed with a view to improving the milling performance. Lastly, the SAG mill was fitted with a trommel screen in the search for increased throughput.

Despite all these efforts, the sulphide ore circuit did not achieve the target recovery and grade in 2017. Assay-by-size analyses have enabled the plant to identify particles coarser than 150 µm and finer than 38 µm as accounting for the greatest copper losses to the flotation tails. This state of affairs has been attributed to inadequate liberation of valuable minerals in the +150 µm size fractions. In contrast, fully liberated particles in the -38 µm size fractions are slow-floating (Kaputula, 2017). It is therefore important to model the sulphide ore circuit and investigate the effects of the milling section on flotation performance. From the simulation model, attempts to reduce the generation of particles outside the desired size range (i.e. -150 +38 µm) are also explored. The production of a steep product size distribution in the range -150 +38 µm is anticipated to potentially lead to better flotation response. In addition to this, the approach may

assist in identifying avenues for reduced copper losses and consequently improved copper recovery and grade around the Kansanshi sulphide ore circuit.

Perhaps the most important note to make is that milling circuits are often geared towards maximizing throughput. This has the adverse consequence of reducing residence time at the downstream flotation stage. Naik and van Drunick (2007) have indicated that the effects of reduced flotation residence time are difficult to estimate without a flotation model. From this point of view, the integration of milling and flotation sections of the Kansanshi sulphide ore circuit is thus expected to help build a simulation tool for mitigating tonnage, recovery and grade.

The milling circuit liberates and conditions valuable minerals in the ore in readiness for recovery in the flotation circuit. The performance of flotation circuit is greatly influenced by the quality of material it receives from the comminution circuit and consequently comminution circuit performance. It is imperative that comminution and flotation circuits are analyzed and optimized together. The impact of changes in comminution operating parameters and equipment capabilities on flotation performance in terms of valuable mineral recovery and concentrate grade can be evaluated and the comminution circuit optimum operating conditions located based of flotation performance. This can be achieved by varying operating parameters and equipment specifications on the comminution circuit and tracking the flotation circuit performance until their optimal is located. Studying, evaluating and optimizing operational and metallurgical performance of mineral processing plants can be easily and efficiently attained by conducting an integrated comminution and flotation surveys, building models and performing simulation to identify optimum operating conditions (Yahyaei et al., 2014). Naik and Drunick (2007) noted that performing integrated survey such as comminution and flotation survey can be employed to simulate the effects of an optimization change in comminution using a flotation model.

1.3 Research objectives

The research project was to be centred on a simulation model integrating milling and flotation of the Kansanshi sulphide ore circuit. For this purpose, the model was built under MODSIM®, a modular simulator for mineral processing operations. The choice for this software package was motivated by the fact that MODSIM® is a flexible and powerful tool relying primarily on fundamental models of mineral processing operations.

Upon selecting MODSIM® as the preferred simulator, two objectives for the research were defined. The first objective was to develop a phenomenological model mimicking the actual behaviour of the milling-flotation section of the Kansanshi sulphide ore circuit. The phenomenological models are developed from a mechanistic description of the mineral processing unit operations in conjunction with process parameters determined from laboratory experiments (Will and Napier-Munn, 2006). The main mineral processing unit operations considered include size-reduction operations, crushing and grinding, classification operations for separation of particles on the basis of size and concentration operations that separate particles according to their mineralogical composition. The simulation model was calibrated against actual plant data collected using a carefully planned sampling campaign. The second objective was to identify viable operating conditions for optimal production of copper sulphide concentrates.

With the above research objectives in mind, the integrated circuit was simulated under various operating conditions guided by current practice at Kansanshi. The simulation output data were then analysed within the attainable region framework. This analysis technique was employed to search for mill operating ranges under product size constraints (i.e. -150 +38 μm) and consequently optimum flotation performance.

1.4 Scope of the research

The research entails constructing a simulation model integrating milling and flotation for the optimal recovery of copper. A plant survey was conducted on the Kansanshi sulphide ore circuit where samples were collected from key streams. Streams sampled were the feeds and discharges of the SAG and ball mills as well as the feed, underflow and overflow around the hydrocylones. Other streams sampled were rougher flotation feed, rougher concentrate and rougher tailings. It must be noted that the samples consist of feed (input) and discharge (output) from processing unit for determining individual units and circuit performance. Laboratory analyses were done on the samples in terms of particle size distribution, solids content, and flotation response. Flotation responses which were measured were recovery and concentrate grade. The raw data then served to characterize the ore in terms of breakage and selection functions parameters later used for model calibration and simulation purposes. Equipment specifications were measured directly during the survey while others were obtained from previous work on the sulphide ore circuit as well as equipment datasheets from manufacturers. The equipment whose specification were obtained included SAG and Ball mills, Pebble crusher, Hydrocyclones and rougher flotation cells. Laboratory batch test-work was carried out to gather flotation kinetics data for use in the flotation model under MODSIM®. This model known as the discrete distributed flotation kinetic constant model offers scale-up capability of batch flotation data. It does also capture the effects of feed size on flotation performance (King, 1972 & 2012).

Parameters investigated in the comminution circuit were SAG mill feed rate, ball filling, total filling, mill rotational speed, slurry concentration and ball mill filling with a view to identifying the combination of these parameters which would generate a product size predominately -150+38 µm. The aforementioned parameters were shortlisted for investigation because they influence the rate of

breakage and product size distribution in tumbling mills (Austin et al., Napier-Munn et al., 1999). To this end, an integrated milling-flotation model of the sulphide ore circuit was built under MODSIM®, a modular simulator for mineral processing operations. After calibration, the effects of the aforementioned milling parameters on production of -150+38 µm were simulated and the output data analysed within the attainable region framework. The simulations focused on changes in SAG mill feed rate, ball filling, total filling, rotational speed, slurry concentration and ball mill filling. It was expected that this would result in process changes in terms of flotation recovery. It was also envisaged that production of material in the range -150+38 µm would result into optimisation of recovery and concentrate grade for the sulphide ore circuit.

The main objective of this work was to find operating conditions of the Kansanshi sulphide ore circuit that will guarantee optimised flotation recovery. The following research questions were central to meeting the goal set out within the scope of the research:

- What is the optimum mill throughput for the Kansanshi sulphide ore circuit that can be attained without compromising flotation recovery?

- What SAG and ball mills conditions of ball size, charge filling, rotational speed, and slurry concentration will generate a final product falling predominantly in the range -150 +38 µm?

- Can the attainable region technique be used to determine a global optimum of flotation recovery and concentrate grade across the entire milling-flotation circuit?

The research focused on answering the questions posed above. The questions served as guideposts and were fundamental to the approach taken in data collection methodology, simulations and data analysis.

1.5 Layout of the dissertation

This dissertation is organized into seven chapters including the introduction. The introductory chapter gives a brief description of the mine were the research was conducted, the background to the research, defines research problem and objectives and also presents the research questions.

The second chapter presents a detailed review of grinding and flotation underpinning principles, comminution and flotation processes. The population balance model and the attainable region methodology are also presented in the context of the current research.

Chapter three gives a description of the survey conducted on the milling and flotation circuit processing the sulphide ore at Kansanshi. The experimental methodology and the equipment used are also covered. Here, the information presented comprises the streams sampled, sampling equipment and methods, as well as the protocols for the experimental work conducted in the laboratory.

Chapter four presents the processing methodology of the analysis of data collected from the Kansanshi sulphide ore circuit and laboratory work. The results from the data are produced in order to build the computer model of the circuit. This is done in chapter five in which a computer version of the Kansanshi sulphide ore circuit is implemented. MODSIM®, a software package specialised for the simulation of mineral processing circuits, was used for the purpose of modelling building, simulation, and optimisation.

In chapter six, the computer model built in MODSIM® is simulated under various operating conditions with a view to optimise the recovery of the entire circuit. In chapter seven, key findings brought about from the industrial survey, laboratory tests, and simulation work are summarised in line with the initial intent of the research. Finally, recommendations for future work are made in Chapter 7.

Chapter 2 Literature review

2.1 Introduction

The primary objective of mineral processing is to produce a good quality concentrate at maximal recovery and minimal operating costs. Comminution and concentration processes are employed to liberate the valuable minerals from the host rock and separate the valuable minerals from the gangue, that is, the valueless fraction of material accompanying the ore.

In the context of the present research work, the following comminution and concentration techniques are reviewed: crushing, milling, and froth flotation.

Literature on comminution and flotation is reviewed in this chapter in line with the objectives set out for the research. The review specifically focuses on the population balance framework with applications to comminution and froth flotation. Fundamental concepts and selected processing equipment associated with the two processes are succinctly presented. A description of key operating parameters and relevant models, then, follows from the theoretical description of comminution and flotation operations. The optimisation of comminution and flotation circuits is also reviewed. Here, the optimisation of mineral processing circuits by modelling and simulation is covered since this has taken centre stage in the industry. Finally, the attainable region framework is presented as an alternative methodology for the optimisation of mineral processing circuits.

2.2 Crushing equipment

Crushing is accomplished by compression of ore particles between the crushing head and the shell liners or by impact of surfaces in a constrained motion (Napier-

Munn et al., 1996). It is usually carried out in stages with each stage employing a different type of crushing equipment.

The most widely used crushing machines are the jaw, the gyratory, and the cone crushers. The working principle and key operating parameters of the cone crusher was reviewed because it was relevant to the research.

The cone crusher consists essentially of a spindle on which is mounted a crushing head housed in a crushing shell. The main operating parameter that determines the cone crusher product size and capacity is the closed side setting (CSS). All the particles in the crusher cavity receive at least one nip prior to exiting the crusher; hence, crusher products are predominantly the size of the CSS.

2.3 Tumbling mills

A tumbling mill is basically a cylindrical shell loaded with loose crushing bodies that tumble when the mill is rotated thereby occasioning ore breakage. Steel rods or balls, ceramic balls, pebbles, hard rock or oversize ore itself are used as grinding media (Schlanz, 1987). The working principle is the same in all tumbling mills regardless of the grinding media used. The charge is lifted to a certain height then falls and tumbles down over the charge mass as the shell rotates with charge slippage being prevented by shell liners.

2.3.1 Breakage mechanisms of tumbling mills

The performance of tumbling mills is greatly dependent on the make-up and the motion of the mill charge. Size reduction in tumbling mills is a combination of three types of breakage mechanisms in some proportion: abrasion, attrition, and impact (Schlanz, 1987; Gupta and Yan, 2016; Austin et al., 1984). Impact breakage is occasioned by an impacting object falling perpendicularly on other particle

thereby transferring energy to it as shown in Figure 2.1. The resultant breakage is proportional to the energy transferred from the impacting to the target particle.

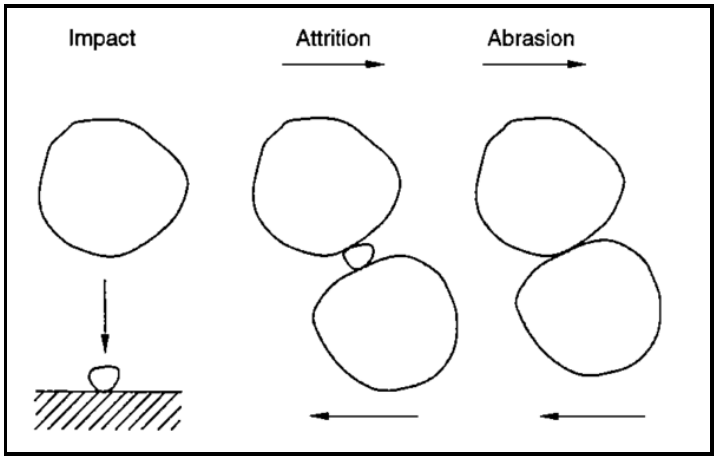

Figure 2.1 Summary of the breakage mechanisms commonly found in comminution equipment (Napier-Munn et al., 1996)

When particles in a mass move at different speeds relative to each other, they rub against each other and wear off rough solids on the surface in a process referred to as abrasion. Similarly, attrition breakage occurs on the surface of the particle which is nipped between two relatively larger particles as shown in Figure 2.1. The smaller particle which is nipped is broken due to the relative motion of the particles. Abrasion and attrition breakages are predominant in the rising body of the tumbling charge. Indeed, the charge does not move as a solid block but comprises of layers moving relative to each other thereby occasioning attrition and abrasion breakages. Note that impact breakage is predominant around the toe of the mill as shown in Figure 2.2.

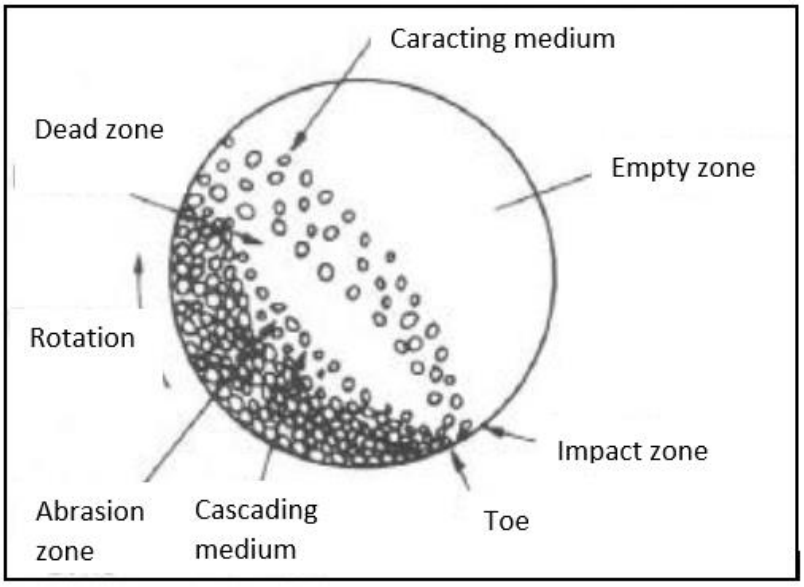

Figure 2.2 Charge motion in tumbling mills (Wills and Napier-Munn, 2006)

2.3.2 Autogenous and semi-autogenous milling

Autogenous (AG) mills are tumbling mills that employ large pieces of hard ore as grinding media (Schlanz, 1987). The large ore pieces must be competent enough to be effective as grinding media. In contrast, semi-autogenous (SAG) mills employ a combination of steel balls and large pieces of hard ore as grinding media (Schlanz, 1987). SAG mills are usually operated with a total filling between 30 % and 35 % of which between 5 % and 15 % are steel balls (Gupta and Yan, 2016).

The breakage taking place in AG and SAG mills can be described as normal, abnormal and self-breakage (Stanly, 1974; Austin, 1987). These are attrition, abrasion and impact breakage (Austin et al., 1984; Gupta and Yan, 2016). These breakage mechanisms are greatly influenced by the rotation speed and charge filling level which determines whether the charge motion will be predominately cataracting or cascading. Attrition and abrasion are prevalent in sections of the mill where the charge is cascading (Austin, 1987). The products from attrition and abrasion processes are fine, though the parent particles remain intact to a larger extent. Particles in the charge suffer breakage as they fall onto the toe of the

charge and as they tumble in the cataracting regions of the mill charge due to impact (Austin, 1987; Wikedzi, 2018).

2.3.3 Ball milling

Ball mills are loaded with steel balls, pebbles or ceramics as grinding media. Breakage of ore particles is done by point contact of steel balls and ore particles. The charge motion in ball mills can be either cascading or cataracting or a combination of the two depending on the mill rotational speed and mill filling. Cascading motions are pronounced at a lower speed whereas cataracting motions come into play when mill speed is increased (Wills and Napier-Munn, 2006).

Factors which affect milling efficiency include ball and powder/slurry loading, ball size, rotational speed, internal slurry concentration and shell liners profile. The particle size fed to ball mills does not have much capacity to induce breakage on itself; hence, breakage is mostly dependent on steel balls. It is common knowledge that a single steel ball or few of them cannot produce reasonable particle breakage; hence, the mill has to be filled with sufficient steel balls to increase breakage frequency. When ball filling is low, cataracting motion of the charge will be predominant resulting in a coarse mill product. Conversely, high ball filling generates predominant cascading motions and more grinding surface area giving more fines in the product and increased breakage rate (Shoji et al., 1982; Austin et al., 1984). Low powder filling translates into low filling of steel balls interstices by powder resulting in high steel ball to steel ball contact. This in turn results in high steel balls and liner wear. On the other hand, too high powder or slurry filling provide a cushioning effect thus reducing the effect of impact from steel ball to steel ball on contact. This invariably reduces the breakage rate. It is important to also consider the volume of interstices in the steel balls filled by powder referred to as powder filling. Low powder filling result in little collision spaces translating in low breakage rates while very high powder filling will cause the ball load to dilate and reduce the breakage rate as a result of reduced ball to ball nipping collision.

Austin et al. (1984) observed that effective breakage rate was feasible with ball filling between 0.6 to 1. Several researchers have proposed operating mills with a powder filling of 1 (Latchireddi and Morrel, 2003; Tangsathitkulchai, 2003). Kutubilwa (2012) also had a similar conclusion from his experimentation that operating mills with a high ball filling with a powder filling of unity guarantees high breakage rate with production of a finer product. When the slurry concentration is very low the ore passes through the mill at a faster rate. As a consequence, residence time will be reduced translating in a coarser product and also high ball to ball collisions. When the slurry concentration is very high a cushioning effect ensues. Mills are usually operated with slurry concentrations ranging between 65 % and 80 % solids (Schlanz, 1987). Mill rotational speed and ball filling have a complimentary effect on the motion of the charge. Lower rotational speed result in predominant cascading motion yielding a fine product and giving high steel balls and liner wear rate. On the other hand, high mill rotational speeds results in predominantly cataracting motion giving a coarser product. Mill speed is usually quoted as a percentage of critical speed. King (2001) proposed that industrial mills should be operated between 70 % and 80 % of critical speed. It has been observed that small diameter steel balls are effective for breaking smaller particles giving a finer product owing to the increased surface area. On the other hand, bigger diameter steel balls are effective for hard and big particles breakage because of their higher impact energy (Austin et al., 1984; King, 2001; Katubilwa, 2009). Liners and lifter are installed inside tumbling mills to protect the mill shell from wear and prevent the charge from slippage respectively. Mill filling, rotational speed and liner profile have a complimentary effect on charge motion. Liners which promote cataracting motion are said to be more aggressive while those promoting cascading motion are said to less aggressive.

2.3.4 Material transport through tumbling mills

In practice, tumbling mills do not conform to the ideal flow of material through a perfectly mixed reactor. This arises from the fact that there is considerable resistance to the flow of material through the mill ascribed to the tumbling load. The actual transport profile of a tumbling mill can be modelled by considering a series of several well mixed segments in the mill. Material at the end of one well-mixed segment feeds the next segment; however, the discharge from the last segment may experience classification from the discharge grate acting like a classifier (Austin et al., 1984; King, 2001).

Several experimental results have shown that operating mills can generally be modelled as three perfectly mixed segments of varying sizes (King, 2001; Austin et al., 1984; Marchand et al., 1980; Weller, 1980). Post-classification may be pronounced or not depending on the particle size of the product exiting the last segment. The time the material will spend in the mill is largely depends on the feed rate, mill speed, ball loading and slurry density (Makokha et al., 2014).

It has been observed that industrial mills do not conform to a perfectly mixed reactor system model but instead contain several perfectly mixed segments in series (Austin et al., 1984; Marchand, 1980). Fresh feed enters the first segment and after undergoing breakage exits the segment entering the second segment. The product from one segment becomes feed to the following segment and so on. The number of perfectly mixed segments in operating mills can be determined from the residence time distribution function. Generally, it has been concluded that industrial mills comprise of two small and one big perfectly mixed segments with the discharge end of the mill providing classification by returning oversize material back into the mill. The residence time distribution can be determined by monitoring the concentration of a tracer from the mill discharge. The residence time distribution (RTD) is determined from the plot of tracer concentration against time as shown in Figure 2.3 by normalising the graph with respect to the area under the curve. The RTD function $\varepsilon(t)$can be determined as follows

$$\varepsilon(t) = \frac{C(t)}{\int_{t=0}^{+\infty} C(t).dt} \qquad \textbf{(2.1)}$$

where $C(t)$ is the concentration of tracer exiting the mill.

RTD can also be presented as a cumulative plot of the total fraction of the tracer that has left the mill, graphed against time as shown in below.

$$E(t) = \int_{t=0}^{t} \varepsilon(t).dt \qquad \textbf{(2.2)}$$

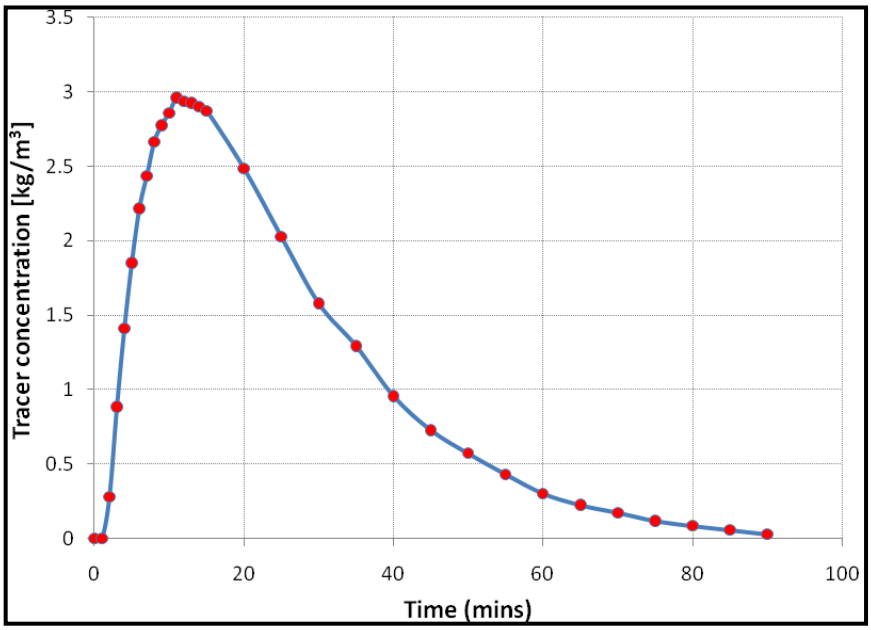

Figure 2.3 Example of tracer response of a full-scale mill of overflow discharge design (Makokha et al., 2011)

Marchand et al. (1980) proposed the model below for one large fully mixed reactor τ_1 and two small fully mixed reactors τ_2.

$$\varepsilon(t) = \frac{\tau_1}{(\tau_1 - \tau_2)^2}\left[\exp\left(-\frac{t}{\tau_1}\right) - \exp\left(-\frac{t}{\tau_2}\right)\right] - \frac{t}{(\tau_1 - \tau_2)\tau_2}\exp\left(-\frac{t}{\tau_2}\right) \qquad \textbf{(2.3)}$$

The average residence time in the mill can be determined as follows:

$$\tau = \frac{M}{W} \quad \textbf{(2.4)}$$

Where *M* is the mass of material in the mill and *W* the mass flow rate through the mill

2.3.5 Operating parameters of tumbling mills

The efficiency of tumbling mills is dependent on a host of design and operating parameters. These factors include rotational speed, ball filling, powder filling, slurry density and ball size distribution (Yekeler, 2007). The total filling and the ore filling are applicable to SAG and AG mills respectively.

The speed at which the mill is rotated is referred to as mill speed, usually quoted in revolutions per minute. It has now become common practice to quote the mill rotational speed as a percentage of critical speed. The volume of the mill occupied by steel balls is called ball filling (Austin et al., 1984). As the mill operates, steel balls wear off as a result of friction within the charge and with mill liners. This leads to the reduction of ball size and ball filling. To maintain ball filling level, the steel balls must be replenished. Eventually, the charge comprises of steel balls of varying sizes commonly referred to as a seasoned charge or ball size distribution (Schlanz, 1987). The volume occupied by ore in the mills is referred to as powder filling (Austin et al., 1984).

In mineral processing, milling is usually carried out wet; the presence of water imparts rheological properties to slurry which are favourable for comminution. This gives rise to the term slurry or pulp density which refers to the fraction of solids present in the solids/water mixture. In SAG mills, grinding media comprises of both steel balls and ore or pebbles, hence the combined load of steel balls and powder or ore is referred to as total filling. Similarly, for AG mills, the grinding media is essentially ore or pebbles. This is referred to as ore filling.

The critical speed can be defined as the speed at which the mill content begins to centrifuge and not tumble (Schlanz, 1987). At this speed, the gravitational force on the mill charge balances the radial force thus preventing the charge from tumbling. It is determined for a tumbling mill as follows (Austin et al., 1984; King, 2001):

$$N_c = \frac{42.2}{\sqrt{D-d}} \quad \textbf{(2.5)}$$

Where N_c is the critical speed in revolutions per minute; D is the internal mill diameter in metres; and d is the largest steel ball diameters in metres.

The fractional ball filling J is defined as the fraction of the mill occupied by steel ball bed at rest (Austin et al., 1984):

$$J = \frac{\text{Mass of balls}/\text{Ball density}}{\text{Mill volume}} \times \frac{1.0}{0.6} \quad \textbf{(2.6)}$$

The fraction of the mill filled by powder or slurry is given by:

$$f_c = \frac{\text{Mass of powder}/\text{Powder density}}{\text{Mill volume}} \times \frac{1.0}{0.6} \quad \textbf{(2.7)}$$

Similarly, the powder filling U is defined as a fraction of the ball interstices at rest filled by powder (Austin et al., 1984):

$$U = \frac{f_c}{0.4\,J} \quad \textbf{(2.8)}$$

In mineral processing operations, grinding is generally done wet; hence, it is important to define the pulp density by considering the quantity of solids in the mixture. In the same vein, the rheological properties of the slurry are better described by the percent solids in the mixture as shown below:

$$C_w = \frac{\nu_s}{\rho_s}\left[\left(\frac{\nu_s}{\rho_l}\right)\left(\frac{1-\nu_s}{\rho_l}\right)\right]^{-1} \quad \textbf{(2.9)}$$

Where ν_s is the weight fraction of solid, ρ_s is the specific density of solid, and ρ_l is the specific density of the liquid

2.4 Size classification

Screens and classifiers are installed in comminution circuits to ensure that material that has attained a set criterion is passed on to the next stage whereas that which has not is returned for further breakage. The evaluation of classification focuses on the extent to which a classifier passes undersize material to the oversize fraction and vice-versa.

Sizing equipment can be classified into screens and classifiers based on the size of the material they separate and the mechanism of separation. Screening is used to separate particles into two or more fractions on particle sizes ranging from 300 mm down to 40 µm (Wills and Napier-Munn, 2006). The choice of whether to use screening or classifications devices is guided by the fact that finer particles would require enormously large screening surfaces for efficient separation as compared to classification devices. In this section the partition curve, vibrating screens and hydrocyclones design and operating parameters as well as models for predicting screening and classification efficiency are reviewed.

2.4.1 Vibrating screens

A screen is a device with a surface which has holes used to separate solids into two or more fractions. The performance of vibrating screens depends on design as well as operating parameters. Screen design parameters include the open area on the screen surface, aperture size and shape and inclination angle. Operating

parameters, on the other hand, include feed rate, screen spray water and vibration amplitude (Napier-Munn et al., 1996; Gupta and Yan, 2006). Figure 2.4 shows a schematic presentation of a screen.

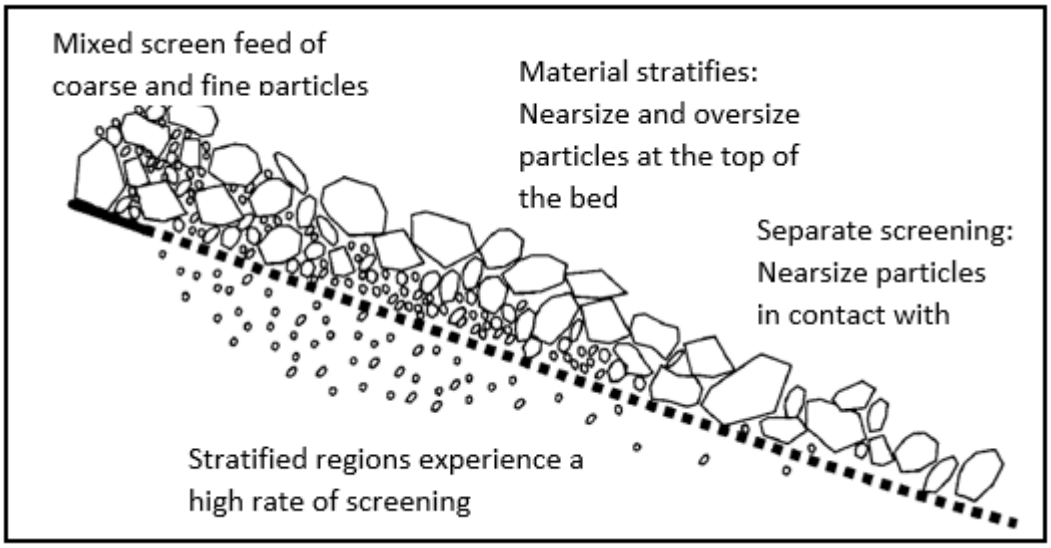

Figure 2.4 Schematic representation of a vibrating screen
(Will and Napier-Munn, 2006)

For screening to be effective, each particle must be afforded a number of opportunities to reach the screen surface and be exposed to the holes. The efficiency of a screen is evaluated in terms of how perfect the separation is between undersize and oversize fractions (King, 2001). The rate of presentation of each particle to the surface is increased and the movement of oversize material over the surface is enhanced by the vibrating motion.

2.4.2 Hydrocyclones

The major role of hydrocyclones in milling circuits is to pass material which meet particle size requirements for downstream operations and retain coarse material for further breakage. Operation and design of hydrocyclones focus on meeting

criteria such as throughput at a specified cut-size, attain specified water split and overflow as well as underflow densities. Note that the performance of a hydrocyclone hinges on geometry (design) and operating parameters. Critical design parameters are shown in Figure 2.5.

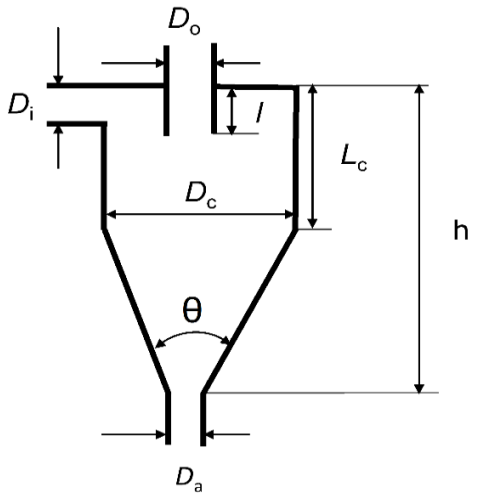

Legend	
D_c	Cyclone diameter
D_o	Vortex finder diameter
D_i	Inlet diameter
L	Vortex finder length inside the cyclone
L_c	Cylindrical section length
h	Hydrocyclone length
θ	Cone angle
D_a	Apex diameter

Figure 2.5 Key design parameters of a hydrocyclone (from Wikedzi, 2018)

The principal design parameter for hydrocyclones is the diameter denoted by D_c in Figure 2.5. Large diameter hydrocyclones have larger capacities but suffer from increased cut-size thus producing a coarse overflow. The opposite is true for smaller diameter hydrocyclones. The increased cut-size in large diameter hydrocyclones is attributable to low tangential feed velocities which translate into equally low centrifugal forces (Napier-Munn et al., 1996). Centrifugal forces are the main drivers of the hydrocyclone classification process. Other equally important design parameters on hydrocyclones are the overflow and underflow diameters referred to as vortex finder and spigot or apex respectively. Large vortex finder and smaller spigot result in higher cut-sizes, thus giving a coarser overflow and vice versa. Major operating parameters are feed flowrate and slurry pulp

density. Higher feed flowrates generate higher centrifugal forces inside hydrocyclone and consequently a finer product (Wills and Napier-Munn, 2006). The opposite holds for lower slurry feed rates. Higher slurry feed densities on the hand will give a coarser overflow and vice versa.

2.4.3 Partition curve of size classifiers

Operating hydrocyclones will always pass a portion of oversize to the overflow and undersize to the underflow no matter the design and operating efficiency. The distribution function is used to evaluate the efficiency of separation attained by a classifier. The steeper the distribution curve the higher the separation efficiency and vice versa. The partition curve or tromp curve shown in Figure 2.6 gives the representation of the classifier distribution function.

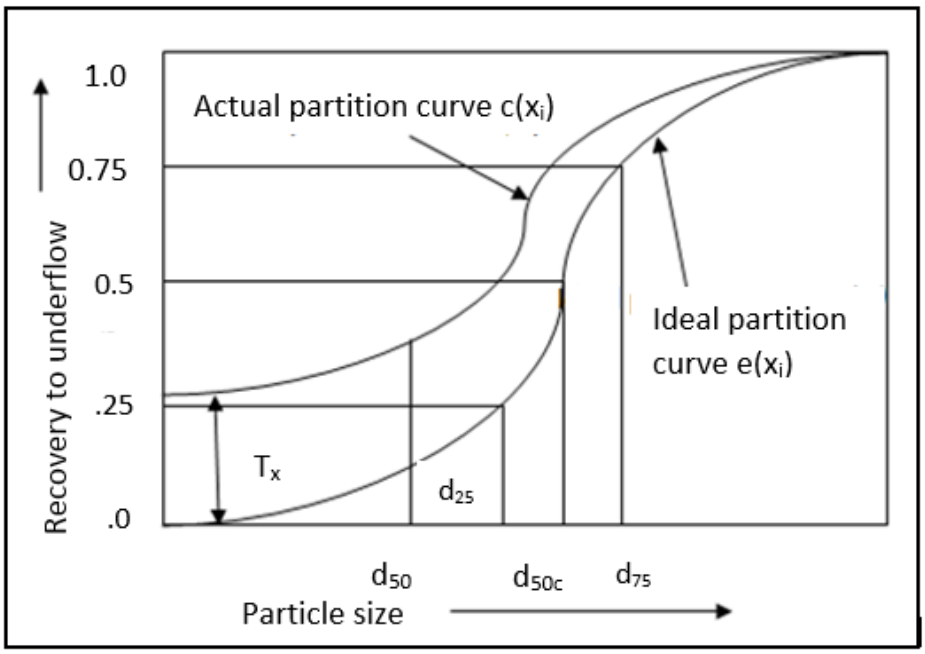

Figure 2.6 Typical partition curve of a hydrocyclone

The efficiency of hydrocyclones as presented by the partition does not start at zero because of short-circuiting (T_X). This phenomenon arises from the entrainment of very fine particles in the water which reports to the underflow without being subjected to the influence of classification. That is why the actual partition curve is corrected by eliminating the particles entrained in the water to the underflow. In doing so, an ideal partition curve is generated that accounts for the efficiency due to classification only.

In Figure 2.6, T_X represents the portion of undersize material in the feed that reports to the underflow by short-circuiting. The actual classification function $c(x_i)$ can be calculated as shown below (King, 2001):

$$c(x_i) = T_X + (1 - T_X)\, e(x_i) \qquad \textbf{(2.10)}$$

Where $e(x_i)$ describes the ideal classification function with no short-circuiting. The particle size which has equal chances of reporting either to the overflow or underflow is known as the cut-size. In the context of Figure 2.6, two cut-points can be calculated: the actual d_{50} and the corrected d_{50c}. The term d_{50} refers to the cut-size which is the size of particles which have an equal chance of either reporting to the under or overflow in real operation. The corrected cut-size d_{50c} has the effect of short-circuiting eliminated so that classification is only as a result of the separation action of the hydrocyclone.

The factors hindering transmission of undersize material reporting to the underflow are summed up in the partition function. The empirical model by Karra (1979) can be used to describe the classification function as shown below:

$$c(d_p) = 1 - \exp\left[-0.693 \left(\frac{d_p}{d_{50}} \right) \right]^{5.9} \qquad \textbf{(2.11)}$$

where λ = 5.9 quantifies the sharpness of classification.

and $x = \frac{d_p}{d_{50c}}$ **(2.12)**

The parameter λ is a qualitative description of the behaviour of classification equipment indicative of the degree of classification sharpness. This parameter together with T_X and d_{50} must be evaluated using actual data from the classifier in terms of operating conditions and physical dimensions.

When the values for d_{50} are higher than the screen mesh size the screening efficiency is high and vice-versa.

2.4.4 Empirical models of size classifiers

Two empirical models of size classifiers are covered here: the Karra model and the Plitt model. The first finds wide applications with screens while the second is favoured for hydrocyclones.

Karra (1978) proposed the expression in Equation (2.13) for determining the theoretical amount of undersize that a screen can transmit to the undersize. Karra's model is capable of accurately predicting how the screen will perform under actual plant operating conditions (King, 2001; Karra, 1978)

$$Ths = AS \times BS \times CS \times ES \times FS \times GS_C \times (\text{Screen area}) \quad \textbf{(2.13)}$$

The letters denote factors applied to compensate for changes in screen and feed from standard to actual conditions as explained earlier. The letters represent the following: basic capacity (AS), oversize (BS), half size (CS), screen deck position (DS), wet screening (ES), bulk density (FS) and GS_C for near size particles. For nominal standard operating conditions, all the capacity factors are unity. They will increase or decrease as the screening duty becomes more or less arduous (King, 2001).

The model developed by Plitt is shown below (Napier-Munn et al., 1996; Nageswararao et al., 2004; Wills and Napier-Munn, 2006):

$$d_{50c} = \frac{39.7\, D_c^{0.46}\, D_i^{0.6}\, D_o^{1.21}\, \eta_F^{0.5}\, \exp(0.063 C_v)}{D_a^{0.71}\, h^{0.38}\, Q_f^{0.45} \left(\frac{\rho_S - \rho_F}{1.6} \right)^K} \quad \textbf{(2.14)}$$

Where D_c, D_a and h are expressed in cm and are defined in Figure 2.5; C_v is solids content by volume; η_F is fluid viscosity (mPa.s); K is hydrodynamic exponent. The value of is K = 0.5 for laminar flow.

Plitt's model has proved to very robust and found application in modelling hydrocyclone with large diameters with high percent solids in the feed over a wide operating range (Napier-Munn et al., 1996; King, 2001). It is capable of predicting the performance of hydrocyclone using data obtained from operating hydrocyclones. The model suffers from a weakness in its prediction of flow split between the over and underflow streams.

2.5 Froth flotation

Froth flotation is a complex physico-chemical process used to separate minerals based on their differences in surface properties and their ability to selectively attach to air bubbles in an aerated mineral slurry pulp (Rahman et al., 2012; Bu et al., 2016; Wills and Napier-Munn, 1996). The principles and kinetics underpinning the flotation process are presented in this section. Also presented are parameters which determine the performance of the flotation process and associated flotation models.

2.5.1 Principle of froth flotation

Froth flotation involves three phases: liquid, solids and froth (Hu, 2014; Morar et al., 2012; Bu et al., 2016; Neethling et al., 2008; Hanumanth et al., 1992; Ali et al., 2009; Ergün et al., 2009; Jovanović and Miljanović, 2015; Wills and Napier-Munn, 1996). Figure 2.7 shows a schematic presentation of the flotation process.

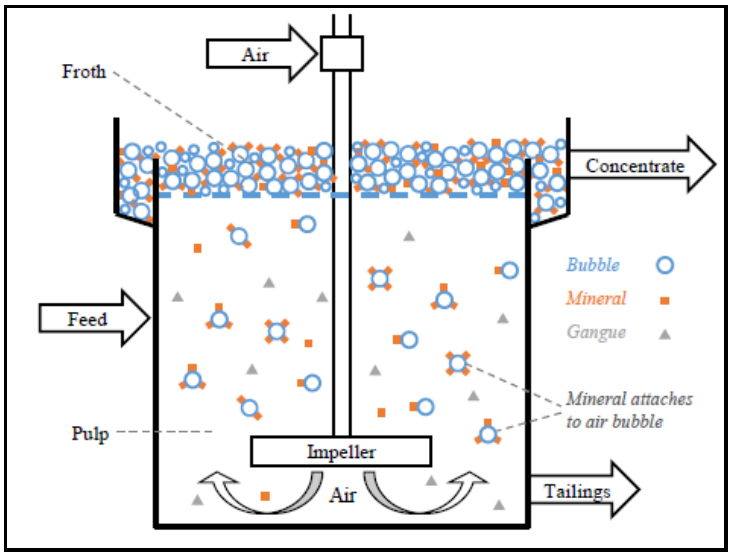

Figure 2.7 Simplified representation of the flotation mechanism (Hu, 2014)

The separation of valuable minerals from the gangue in froth flotation is accomplished by conditioning the valuable particles in the agitated pulp with chemicals to become hydrophobic and blowing air which is sheared into small bubbles. The hydrophobic valuable minerals will selectively attach to the air bubbles and rise to the top of the flotation cells to form a mineralised froth as shown in Figure 2.7 (Lynch et al., 1974).

2.5.2 Kinetics of batch flotation tests

Laboratory flotation testing is conducted in batch flotation cells on representative ore samples or slurry being fed to the flotation cells. In the former the samples are crushed and milled in the laboratory prior to flotation testing. Batch flotation test runs are usually conducted in duplicate for reproducibility and control of wild

results or outliers. The feed, concentrate and tailings samples are weighed and analysed for the minerals of interest. The assays along with the sample weights are used to determine recovery which can be plotted against flotation time to generate grade-recovery time profiles (Dowling et al., 1985; Bu et al., 2017; Jovanović and Miljanović, 2015). Flotation rates and kinetic data can be obtained from these graphs.

Zuniga (1935) pioneered the development of kinetic flotation models when he expressed the flotation process with a differential equation of a chemical reaction. He then observed that flotation recovery was an exponential function of flotation time as shown below:

$$\frac{dC}{dt} = FRC.C(t)^n \qquad \textbf{(2.15)}$$

Where $C(t)$ is the concentration of floating particles left in the flotation cell at time t; FRC is the flotation rate constant; and n is the order of the flotation process.

Laboratory experiments have proved that the flotation process can be represented by a first order kinetic model (King, 2001; Zuniga, 1935; Bu et al., 2016). The rate at which particles in a well agitated flotation cell are recovered by bubbles is proportional to the concentration of the particles in the pulp phase (Bu et al., 2016; Woodburn, 1970; King, 2001).

The rate of capture of particles of different species in the pulp phase is a function of the degree of hydrophobicity and as a result they are captured at different rates (Lynch et al., 1974; Yianatos, 1989). The rate of transfer of particles from the pulp to the froth phase is a strong function of particle size and composition (Lynch et al., 1974; Morris, 1952; King, 2001; Johnson, 1972). This results in particles being classified into fast, medium and slow floating based on their rate of capture during flotation which can be attributed to the rate constant. Jameson (2012) explained that the variation in the rate constant is a function of the particles degree of

liberation and size. Good flotation performance occurs in the middlings size range (Gaudin et al., 1931). This can be attributed to adequate valuable minerals liberation and particles not being too heavy to be lifted by air bubbles and not too fine to create slimes. Poor flotation recoveries with fine can be attributed to poor efficiency of bubble-particle collisions and formation of slimes which coat particles thereby preventing collector adsorption on the particles. The poor recovery of coarse particles is attributed to inadequate valuable mineral liberation, bubble-particle detachment because air bubbles cannot lift coarse particles. Flotation can be modelled as a first order process as shown below (Lynch et al., 1981):

$$R = 1 - \exp(-f_r\, t) \qquad \textbf{(2.16)}$$

Where R is the cumulative recovery after time t and f_r is the first order rate constant. The rate of capture of valuable minerals in the flotation process is primary influenced by concentration of valuable minerals present and degree of valuable minerals liberations (King, 2001). Liberation of minerals is a function of particles size, hence modelling the flotation process must incorporate the effect of particle size on flotation.

The effect of particles size is introduced in modelling the flotation process by splitting the specific flotation rate constant FRC_{ij} in three components (King, 2001):

$$FRC = r_{fc}\, \Im(d_{pi})\, S_{av} \qquad \textbf{(2.17)}$$

where $\Im(d_{pi})$ account for all the effect of particle size and type; S_{av} is the available bubble surface area averaged over the entire bubble population in the flotation cell; r_{fc} is the residual constant specific to the particle type but independent of particle size.

King (2001) proposed an empirical model for the dependency of particle size on the rate of flotation by introducing the function $\Im(x_i)$ to describe variations in flotation rate:

$$\Im(x_i) = 2.33\left(\frac{\varepsilon}{x_i^2}\right)^{0.5}\left[1-\left(\frac{x_i}{x_{\max}}\right)^{1.5}\right]\exp\left(-\frac{\varepsilon}{x_i^2}\right) \quad \textbf{(2.18)}$$

where $x_{\max}$ is the largest particle size that can be floated while ε is the level of turbulence in the flotation pulp.

Recovery-by-size data collected from batch flotation tests can be used to determine parameters in Equation (2.18). This in turn can be used to estimate the recovery of an industrial flotation cell processing an ore similar to that tested under laboratory conditions (King, 2001):

$$R_i = 1-\exp\left[-r_{fc}.\sigma.\Im(x_i)t_f\right] \quad \textbf{(2.19)}$$

where t_f is the average residence time in the flotation cell; σ is the average surface area per unit volume of air bubbles in the flotation cell; and r_{fc} is the specific flotation rate constant of particles of size x_i. This rate constant can be determined by curve-fitting batch flotation data using the first-order kinetics law. These equations can be used to model a bank of flotation cells and simulate the operation of the continuous process.

2.6 Population balance framework

The population balance framework has been applied successfully to describe the operation and performance of mineral processing equipment (King, 2001). It is important to note that mineral processing operations host millions if not billions of particles in the process at any given time thus making it impossible to describe each particle in detail. This dilemma has been resolved by grouping particles into

discrete categories based on some significant characteristic such as particle size, mineralogical and chemical composition, shape and surface specific energy. This has been the principle behind population balance modelling.

The application of population balance modelling to comminution and froth flotation processes are reviewed in the following section.

2.6.1 Application to comminution machines

The general population balance for comminution machines can be applied to describe and optimise the operation of rod, ball, semi-autogenous and autogenous grinding mills. This approach only considers the particle size and assumes that particle breakage and wear is not influenced by the position of particle in the mill. The general population balance model must account for all the breakages mechanisms which include self, impact, abrasion and attrition breakages. The population balance applied to batch grinding take account of the quantity of particles within discrete size ranges otherwise referred to as complete size-mass-balance. The population balance of material in a batch grinding system can be summarised as follows:

The rate at which material disappears from the largest size interval j into smaller sizes by breakage action is $= S_j w_j(t) W$

The material in size interval class i broken from size interval j will appear at the rate $= b_i S_j w_j(t) W$

Material in size interval class i will break into a smaller size class and disappear at the rate $= S_i w_i(t) W$

The composition of material in the size class interval i in the final product of the batch grinding process will be equal to material being broken from a size interval larger than i, denoted as j plus materials of size i already in the feed minus material

broken from i into a size interval smaller than i. This can be expressed in mathematical terms as:

$$\frac{d[w_i(t)W]}{dt} = -S_i w_i(t)W + \sum_{\substack{j=1 \\ i>1}}^{i-1} b_{ij} S_j w_j(t)W \qquad \textbf{(2.20)}$$

2.6.2 Population balance model of ball milling

The ball mill population balance has necessitated the mathematical description of breakage process that happens in the ball mill. When the feed and ball mill operating conditions as well as the ball mill geometry are known, the size distribution of the ball mill product can be determined. Austin et al. (1984) proposed an empirical model for determining the product size distribution discharged from a ball mill after the mean residence time τ for a steady state continuous plug flow ball mill without exist classification:

$$p_i = p_i(t) = \sum_{j=1}^{i} d_{i,j}(t)\, f_j \quad \text{with } n \geq i \geq j \geq 1 \qquad \textbf{(2.21)}$$

$$\text{where } d_{i,j} = \begin{cases} 0, & i < j \\ e_j, & i = j \\ \sum_{k=j}^{i-1} c_{i,k}\, c_{j,k}\, (e_k - e_i), & i > j \end{cases} \qquad \textbf{(2.22)}$$

$$c_{i,j} = \begin{cases} -\sum_{k=i}^{j-1} c_{i,k}\, c_{j,k}, & i < j \\ 1, & i = j \\ \frac{1}{S_i - S_j} \sum_{k=j}^{i-1} S_k\, b_{i,k}\, c_{k,j}, & i > j \end{cases} \qquad \textbf{(2.23)}$$

$$e_j = \int_0^{+\infty} \exp(-S_j\, t)\, \varphi(t)\, dt \qquad \textbf{(2.24)}$$

Where $p_i(t)$ is the mass fraction of particles of size x_i discharged by the mill after having undergone size reduction for an average processing time *t*.

f_i is the feed of mass fraction of particles of size x_i.

$d_{i,j}(t)$ represents the transformation of particles in the feed of size x_j into particles in the product of size x_i.

S_i is the selection function describing the selection of particles for breakage in the ball mill.

$b_{i,j}$ is the breakage function which describes the mass fraction of fragments of size x_i resulting from the breakage of selected particles of size x_j.

$\varphi(t)$ is the residence time distribution function of the mill describing the transport of particles through the mill while size reduction is in progress.

The selection and breakage function parameters can be obtained from laboratory batch milling data (Austin et al., 1984). Selection function varies with particle size as shown as shown below:

$$S_i = a\, x_i^{\alpha} \frac{1}{1+\left(\frac{x_i}{\mu}\right)^{\Lambda}} \qquad \textbf{(2.25)}$$

where α and Λ are dependent on the material being treated; a and μ depends on milling conditions.

The cumulative breakage function can be fitted using the empirical model below (Austin et al., 1984):

$$B_{i,j} = \Phi\left(\frac{x_{i-1}}{x_j}\right) + (1-\Phi)\left(\frac{x_{i-1}}{x_j}\right),\ 0 \le \Phi \le 1 \qquad \textbf{(2.26)}$$

where β, γ, and Φ are parameters that depend on the material being broken.

When grinding kinetic data is obtained from batch laboratory test mills it becomes imperative that it is scaled up to industrial mills data for practical application purpose. Austin et al. (1984) proposed a method of scaling up batch laboratory data to industrial mills data to predict how selection function parameter varies with ball and mill diameter, ball filling, powder filling and mill rotational speed as shown in Equations (2.27– 2.32). An important point to note is that parameters which are dependent on the material undergoing breakage and which are dependent on the conditions and geometry of the mill used must be identified.

$$S_i(d) = a_T \left(\frac{x_i}{x_0}\right)^{\alpha} \frac{1}{1+\left(\frac{x_i}{C_1 \mu_T}\right)^{\Lambda}} C_2\, C_3\, C_4\, C_5 \qquad \textbf{(2.27)}$$

where $C_1 = \left(\frac{D}{D_T}\right)^{0.2} \left(\frac{d}{d_T}\right)^{2}$ **(2.28)**

$$C_2 = \frac{d_T}{d} \qquad \textbf{(2.29)}$$

$$C_3 = \begin{cases} \left(\frac{D}{D_T}\right)^{0.5} & \text{for } D \le 3.81\text{m} \\ \left(\frac{3.81}{D_T}\right)^{0.5} \left(\frac{D}{3.81}\right)^{0.3} & \text{for } D > 3.81\text{m} \end{cases} \qquad \textbf{(2.30)}$$

$$C_4 = \left(\frac{1+6.6\, J_T^{2.3}}{1+6.6\, J^{2.3}}\right) \exp\left[-c\,(U - U_T)\right] \qquad \textbf{(2.31)}$$

$$C_5 = \left(\frac{\phi_c + 0.1}{\phi_{cT} + 0.1}\right) \frac{1+\exp\left[15.7\,(\phi_{cT} - 0.94)\right]}{1+\exp\left[15.7\,(\phi_c - 0.94)\right]} \qquad \textbf{(2.32)}$$

In Equation (2.27), a_T, μ_T, α, and Λ are the selection function parameters of the ore measured using the laboratory test mill. They are characteristic of the ore being processed by the industrial mill. The following should be noted from

Equations (2.27 – 2.32): D_T , d_T , J_T , U_T , and ϕ_{cT} represent the internal diameter, ball size, ball filling, powder filling and rotational speed of the laboratory batch mill. Batch results from the test mill are scaled up to the industrial mill characterised by parameters D, d, J, U, and ϕ_c .

In Equation (2.31), the term c accounts for whether scale-up is to be done either under dry milling or wet milling. Austin et al. (1984) proposed c = 1.20 for dry milling while a value of c = 1.32 is used when wet milling is involved.

2.6.3 Population balance model of fully- and semi-autogenous mills

The population balance for fully autogenous (FAG) and semi-autogenous (SAG) mills provides means for determining the products size distribution from these units given feed and operating conditions as well as mill geometry. The major breakage mechanisms in FAG mills are attrition and abrasion because the charge density is low leading to low impact energy and consequently low impact breakages (King, 2001). Self-breakage happens when a lump of ore falling freely breaks on impact at the toe of the mill. Steel balls are added to the charge in SAG mills to increase the charge density and consequently impact energy and breakage. Attrition breakage can be determined using a laboratory mill loaded with only ore lumps to be abraded whereas impact energy can be modelled using Austin's standard breakage and selection function models. Self-breakage can be modelled using the t_{10} index in which a lump of ore is drop the distance equivalent to the fall distance in an operating mill. When conducting the material balance for AG and SAG mill, three distinct size classes are identified. These are size class interval of interest usually denoted as i, the size class interval larger than i, usually denoted as j, and the size class interval smaller than i. Taking a mass balance around the size class of interest i, after grinding gives:

> Mass in size interval i in feed + mass of size i generated from breakage of j = mass of i broken to smaller size + product.

The three size interval classes can be defined using three impact breakages and abrasion parameters A, b and t_{10}. These parameters are size-energy dependent and are influenced by ball size and loading. Ore breakage resulting from impact of balls can be deduced from drop test where a known weight is dropped from a given height and the size distribution arising from the breakage analysed. A computer program is employed to conduct an analysis and generate results. The data generated by the computer program includes the mass before and after impact, input energy, particle size distribution, number of particles and t-values. The breakage index t_{10}, representing the one tenth of the initial mean size, can be determined using the equation below (Napier-Munn et al., 1996):

$$t_{10} = A\left[1 - \exp\left(-b\, E_{cs}\right)\right] \qquad \textbf{(2.33)}$$

where E_{cs} is the specific comminution energy in kWh/t while A and b are the impact breakage characteristics of the material undergoing testing.

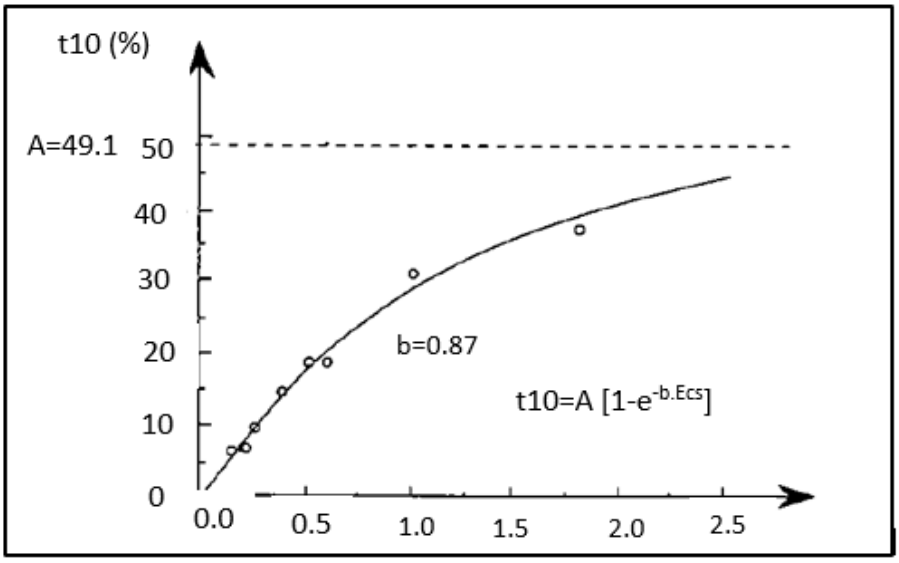

Figure 2.8 Effect of the specific comminution energy E_{cs} on the breakage index t_{10} (Napier-Munn et al., 1996)

The parameter t_{10} in Equation (2.33) is sometimes also referred to as fineness index. Higher values of t_{10} indicate a finer product size distribution.

2.6.4 Population balance model of froth flotation

The flotation process treats millions of particles at any given time and classifying each particle would be impossible. This dilemma has been resolved by grouping particles into discrete classes based on property similarities such as particles size and mineralogical composition (Jovanovic and Miljanović, 2015; King, 2001).

The population balance model applied to froth flotation considers whether particles in the pulp and froth phases are free or attached to the air bubbles. It can be represented by the differential equation below (Herbst and Harris, 2007):

$$\frac{dV\,\varpi}{dt} = \varpi_{in}\,Q_{in} - \varpi_{out}\,Q_{out} + \sum_{i=1}^{n} r_{ji}\,\varpi_j\,V \qquad \textbf{(2.34)}$$

where ϖ is the concentration of minerals in each of the four states; each state is represented by a single differential equation

ϖ_{in} is the concentration of minerals in each of the four states that will, due to certain mechanisms, pass into the object state, or are already into the object state

ϖ_{out} is the concentration of minerals in each of the four states that are not in the object state, or they will due to certain mechanism leave the object state

V is the volume of the flotation cell

Q_{in} is the volumetric flow rate of input material (water or air) into the pulp or froth phase

Q_{out} is the volumetric flow rate of output material (water or air) into the pulp or froth phase

r_{ji} is the transfer rate between the attachment or detachment of mineral particles to air bubbles and their entrainment into the froth or their drainage out of the froth. In the symbol for the transfer rate r_{ji}, i refers to the mineral particle size while j is its particle composition.

2.7 Optimisation of mineral processing circuits

Optimisation is the locating of the best operating parameters which can yield the best process outputs defined by personnel responsible for the operation so that the best possible use of the equipment or process is attained (Napier-Munn et al., 1996).

Optimisation criteria in milling may focus on the production of particles within a narrow size range as required by downstream operations at a fixed throughput. It may also take the form of increasing throughput while maintaining the particle size distribution constant. Milling circuit optimisation may also focus on reducing operating cost through effective utilisation of energy, steels ball and liners thereby increasing the bottom-line. In flotation, on the other hand, the approach maybe to improve recovery of a valuable mineral by a specific amount at constant grade or vice versa. Flotation optimisation may also take cost reduction approach were savings in consumables such as reagents are pursued. A method which has gained significant ground in the recent past is the application of modelling and simulation off-line and implementing findings on an operating plant. The simulation approach will usually entail carrying out a plant survey and laboratory experimentation to obtain data required for model fitting and then running simulation of many operating variations to obtain the best possible outcome (Chimwani, 2014; Hu, 2014; Naik and van Drunick, 2007; Compan et al., 2015).

In this section, the optimisation of milling and flotation operations are reviewed in terms of energy size reduction, throughput, energy utilisation and recovery.

2.7.1 Optimisation of classical SABC circuits

The comminution circuit usually comprises of the crushing and grinding circuits. Run-of-mine ore is delivered to the crushing circuit where it undergoes two stage crushing; primary and secondary crushing in gyratory and cone crushers respectively prior to being delivered to the fine ore stockpile as shown in Figure 2.9. The grinding circuit can be configured with primary and secondary grinding stages and crushing a setup commonly referred to as SAG mill, ball mill, crusher – SABC circuit. SAG mill pebbles are recycled to the primary mill after crushing by the pebble crusher. A comminution circuit comprising a crusher circuit and a classic SABC design is shown in Figure 2.9.

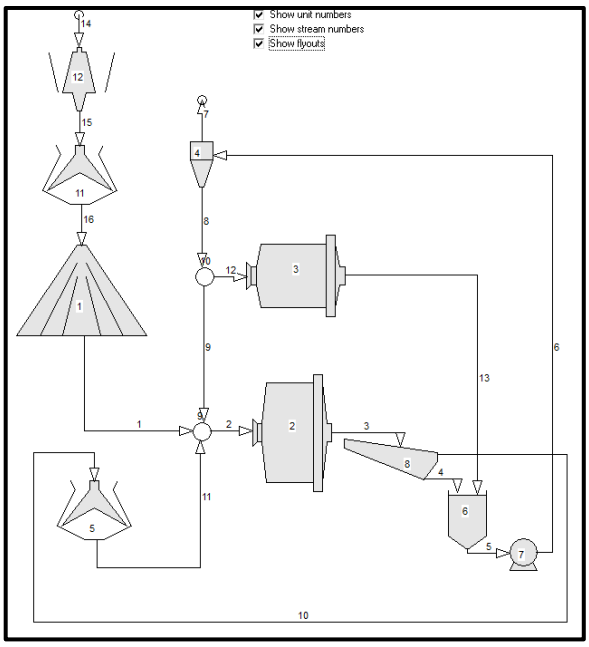

Figure 2.9 Classic design of a Semi-Autogenous mill, Ball mill, and Crusher circuit also known as SABC design

Napier-Munn et al. (1996) summarised steps involved in optimisation of a comminution circuit as comprising selection of the optimisation criteria, surveying the circuit to obtain equipment and operating data as well as current performance and mass balancing data to ascertain the quality of data. Other steps are fitting the data to a mode and running simulations for various scenarios to determine a combination of parameters which would generate optimum performance. Finally,

the optimised results are implemented on the plant. Figure 2.10 depicts a summary of optimisation steps as outlined above.

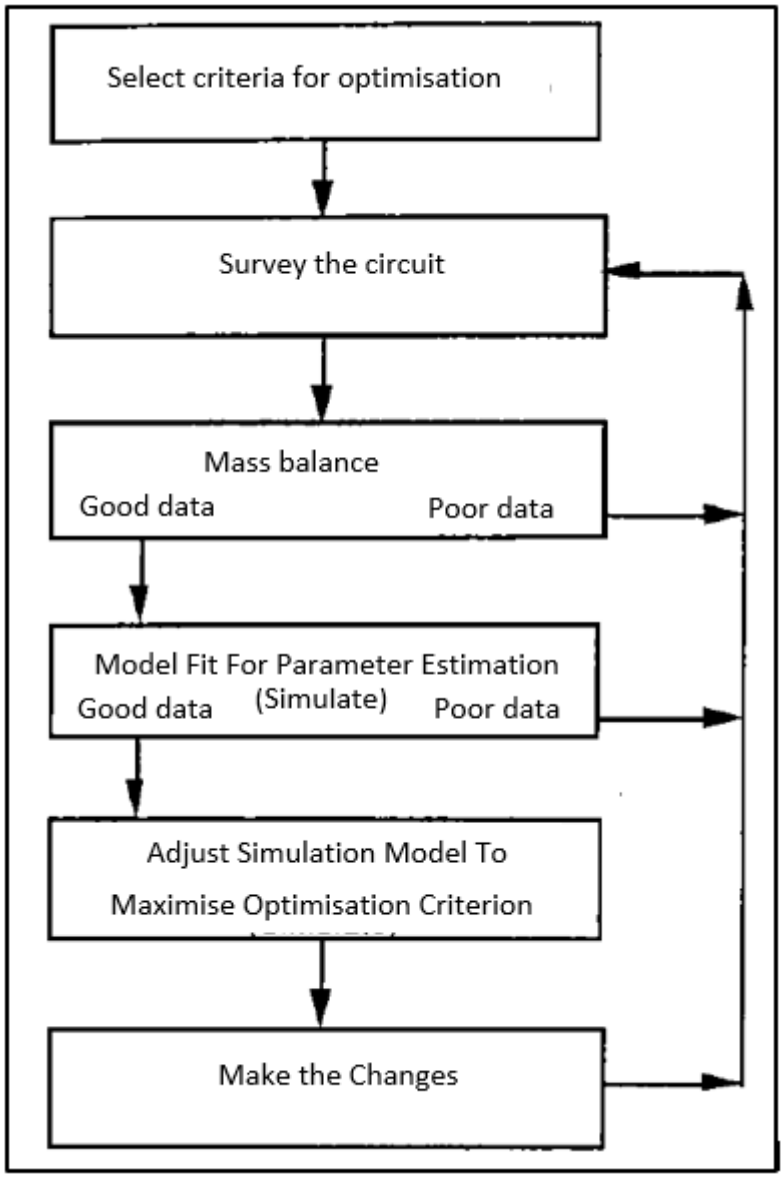

Figure 2.10 Generic methodology for the optimisation of comminution circuits (after Napier-Munn et al., 1996)

Optimisation of the comminution circuit may be achieved through reduction of transfer point between comminution equipment. This would entail reduction of the size that successive comminution units pass on to the next unit. This reduction

in feed size can translate into increased throughput as was demonstrated by Narayanan et al. (1987).

The optimisation criteria referred to in the section above may focus on maximising throughput while maintaining the currently product particle size distribution, changing the product size distribution while maintaining the current throughput. It may also take the form of minimising operating cost while maintaining the current throughput and product size distribution. Having determined the optimisation criteria, the strategy shifts to identifying where weaknesses reside in the process and the approach to resolve the weaknesses. In an instance where the objective is to increase the quantity of material amenable to flotation in final comminution product, the approach may be to operate at the optimum performance of individual units in the SABC circuit. On the SAG mills, circuit consideration maybe given to the current operating power draw, ball size and filling level, slurry concentration and filling as well as mill rotational speed. These factors must be evaluated against design parameters to identify were improvement opportunities exist. Computer simulations can then be employed to located optimum combination of parameters that will guarantee the SAG mill as well as circuit optimum performance. Additionally, the aperture size of the SAG mill discharge screen must be simulated to identify a size that can attain efficient utilisation of the pebble recycle crusher and transfer an appropriate size to the ball mill circuit for optimal performance. The performance of the pebble recycle crusher can be evaluated in terms of utilisation (throughput), power draw, and product size. The optimisation in this case may come from adjusting the SAG discharge screen aperture size and the pebble crusher closed side setting. In the same vein the ball mill circuit feed size, ball size and filling, slurry concentration and filling as well as milling rotational speed can be evaluated against design parameters to identify were opportunities for improvement reside. Performance of hydrocyclone in terms of operating conditions and geometry can be evaluated. Computer simulations can be resorted to when identifying a combination of parameters which would guarantee optimal performance. Napier-Munn et al.

(2019) provides a good example of SABC circuit design were a survey conducted reviewed that the SAG mill was being operated at lower filling level, lower mill feed density and lower power draw compared to design. The discharge classifier also exhibited a coarser cut point. These deficiencies were addressed by increasing the SAG mill filling and closing the SAG circuit with a cluster of hydrocyclones. The increased SAG filling translated into increased power draw and as a consequence increased power for finer grinding. The hydrocyclone cluster resulted into increased flow through the mill and reduced cut size. The combined effect was reduction in the size of material transferred to the ball and increased flowrate to the ball mill. The benefits of reduced feed size on the ball mills circuit was reduced product size. The ball size in the ball mill was reduced because smaller balls are effective on grinding smaller particle sizes. On the ball mill circuit deficiencies identified included larger ball size, low mill feed density, high hydrocyclone feed density and larger hydrocyclone diameter. These deficiencies were addressed by reducing the ball size and ensuring that hydrocyclones were fed with a dilute slurry. The SAG and ball mill feed densities were increased. The hydrocyclone with a smaller diameter was installed to reduce the cut-size. The net effect was reduction of the circuit final product size. The optimisation of grinding circuits can also be linked to downstream operations like flotation. In this instance the objective becomes increasing the percentage of material in the size range amenable to flotation. To attain this objective, changes on the grinding circuit can be simulated under flotation circuit constraints to identify a combination of milling parameters which would produce optimal flotation recovery.

2.7.2 Optimisation of flotation circuits

Optimisation of flotation circuits seeks to locate the circuit configuration and operating conditions which can give the best circuit performance. When optimising the flotation circuits focus is on obtaining the best results for flotation

circuit key performance indicators such as concentrate grade and quality, recovery, throughput and reagent consumption.

Modelling and simulation are applied to identify the particle size range which can yield an optimum recovery in the flotation circuit. It has now become customary to model the flotation and milling circuits together so that the milling circuit is optimised under downstream constraints (Chimwani, 2014). Optimal flotation recovery requires valuable mineral particles in the flotation feed to be adequately liberated because under or over grinding will have a negative impact on flotation performance as alluded to earlier on. To this end, simulations are run with variations in operating parameters in the milling circuit to produce various particles size distributions in the feed to flotation. The particle size range which yields the best recovery is identified and the operation of the milling circuit tailored to give a product with the identified particle size distribution (Chimwani, 2014). This technique was successfully applied to determine conditions necessary to mill a platinum ore to a size distribution required for optimum flotation recovery (Chimwani, 2014).

2.7.3 Attainable region paradigm

The attainable region (AR) technique provides means of quickly identifying the most promising solution to the real problem. It is a data analysis technique used to determine all the possible outcomes from a process given the feed and product conditions and reaction kinetics (Glasser and Hildebrandt, 1997). The AR as a data analysis tool was developed for the analysis of chemical reactor systems but later extended to analysis of comminution systems because of similarities in the two processes. The similarities in chemical reactor systems and comminution which are requirements for the AR technique are the feed, products characteristics and reaction kinetics (Khumalo et al., 2006; Danha et al., 2015). The application of the AR technique involves identifying process fundamentals, choosing state variables, defining and drawing state vectors, constructing the region, interpreting the

boundary as the process and finally locating the optimum (Metzger et al., 2007). Chimwani (2014) successfully employed the attainable region technique to optimise the production of material in the milling circuit which guaranteed the best recovery in flotation. This was achieved by systematically varying ball mill operating parameters such as rotational speed, ball filling and size, slurry filling and concentration and then constructing AR plot. The combination of operating parameters yielding material in the desired range was identified from the AR plots. The strength of AR technique resides in its simplicity in the that the optimum can be read directly from graphs without long tedious calculation and can be applied to any process which can be broken in fundamental processes (Metzger et al., 2007). Additionally, once the universal attainable region is known applying a new objective function is effortless. An example of an AR plot is shown in Figure 2.11.

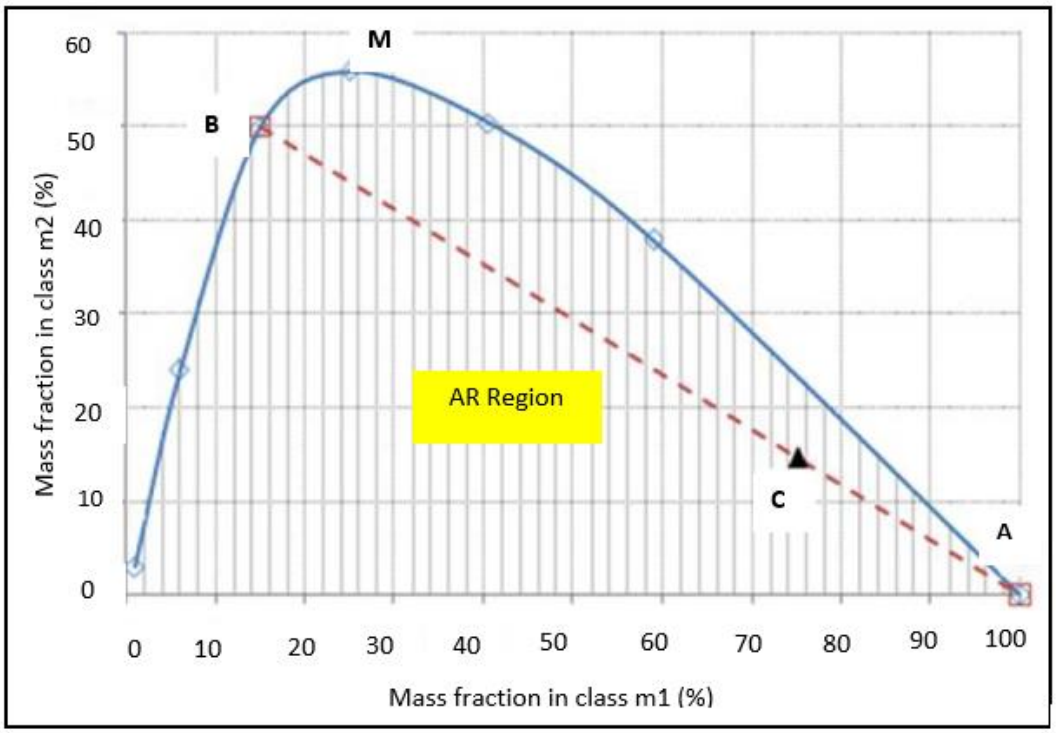

Figure 2.11 Principle of mixing in the AR space (Mulenga and Bwalya, 2015)

The attainable region technique can be employed for the optimisation of the milling and flotation circuit by interfacing the two circuits and generating data under varying conditions which can then be used to generate the AR path. On the

milling front the path required to break particles from the feed size distribution to the product size of interest is identified. Operating parameters responsible for generating the size distribution yielding optimum recovery in flotation are also identified and used to develop the comminution circuit operating procedure.

A third dimension is then added to the attainable region plot so that flotation recovery is monitored as a function of comminution desired product size distribution. Finally, interpretation of the three-dimensional attainable region path may help identify possible combinations of operating conditions for optimised operation of the milling-flotation circuit. It would be appropriate to state at this point that the AR technique is a versatile and powerful tool which can provide visual in-depth insights into the mineral processing data thus providing means for optimisation (Katubilwa, 2012). The limitation of the AR technique is that it can only be applied on the data that is available and does not provide means of trying what if scenarios.

2.7.4 Future outlook

The AR technique as a research and optimisation tool has matured over the last decade. Its simplicity and effectiveness make it a research and optimisation tool of choice. Unfortunately, it has not been fully exploited in the optimisation of mineral processing operations at industrial level. Operating plants have a lot a data in their historical databases which can be exploited through collaboration. This data must be analysed using the attainable region technique with a view to gain ground on its industrial application and buy in from industry. The focus going forward must be to realise the full potential of AR through its contribution to improved plant operations.

2.8 Summary

In this chapter theory, principles and models on crushing, milling, hydrocyclone, flotation, screening and classification were reviewed. Major equipment used in these circuits has been succinctly reviewed in terms of design, operations, modelling and optimisation. The influence that design mostly in terms geometry and operating parameters influence product output and how modelling and simulation can be applied to optimise the processes was reviewed. It was established that the population balance model has been used to describe the milling and flotation process. Optimisation strategies for milling and flotation processes were also reviewed. The attainable region as an analysis and optimisation technique was reviewed. Information is available in literature on the success of AR technique in the optimisation of comminution circuits within downstream constraints such as flotation. However, the technique still needs to find more application in industrial use.

Chapter 3 Laboratory testwork and plant survey programme

3.1 Introduction

The plant surveying campaign and the experimental methodology adopted are described in this chapter. The plant survey was conducted by sampling all key streams in the milling and rougher flotation circuits under steady state conditions. Streams sampled were the feeds and discharges of the SAG and ball mills as well as the feed, underflow and overflow around the hydrocylones. Other streams sampled were rougher flotation feed, rougher concentrate and rougher tailings. It must be noted that the samples consist of feed (input) and discharge (output) from processing unit for determining individual units and circuit performance. Data obtained from the samples included flotation recovery, concentrate grade, moisture content, slurry percent solids and particle size distribution. Batch flotation tests conducted were rates test to determine recoveries tenable at various flotation durations. The data obtained was used to calculate the flotation rate constants.

A plant survey was conducted to collect samples from the Kansanshi sulphide ore circuit. Samples collected on the comminution circuit were the feed and discharge streams of the SAG and ball mills as well as the feed, overflow and underflow around the hydrocyclones. On the rougher flotation circuit, the flotation feed, concentrate and tailings were collected. The wet SAG mill feed sample was weighed, dried and re-weighed to obtain the moisture content. The dried sample was sieved to obtain the particle size distribution. The hydrocyclone samples were weighed, filtered and re-weighed again to obtain the mass fraction of solids in the streams. The samples were later split to obtain representative samples for sieve analysis and construction of the partition curve. The data obtained from the comminution circuit was analysed to ascertain the performance of the individual units and the circuit as a whole with the view to identifying areas of inefficiency

and were capacity for additional material to be treated existed. The data was also used for calibration of comminution units in MODSIM® to mimic circuit behaviour. Data obtained from rougher flotation circuit survey was used to obtain flotation rates data for calibration of flotation units in MODSIM®.

The experimental information comprises of the nature of data collected, sampling points, sampling equipment and methods used. The sample sizes collected, sample processing and technical specifications of plant equipment are also presented. The laboratory and survey data collected was to be used for the estimation of model parameters in subsequent chapters.

3.2 Specifications of the Kansanshi sulphide ore circuit

Kansanshi mine concentrator receives ore from two open pits, namely the main pit and north - west pit. The ore is delivered from the pits to the concentrator run-of-mine pad in haul trucks. The copper in the ore deposit is hosted in a range of copper minerals which include chalcopyrite, secondary copper sulphides, native copper, cuprite, malachite, azurite and chrysocolla. The ore is classified into three distinct categories namely sulphide, mixed, and oxide ores because of the varying proportions of sulphide and oxide copper minerals contained in the ore. Three separate processing circuits comprising of dedicated comminution and flotation circuits are used to process each ore type. The research focused on the sulphide ore circuit. The feed grade to the sulphide ore circuit averaged 0.77 % TCu in 2017.

The run-of-mine sulphide ore undergoes primary crushing in a Metso 54-75 gyratory crusher with 450 kW available power and secondary crushing in a Nordberg MP800 cone crusher with 600 kW available power arranged in open circuit as shown in Figure 3.1. Secondary crusher product in delivered to the semi-autogenous mill ore stockpile. The material is then sent to a classic SABC circuit. Primary milling is conducted using a 9.75 x 6.1 m SAG mill with 12 MW installed power whereas secondary milling is accomplished in a 6.1 x 9.3 m ball mill with 5.8

MW installed power. The sulphide ore circuit primary and secondary grinding stages are serviced by a common discharge sump that supplies a nest of eight 840 mm diameter Krebs hydrocyclones. Pebbles from the SAG mill are crushed in a Terex Cedarapids MVP 450 short head cone crusher with 315 kW installed power and recycled to the primary mill. The hydrocyclone underflow constitutes the only feed to secondary grinding though a small portion of it is re-circulated to the SAG mill. Usually 5 % of hydrocyclone underflow is re-circulated to the SAG mill by means of a regulated pinch valve. The hydrocyclone underflow also provides feed to the heavy mineral pre-concentration employing Falcon and Knelson concentration units for gold recovery.

The hydrocyclone overflow is sent for froth flotation organised as follows: roughing in 6 x 300 m^3 cells, and cleaning in 8 x 30 m^3 cells and two Jameson cells.

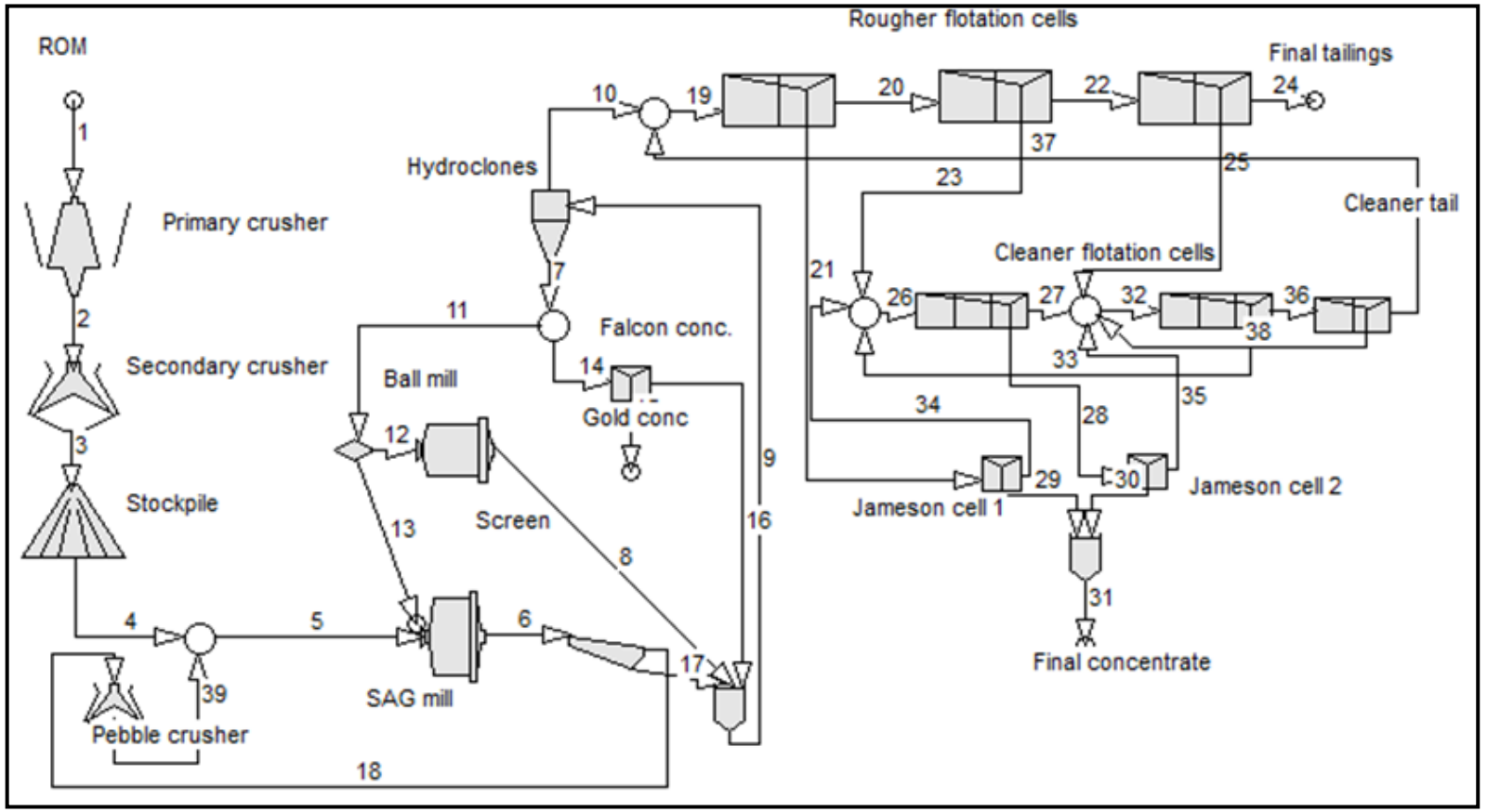

Figure 3.1 Kansanshi sulphide ore circuit

Equipment dimensions for the SAG and ball mills were obtained from previous work conducted on the sulphide ore comminution circuit and equipment datasheet (Bepswa et al., 2015; Faulkner and Mwansa, 2015; Flour Australia PTY Limited, 2006 – 2019). The dimensions obtained for the SAG and ball mills were diameter, centre line length, belly length, trunnion diameter and grate opening. Measurements of ball filling were obtained during the plant shutdown on May 7, 2018 a day after the survey. Hydrocyclones dimensions were obtained from a sulphide hydrocyclone which was being assembled for installation. Hydrocyclone dimensions obtained were cyclone diameter, vortex-spigot distance, inlet and spigot diameter. Rougher flotation cells volume was obtained from the manufacturer's datasheet (S2 Project). Crusher gap setting operating range and target were obtained from internal reports (Chansa, 2018). Power ratings for the crushers and mills were obtained from equipment nameplates (drive motors).

During the survey equipment specification for major units in milling and flotation collected is presented in Table 3.1 below.

Table 3.1 Specifications of the comminution and flotation equipment used in the sulphide ore circuit, Kansanshi

Pebble crusher	Terex Cedarapids MVP 450	
	Available power:	315 kW
	Closed side setting:	12 mm
SAG mill	Internal diameter:	9.75 m
	Internal belly length:	6.10 m
	Centre line length:	8.9 m
	Available power:	11.6 MW
	Grate discharge design	
	Speed (VSD):	75 % of critical
	Ball filling:	19 %
	Top-up ball size:	125 mm
Ball mill	Internal diameter:	6.10 m
	Internal belly length:	9.30 m
	Centre line length:	10.5 m
	Available power:	5.8 MW
	Overflow discharge design	
	Speed:	75 % of critical
	Ball filling:	28 %
	Top-up ball size:	60 mm
Flotation	Volume:	300 m^3
	Air hold-up (%):	15
Hydrocyclones	Number in the cluster:	8 (with 2 on standby)
	Cyclone diameter:	0.84 m
	Inlet diameter:	0.37 m
	Vortex finder diameter:	0.4 m
	Spigot diameter:	0.2 m
	Vortex-spigot distance:	2.09 m
	Pressure drop:	108 kPa
	Head of feed slurry:	31 m
	Slurry viscosity:	0.00014 Pa.s

The data in Table 3.1 was used for model fitting in MODSIM®. The data was collated through direct measurement, read off equipment nameplate and from previous work on the sulphide ore circuit.

3.3 Plant surveying campaign

A survey for the Kansanshi sulphide ore milling and flotation circuit was conducted at conditions as close to steady state as possible. Steady state conditions were assumed to have been attained once mass flow and stream characteristics remained approximately constant during the period of the survey (Napier-Munn et al., 1999). Prior to commencing the sampling exercise, the control room operator observed SCADA trends for SAG mill feed rate, SAG mill power draw, SAG mill weight, hydrocyclone feed pump amperage, feed pressure, flow rate and density, flotation feed flowrate and density. The SAG mill fresh feed set-point was held constant by de-activating the grinding control loop. The sampling team was notified that plant operations were stable when fluctuations in the aforementioned parameters were minimal for about 1 hour as observed on the SCADA trends in the control room. Streams sampled were the feeds and discharges of the SAG and ball mills as well as the feed, underflow and overflow around the hydrocylones. Other streams sampled were rougher flotation feed, rougher concentrate and rougher tailings.

All the samples were collected on May 6, 2018. Samples were collected by a team comprising seven people over duration of 1 hour. Sampling resources used in the campaign are shown in Table 3.2. The stream numbers indicated in Table 3.1 correspond to streams on the sulphide ore circuit flowsheet presented in Figure 3.1. Data from a previous survey on the sulphide ore circuit was consulted when selecting sampling and sieve analysis equipment for the survey (Bepswa et al., 2015; Faulkner and Mwansa, 2015).

It is important to obtain representative samples and data of high quality during plant surveys for modelling. The sampling campaign conducted on the Kansanshi mine comminution circuit was conducted in accordance with guiding principles and techniques proposed by Napier-Munn et al. (1999). The sample sizes, sampling points, sampling methods and sampling equipment employed in the survey conformed to guidelines provided by Napier-Munn et al. (1999). Sample cutters used were of the appropriate design in terms of shape, size and opening in order to eliminate bias due to not collecting coarse particles. In order to obtain an optimum sample cut of the stream flow, and a statistically adequate sample size, customized samplers were employed for some of the points in the circuit. The flotation circuit samples were collected from automatic samplers which were operated in manual mode. This enhanced the integrity of the samples collected on the flotation circuit. A series of 4 samples of every slurry stream was obtained over a 1-hour period, during which the comminution and flotation circuits were held as close as possible to steady state operation.

Members of the sampling team where trained on the sampling methods and a practice sampling session conducted on the actual streams which were to be sampled. The survey campaign involved clearly outlining the survey objectives, preparing survey scenarios, inspecting circuit and sampling points and mobilizing sufficient sampling resources and training the sampling team. This was meant to ensure that representative samples of streams were collected. The researcher coordinated the sampling campaign to ensure that correct sample quantities were collected at planned intervals for a predetermined period. Samples handling, filtration, drying, weighing, splitting and screening were assigned to competent metallurgical technicians who were closely supervised by the researcher to guarantee the quality of samples. On completion of the

Table 3.2 Sampling points and associated resources

Stream No.	Sample name	Sampling Point	Sampling equipment	Sample mass (kg)	People required
5	SAG mill feed	SAG mill feed conveyor belt	Drum, shovels, sampling bags, fork-lift	500 – 800	4
6	SAG mill discharge	Edge of SAG slurry discharge onto vibrating screen	Specially designed half-moon sample cutter, bucket	10 – 15	1
8	Ball mill discharge	Edge of ball mill launder at the discharge hopper	Specially designed half-moon sample cutter, bucket	10 – 15	
9	Cyclone feed	Built-in sampler at cyclone distributor	Poppet sampler, bucket	10 – 15	1
10	Cyclone overflow	Cyclone over-flow launder	Half-moon cutter, bucket	3 – 5	
12	Ball mill feed	Cyclone cluster underflow	Half-moon cutter, bucket	10 – 15	
10	Float feed	Rougher feed OSA	OSA sampler, bucket	3 – 5	1
20	Rougher tail	Rougher tail OSA	OSA sampler, bucket	3 – 5	
21	Rougher Conc.	Rougher con OSA	OSA sampler, bucket	3 – 5	

In Table 3.2, percent solids and sizing were collected as part of the laboratory analysis for streams 5 – 10. In contrast, head, sizing and assays were collected for streams 10 – 21. Furthermore, the solid concentration was also measured for stream 21.

All the samples were collected over 1-hour duration, i.e. between 08:00 and 09:00 a.m. on May 6, 2018. Four samples were cut from each slurry stream in 15 min increments. The conveyor belt sample was collected at once.

The sulphide ore circuit superintendent was notified that the sampling exercise would commence. The SAG mill feed was collected last after confirmation that all the other samples had been collected, because stopping the SAG mill feed conveyor first would have caused upsets to the milling and flotation circuits. The flotation feed, rougher concentrate and tailings samples were collected from the On Stream Analyser (OSA) multiplexer sampler shown in Figure 3.2.

Figure 3.2 On-stream analyser multiplexer sampler

The sample buckets were put into positions and the OSA sample hose inserted into the bucket as depicted on the left picture of Figure 3.1. On the control panel the sampling mode was switched from automatic to manual sampling for the sampler to be operated manually. The sampling knob on the control panel was switched to “cut sample” and held in that position until the sample bucket was filled to a pre-marked level for each sampling cycle (repeated 4 times after 15 min). One person was assigned to collect the flotation feed, rougher concentrate and tailings samples. The hydrocyclone feed sample was collected on the hydrocyclone distributor poppet sampler shown in Figure 3.3.

Figure 3.3 Hydrocyclone distributor poppet sampler

The sample bucket was put into position and the poppet sampler hose inserted into the bucket as depicted on the left picture of Figure 3.3. On the control panel the sampler was switched on and the sampling button pressed and held in that position until the sample bucket was filled to a pre-marked level for each sampling cycle (repeated 4 times after 15 min). The hydrocyclone overflow sample collected from the hydrocyclone overflow combined launder using a half moon sampler. Four scoops were collected to fill the sample bucket at 15 min interval.

The hydrocyclone underflow sample which constitutes the ball mill feed was collected from the hydrocyclone cluster underflow launder using a half moon sample cutter. Four scoops were collected to fill the sample bucket at 15 min interval. The ball mill discharge sample was collected by cutting 4 scoops using a half moon sample cutter at the edge of the launder were the slurry discharges into the combined SAG and ball mill discharge sump at 15 min interval. The SAG mill discharge sample was obtained at the discharge end where the SAG mill discharges slurry on the vibrating screen. Four samples were obtained at a 15 min interval using a half moon sample cutter. It must be noted that the SAG mill has now been fitted with a trommel screen.

The SAG mill feed sample which was supposed to be collected should have been between 500 kg and 800 kg (Napier-Munn et al., 1999). Under the prevailing circumstances, collecting and processing this sample size was not feasible due to

lack of manpower and equipment such as front-end loader. In the compromise method the sample was cut over 2-m belt length from the conveyor belt. The samples are shown in Figure 3.4.

Figure 3.4 A belt cut sample of the SAG mill feed

It must be noted that all applicable site safety precaution such as isolation, lockout and tagging and wearing a safety harness were adhered to. The belt sample was collected from a 2-m length.

3.4 Sample preparation

The SAG mill feed sample was weighed on a 500 kg platform balance and dried in the oven at 110°C, overnight. Then, the dry sample was re-weighed to obtain the moisture content in the sample. The sample is shown in Figure 3.5.

The whole sample obtained from the belt-cut was subjected to sieve analysis.

Figure 3.5 Dry sample of the SAG mill feed

The SAG mill and ball mill discharges, ball mill feed, cyclone feed, underflow and overflow and rougher flotation feed, concentrate and tailing were weighed wet and pressure filtered. The wet samples were dried at 110°C in an oven overnight and the dry sample re-weighed to obtain moisture content.

3.5 Particle size analysis

A complete size analysis for the dry samples was carried out. The SAG mill feed was first sized on a 450 mm screen deck using $\sqrt{2}$ series of sieves from 125 mm down to 3.5 mm. The screens were arranged as follows in mm: 125; 75; 53; 45; 31.5; 25; 19; 13.2; 11.2; 8; 6.7; 4.75; 3.5; and a pan at the bottom as shown in Figure 3.6.

Figure 3.6 Stack of screens spanning from 125 mm down to 3.5 mm

The big ore chunks were hand sized on 125, 75 and 53 mm screens. This portion of the sample accounted for approximately 40% of the total sample. Hand screening was done by removing larger rocks from the sample by hand, brushing off any fines into a bucket, and passing them along the row of screens. A rock was tested on the screen size below the final one it passed, so as to ensure it was in the correct size fraction. The remaining dry sample which was approximately 60% of the total sample was split into two equal parts A and B. Sample A was loaded on the first stack placed on the 450 mm diameter non-adjustable vibration amplitude sieve shaker and the screens strapped. Screen size 125, 75 and 53 mm were also included on the screen stacks. It must be noted that as the sample was being loaded the bulk of fine material sunk through the screens. The sample was screened for 15 min. Afterwards, the shaker was stopped and material on each sieve weighed to ascertain the mass retained. The samples were re-loaded on

screens, then restacked and operated for a further 5 min and the weight of material on each sieve weighed again. There was no change in the weights. Screening time was set at 15 min. The material retained on each screen was loaded in polyurethane sample plastics bags pre-marked with the screen size. The screening process was repeated for sample B. The material retained on each screen in the second run was combined with material from the corresponding screen from sample A. Samples from each screen size were weighed and recorded. The sink was split using a rotary sample splitter to obtain a 1000 g sample. The 1000 g sample obtained was wet screened on the 25 µm screen to remove fines which would cause blinding of the screens to be used in the second sieve analysis. The sample was dried in an oven at 110°C overnight. The 1000 g dry sample was sieved on the 320 x 380 x 850 mm diameter Wagtech electromagnetic sieve shaker shown in Figure 3.7 for 15 min and the sample retained on each sieve was weighed to ascertain the mass of material retained. The samples were re-loaded to the respective screens and screened for a further 5 min. Samples from each screen were re-weighed. There was no change in the screen samples weighed. Fifteen minutes was adopted as the sieving time. It is the standard time adopted for sieving a 1000 g sample at Kansanshi mine metallurgical laboratory. The shaker settings were set as follows: vibrating intensity H = 94, sieving time L = 12 min, on time F = 960 min and continuous sieving C = 1. Using ratios of weights of the total sink sample and 1000 g sample obtained from the rotary splitting the weights retained on each screen was back-calculated.

Figure 3.7 Stack of screens spanning from 2500 µm down to 25 µm

SAG and ball mill discharge as well as ball mill feed (also hydrocyclone underflow) dry samples were split on the rotary splitter and a 1000 g sample obtained. Hydrocyclone feed and overflow as well as the rougher concentrate and tailing dry samples were also split on the rotary splitter and a 1000 g sample obtained. The 1000 g of each sample was wet screened. The samples were dried in an oven at 110°C overnight. The 1000 g dry samples were sieved for 15 min and the samples retained on each sieve were weighed to ascertain the mass of material retained. Fifteen minutes sieving time was used for sieving a 1000 g sample on the 320 x 380 x 850 mm diameter sieve shaker as shown in Figure 3.7 above. The results from the sieve analysis were recorded.

Operational data was obtained from the supervisory control and data acquisition (SCADA) to be used for model validation. The data acquired from SCADA was SAG mill feed rate and power draw, ball mill power, hydrocyclone feed density, flowrate and pressure and flotation feed density and flowrate.

3.6 Challenges faced as part of the experimental work

As far as the laboratory work was concerned, the initial plan was to obtain a large sample of the SAG mill feed and conduct batch grinding and flotation testing. Batch grinding testing was not done because Kansanshi metallurgical laboratory does not have a batch ball mill. Employing the available rod mill using worn out steel balls from the plant mills was not consented to. It was also intended to collect small samples along the sulphide ore circuit under various operating conditions. These samples were to be analysed in order to model the response of the circuit with feed flowrate. This was not done because management did not consent to altering operating conditions during the survey. It was also desired to crash stop the mills to obtain the slurry filling and later grind out the mills to obtain the ball filling. Permission to crash stop the mills was equally not granted. According to Napier-Munn et al., (1999), the sample to be collected from the SAG mill feed under the circumstances was supposed to be between 500 and 800 tons. Collecting and processing a sample of this size required a front-end loader and 6 people. These resources were not available, hence a compromise made were a sample was collected over a 2-m conveyor belt length. Obtaining samples for the SAG discharge was challenging for two reasons; firstly, access to the sampling point was difficult, hence a cutter with a long handle was fabricated. Secondly slurry discharging from the SAG mill was at a very high velocity. This required a special sample cutter proposed by Napier-Munn et al. (1999) to be fabricated. Resources to fabricate the special sample cutter were not available. Lack of sufficient personnel to sample all the key streams in the milling and flotation circuits was also a challenge. The initial plan was to assemble a sampling team

comprising twelve people, but only seven were available. The SAG mill discharge pebble crusher feed and product as well as the rougher flotation scavengers 1 and 2, cleaner flotation circuit as well as the Jameson cells were not sampled due to the lack of manpower. Sieving samples was to be done using $\sqrt{2}$ screen sequence. However, above 850 µm, screens in the $\sqrt{2}$ screen sequence were not available, hence the $\sqrt{2}$ sequence was not adhered to above 850 µm. Dimensions for hydrocyclones were obtained from a hydrocyclone which was being constructed for installation on the sulphide mills hydrocyclone cluster which was identical to the operating hydrocyclones. It must be noted that hydrocyclone components wear off during operation; hence, minor differences would exist between a hydrocyclone in operation and a new one. It was not feasible to obtain dimensions from an operating hydrocyclone.

The shortcoming for not adhering to the minimum sample for the SAG mill feed and non-adherence to $\sqrt{2}$ screen sequence above 850µm may be the reason for lack of smoothness in the SAG mill particle size distribution curve above 1000µm. The same trend was noted on the ball mill feed and product particle size distribution curve above 1000µm. Parameters for impact, abrasion and attrition breakage used for the SAG mill model in MODSIM were obtained from previous work on the sulphide milling circuit on a similar ore (Bepswa et al., 2015). The ore properties are expected to change as mining progresses, hence it must be expected that the properties used are not a true reflection of what was obtaining on the ground at the time of the survey. When curve fitting the data on the SAG and ball mills to determine parameter for breakage and selection functions parameters the researcher ensured that the best possible much between survey and MODSIM generated curves was attained to improve the confidence in the

values obtained. The difference between the new and actual hydrocyclone dimensions may have contributed to the differences between the survey and simulated hydrocyclone feed, underflow and overflow particle size distribution. The pebble crusher was not surveyed due to lack of resources and as such no particle size distribution was available for calibration and comparison. Failure to survey the entire flotation circuit meant that only the rougher flotation circuit was investigated and not the overall flotation circuit recovery. Parameter for the flotation rate constant were obtained by adjusting the values parameters in MODSIM® until the MODSIM® predicted values for concentrate grade and recovery were very close to survey values. Modeling the sulphide circuit response with feed flow-rate could have enabled the researcher to fine tune the MODSIM calibration as the this could have been done at several operating conditions thus improving the confidence of the MODSIM response to the Kansanshi sulphide ore circuit.

Chapter 4 Reconciliation of surveyed industrial data

4.1 Introduction

This chapter presents comminution and flotation circuits performance data obtained during the survey. The influence of design and operating parameters on mills, crushers and flotation on the performance is also presented. These parameters include rotational speed, ball filling, powder filling, slurry density and ball size distribution (Yekeler, 2007). The total filling and the ore filling are applicable to SAG and AG mills respectively.

The performance data was analysed to get the performance of the plant at the time of the survey included hydrocyclone particle size distribution, Tromp or partition curve as well as the ball and SAG mills feed and discharge particle size distribution.

4.2 Particle size distributions

Samples collected from hydrocyclones were used for particle size analysis. The particle size distribution for the hydrocyclone feed, overflow and underflow are presented in Figure 4.1.

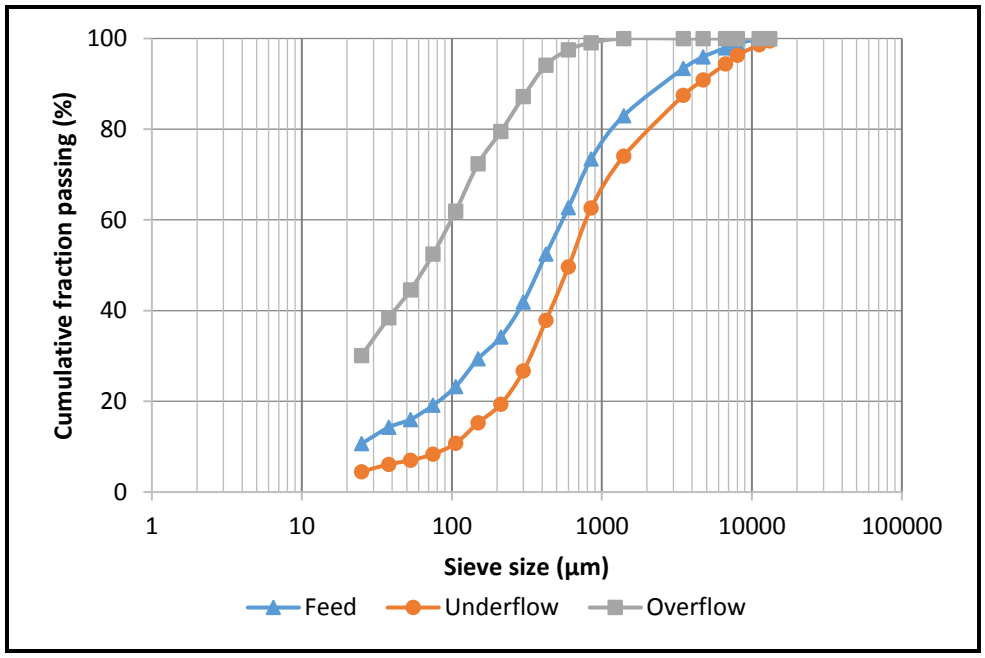

Figure 4.1 Particle size distributions of the feed, overflow and underflow of the nest of hydrocylones

The hydrocyclone efficiency is represented by a *performance* or *partition* curve also known as tromp curve shown in Figure 4.2. It relates the weight fraction, or percentage, of each particle size in the feed which reports to the underflow, to the particle size. The *cut-size* of the hydrocyclone which is the size for which 50% of the particles in the feed report to the underflow can be obtained from the tromp curve. When constructing the tromp curve, firstly the dilution factors in the feed, overflow and underflow were determined. The data used for obtaining the dilution factors as well as dilution factors are presented in Table 4.1. The tromp curve for the hydrocyclone was constructed using an electronic spreadsheet as shown in Table 4.2. Columns 1 and 2 represents the screen size and geometric mean of screen sizes respectively, columns 3 and 4 represent the screen analyses of the overflow and underflow, and columns 5 and 6 relate these results to the feed material. For example, column 5, is prepared by multiplying the results of column 3 by 0.75 the mass yield to the underflow; adding column 5 to column 6 produces gives column 7 which is the reconstituted size analysis of the feed material. Column 8 is determined by dividing each weight in column 5 by the corresponding

weight in column 7. Plotting column 8 against column 2, the arithmetic mean of the sieve size ranges, produces the partition curve. Column 9 represents the corrected partition curve.

Table 4.1 Performance data of the cluster of hydrocyclones

	Feed	Underflow	Overflow
Wet weight	4.69	11.06	3.13
Dry weight	3.06	9.07	1.26
Solid concentration (%)	65.20	82.01	40.30
Water split	34.80	17.99	59.70
Dilution factor	0.53	0.22	1.48
Mass yield	-	0.75	0.25

Table 4.2 Computation of the Tromp curve data

Sieve size (µm)	Geometricmean size,µm	Wt%		Wt % of feed		Reconstituted Feed	% of feed to u/f	Corrected Partition no.
		U/F	O/F	U/F	O/F			
18668								
13200	15697.5	0.52	0.00	0.39	0.00	0.39	100.00	100.00
11200	12158.9	0.87	0.00	0.65	0.00	0.65	100.00	100.00
8000	9465.7	2.29	0.00	1.72	0.00	1.72	100.00	100.00
6700	7321.2	1.94	0.00	1.46	0.00	1.46	100.00	100.00
4750	5641.4	3.50	0.00	2.63	0.00	2.63	100.00	100.00
3500	4077.4	3.42	0.00	2.57	0.00	2.57	100.00	100.00
1400	2213.6	13.40	0.00	10.06	0.00	10.06	100.00	100.00
850	1090.9	11.41	0.94	8.57	0.24	8.80	97.33	96.14
600	714.1	12.98	1.55	9.74	0.39	10.13	96.20	94.50
425	505.0	11.81	3.35	8.87	0.84	9.70	91.39	87.55
300	357.1	11.18	6.95	8.40	1.73	10.13	82.92	75.29
212	252.2	7.30	7.73	5.48	1.93	7.41	74.02	62.42
150	178.3	4.12	7.07	3.09	1.76	4.85	63.73	47.53
106	126.1	4.50	10.48	3.38	2.61	5.99	56.44	36.99
75	89.2	2.41	9.46	1.81	2.36	4.17	43.50	18.27
53	63.0	1.36	7.93	1.02	1.98	3.00	34.13	4.72
38	44.9	0.87	6.14	0.66	1.53	2.19	30.02	-1.23
25	30.8	1.61	8.29	1.21	2.07	3.28	37.00	8.86
1	5.00	4.50	30.11	3.38	7.50	10.88	31.08	0.30

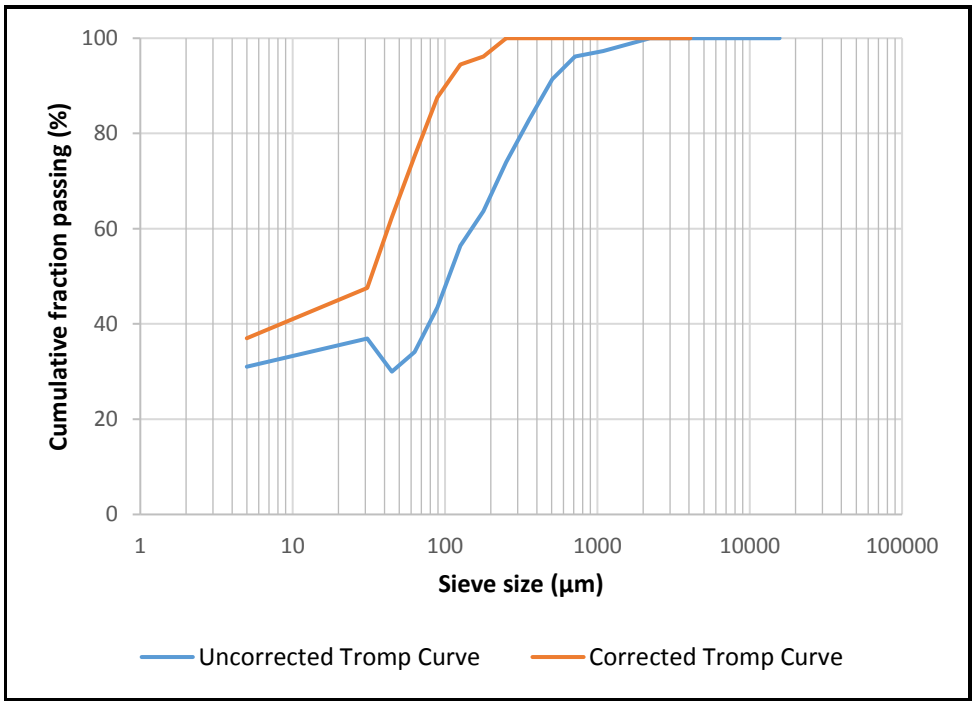

Figure 4.2 Tromp curves of the nest of hydrocyclones

During the survey, samples for the feed and discharge of the SAG and ball mills were obtained for evaluating the current performance of the two units. The 80 % passing size of the feed and product as well as the reduction ratios for the ball and SAG mills can be obtained from the graphs in Figures 4.3 and 4.4 respectively. The narrower the gap between the feed and discharge the lower the reduction ratios and vice versa.

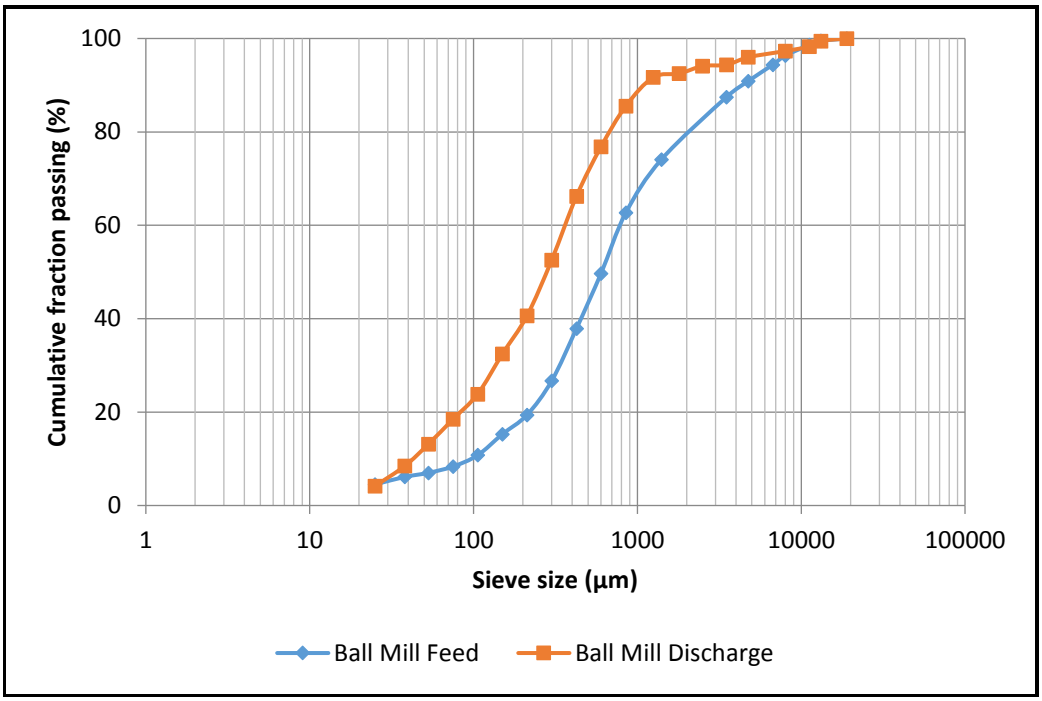

Figure 4.3 Particle size distributions of the feed and discharge of the ball mill

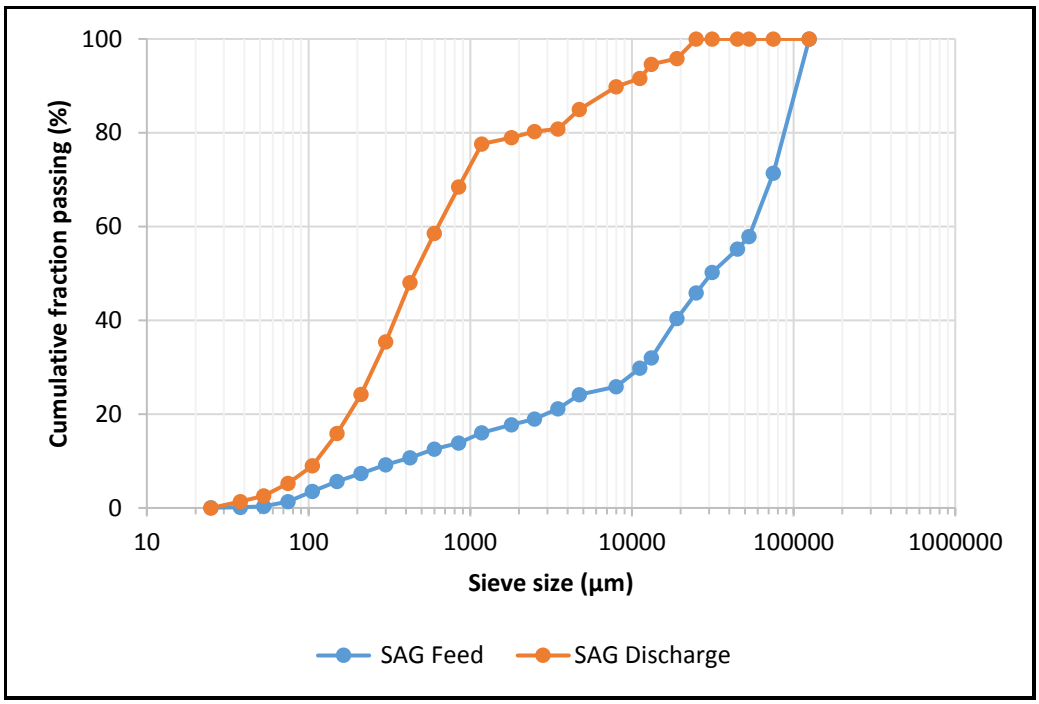

Figure 4.4 Particle size distributions of the feed and discharge of the SAG mill

The next section presents the mass balance of the data obtained from the survey to evaluate its quality. An analysis of the data is performed to ascertain the performance of the SAG and ball mill, hydrocyclone and pebble crusher.

4.3 Mass balancing and data reconciliation

The survey data was mass balanced to confirm their quality and also to infer any stream that could not be measured. For the comminution circuit, flow rates for the SAG mill and feed and overflow of the hydrocyclone could be measured. Flow rates for the hydrocyclone underflow and ball mill discharge streams were determined through mass balance. Table 4.3 gives a summary of key stream tonnages and 80% passing sizes of the feeds and products of the SAG mill and ball mill as well as the hydrocyclone overflow.

Table 4.3 Operational and mass balanced streams around Kansanshi milling circuit (tonnage rates on dry basis)

	Stream/Unit name	**Survey**
SAG Mill	Feed	1 740 tph
	F80	90 mm
	T80	2 360 µm
	Power	11.50 MW
	Recycle pebbles	190 tph
	Discharge pulp density	81.60 % solids
Ball Mill	Discharge (t/h)	-
	Discharge pulp density	78.29 % solids
	F80	2 330 µm
	P80	692 µm
	Power	5.1 MW
	%<150 µm in discharge	24
Hydrocyclone	Feed	7 655 tph
	Feed pulp density	68.50 % solids
	Overflow	1 233 tph
	Overflow pulp density	40.89 % solids
	Underflow	6 419 tph
	Underflow pulp density	82.01 % solids
	Overflow P80	217 µm
	Circulating load, CL	520 %
	Feed pressure	126 kPa
Flotation	Feed	0.78 % TCu
	Concentrate grade	10.90 % TCu
	Tailing	0.17 % TCu
	Recovery	79.44 %

SAG mill feed rate at 1740 tph was 29 % above the design capacity of 1350 tph. This could be attributed to the smaller feed size at 90mm against design of 112 mm as shown in Table 4.4. The higher throughput compared to design could be translating into reduced residence time leading to a low reduction ratio. The gap between the SAG mill feed and discharge particle size distribution as shown in Figure 4.4 is not wide enough indicating low size distribution. The specific input energy at 6.6 kWh/t against design specific energy of 9.2 kWh/t (see Table 4.4) could be indicative of a softer ore being treated which would also be a reason for the higher throughput. When higher energy input is applied, the mill product is finer and vice versa. The product transfer size of transfer size (T80) at 2.36 was higher than design of 1.2 to 2.0. Softer ores are usually broken by impacts of grinding media thus yielding a coarser product while hard ore are broken by attrition and abrasion giving a finer product. Mill power draw at 11.5 MW against available power of 12 MW as shown in Table 4.4 is indicative of capacity still not being utilised which can be exploited. The low power draw compared to design could provide an opportunity for addition steel balls to be added. The ball filling at 16 % against the design ball charge of 12 % to 18 % still provides an opportunity for additional steel balls to be added.

Table 4.4 Performance indicators of the SAG mill and pebble crusher

Parameter	**Survey value**	**Design**
SAG mill feed rate (t/h)	1 740	1 350
SAG mill feed, F80 (mm)	90	112
Transfer size, T80(mm)	2.36	1.2 – 2.0
Reduction ratio	38	
Ball charge (%)	16	12 – 18
Power (MW)	11.5	12
Input specific energy (kWh/t)	6.61	9.2
Pebble crusher feed (tph)	190	325

4.4 Performance of the recycle pebble crusher

The pebble crusher was not surveyed due to lack of resources as pointed out earlier. The feed rate to the pebble crusher at 190 tph as shown in Table 4.4 above against design feed rate 375 tph indicated that there was capacity which can be exploited here.

4.5 Performance of the ball mill

The fraction of particles less than 150 µm the product target size for Kansanshi milling circuit in the ball mill product is considered as an indicator for the efficiency of the grinding stage. This size fraction was only 24 % in the ball mill discharge as shown in Table 4.5 signifying poor performance.

Table 4.5 Performance indicators of the ball mill

Parameter	**Survey value**	**Design**
Ball mill feed, F80 (µm)	2 330	
Ball mill discharge, P80 (µm)	692	
Ball mill reduction	3.4	
% < 150µm in the product	24	
Ball load, J (%)	28	25 – 33
Circulating load (%)	520	200

This poor performance might be caused by a coarse SAG mill transfer size, poor hydrocyclone performance and high circulating load. The gap between the ball mill feed and product as shown in Figure 4.3 is very narrow indicting very low size reduction ratio. The ball mill operating power was at 5.1 MW against the design of 5.8 MW implying that there is still capacity for more steel balls. The steel ball filling was at 28 % within the design range of 25 – 33% provides additional capacity for steel balls addition (Flour Australia PTY Limited, 2006 – 2017). Low power draw could be another cause of low size reduction ratio. When higher energy input is applied, the mill product is finer and vice versa.

4.6 Performance of the nest of hydrocyclones

Survey data for the Kansanshi sulphide ore milling hydrocyclone cluster is presented in Tables 4.6 and 4.7 below.

Table 4.6 Efficiency indicators for the cluster of hydrocyclones

Feed density	68
Overflow 80% percent (µm)	217
By-pass fraction B_{pf} (%)	30
Cut-size d50 (µm)	190
Imperfection (I)	0.66
Sharpness index (SI)	0.29

Where

Bypass fraction B_{pf}

$$B_{pf} = \frac{\text{Mass yield in Underflow} \times \text{Dilution to Underflow}}{100 - \text{Dilution in feed}} \quad \textbf{(4.1)}$$

Imperfection $I = \frac{d_{75} - d_{25}}{2 \times d_{50}}$ **(4.2)**

Sharpness Index $SI = \frac{d_{25}}{d_{75}}$ **(4.3)**

The selection of cut size for hydrocyclones can be done using criteria proposed by Metso minerals (2010). The cut-size can be determined by multiplying target 80% passing overflow size by the corresponding factor presented in Table 4.7. This criterion was used to determine the expected cut-size on the hydrocyclones investigated.

Table 4.7 Factors for conversion of fraction passing in the overflow to the short-circuiting T_X (Metso Minerals, 2010)

Fraction passing in overflow (%)	Factor
99	0.49
95	0.65
90	0.79
80	1.06
70	1.36
60	1.77
50	2.34

The criteria in Table 4.8 were used to evaluate the efficiency of the hydrocyclones in terms of imperfection.

Table 4.8 Categorisation of hydrocyclone efficiency based on imperfection I (Murthy and Basavaraj, 2012)

Imperfection I	Separator category
I< 0.2	Excellent separator
0.2 <I< 0.3	Very good separator
0.3 <I< 0.4	Medium separator
0.4 <I< 0.6	Poor separator
I> 0.6	Bad separator

The criteria in Table 4.9 were used to evaluate the efficiency of the hydrocyclones in terms of water recovered to the underflow.

Table 4.9 General guide to evaluating hydrocyclone by-pass to underflow B_{pf} on performance (Napier-Munn et al., 1996)

Water fraction to underflow (%)	**Efficiency**
> 50	Very poor
40 – 50	Poor
30 – 40	Reasonable
20 – 30	Good
10 – 20	Subject to underflow density and roping
< 10	Achievable only with underflow valve

The 80% passing value of the hydrocyclone overflow at 217 µm against the target feed size for the flotation circuit 80 % passing 150 µm was very coarse for good flotation performance. Recovery-by-size assays reviewed that the major copper loses to the tailing are in -38 µm and +150 µm. The copper loses in the sub 38 µm accounted for 27 % while for +150 µm particles, it was 46 % as shown in Figure A.1 in the Appendices. It is important to note that the hydrocyclone overflow had 38 % of the material in the sub 38 µm and 28 % +150 µm as can be deduced from Table A.1 in the Appendices. It would be necessary to operate the mills in a manner that optimises the production of middlings in -150 +38 µm fraction. The hydrocyclone imperfection I was 0.66 which can be categorised as very poor performance according to the criteria proposed by Murthy and Basavaraj (2012), Table 4.8. The sharpness index SI was found to be 0.29 as shown in Table 4.6 which also signifies poor performance. The closer the SI values to unity the better the performance while the close the value to zero the poorer the performance (Gupta and Yan, 2016). The cut-size d50 obtained was 190 µm. This is very poor

considering that the target size obtained by multiplying the target 80% passing overflow size by an appropriate factor recommended by Metso Minerals (2010) in Table 4.7 is 159 µm. The by-pass to underflow B_{pf} at 30 % is good going by the evaluation criteria proposed by Napier-Munn et al. (1996) shown in Table 4.7.

4.7 Summary

The analysis of data from the survey indicated that the SAG mill performance was inefficiency as the transfer at 2.36 mm was above design of 1.2 mm to 2.0 mm and the reduction ratio was low as evidenced by the narrow gap between the feed and discharge curves on the particle size distribution in Figure 4.4. The pebble crusher was underutilised as the pebbles generated at 190 tph was almost half the design capacity of the pebble crusher at 375 tph. The ball mill discharge contained only 24 % of material in the desired size internal signifying poor performance. The hydrocyclone performance was poor as the cut-size was way above design. The cut-size at 190 µm for the hydrocyclone was also way above the target of 159 µm. Generally, the milling circuit performance was poor.

Chapter 5 Model building of the Kansanshi sulphide ore circuit

5.1 Introduction

Modelling and simulation have gained significant ground in the recent past in design, performance evaluation and optimisation of processes. A host of commercial software packages are available for achieving the aforementioned objectives. For this research, MODSIM® was selected for simulation and optimisation of the Kansanshi sulphide ore comminution and rougher flotation circuits. This chapter provides details of data obtained from survey of the Kansanshi sulphide ore circuit and laboratory batch flotation testing. Additionally, details of MODSIM® models for the units simulated are presented. MODSIM® is a modular simulator software that is used to simulate ore dressing plants. It calculates detailed mass balances for ore dressing plants. The mass balances calculated includes total flowrates of water and solids, the particle size distribution of the solid phase, the distribution of particle composition and the average assay of the solid phase (King, 2012). The assays calculated include mineralogical composition, metal content and element content. The main unit operations of ore dressing plants found in MODSIM® include the size-reduction operations such as crushing and grinding, classification operations for separation of particles on the basis of size, concentration operations that separate particles according to their mineralogical composition and solid liquid separations. MODSIM® generates comprehensive reports for the performance of each unit in the plant. The academic version 3.6 of the software was used in this research.

5.2 Creating the project in MODSIM®

Simulation with MODSIM® can be done on a single unit, circuit or the entire plant. When simulating a circuit or plant the process flowsheet replicating the actual is drawn, the systems data specified, and appropriate model selected for the units

incorporated in the simulations. The system data describe the characteristics and quantities of the ore that is processed in the unit or flowsheet. The characteristics of the ore remain fixed throughout its sojourn in the unit or flowsheet. The models are then calibrated to mimic the performance of the actual operating units before running simulation and analysing data. The flowsheet for the Kansanshi sulphide ore milling and rougher flotation circuit drawn in MODSIM® is shown in Figure 5.1. Examples of a system and model data input form used for the Kansanshi mine sulphide ore grinding circuit simulation are shown in Figures 5.2 and 5.3 respectively.

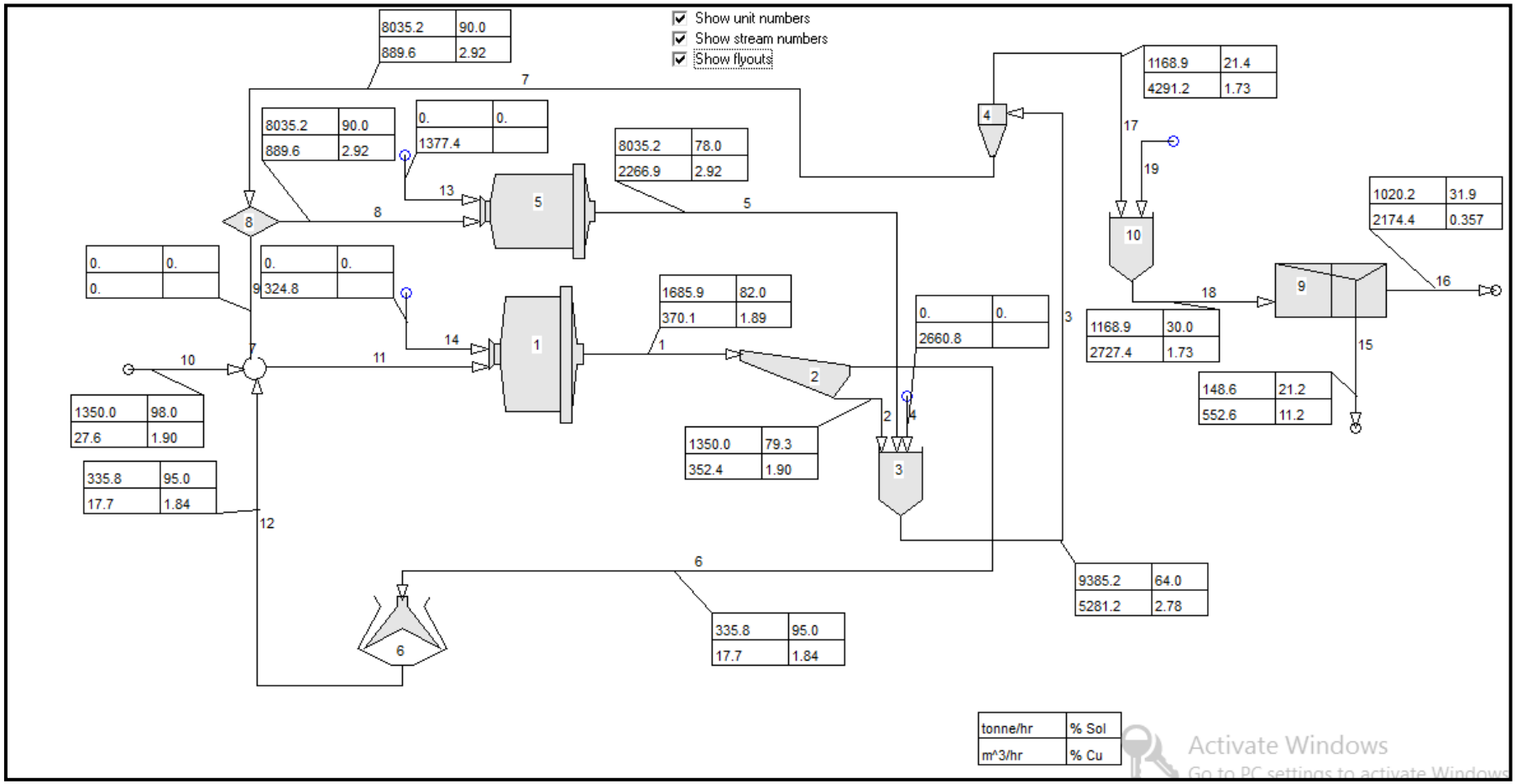

Figure 5.1 Flowsheet of the Kansanshi sulphide ore milling and flotation circuits in MODSIM®

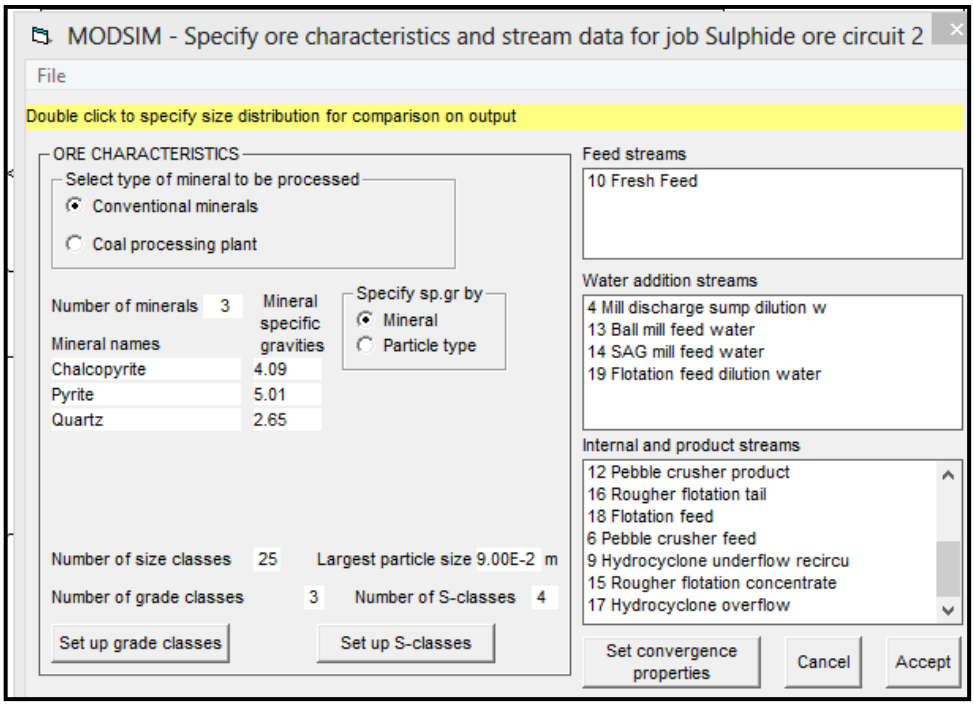

Figure 5.2 MODSIM® systems data entry form with data for Kansanshi milling circuit

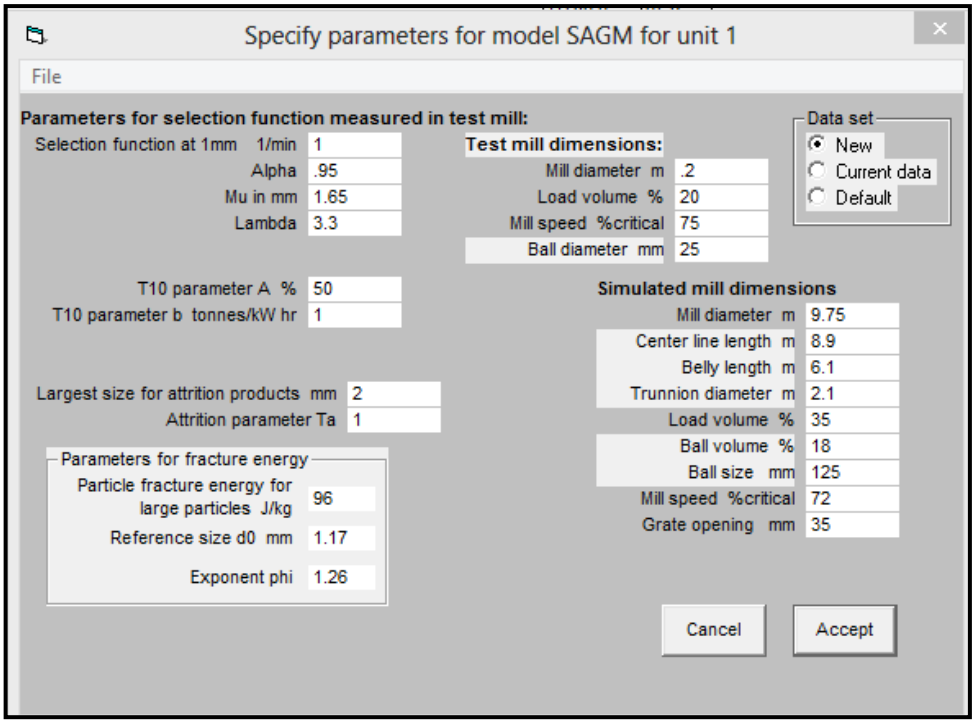

Figure 5.3 MODSIM® model data specification form with SAG mill data

As a starting point for simulating the performance of an existing operation, a reference case or benchmark performance must be established. The data

obtained for the feed stream feed rate and particle size distribution during the plant survey are assumed correct. As an example, the Kansanshi mine milling circuit feed stream data which were used as input to MODSIM® are shown in Figure 5.4.

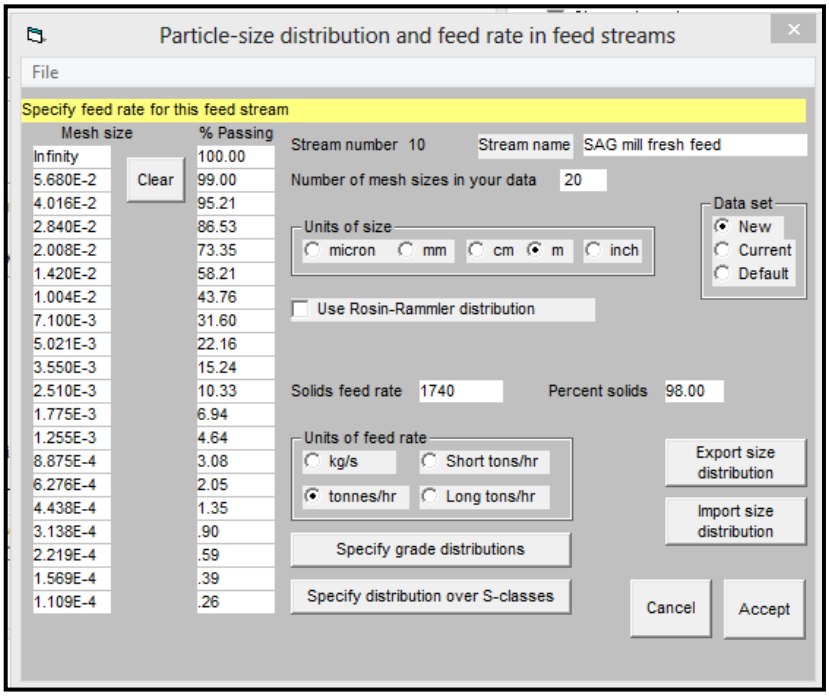

Figure 5.4 Particle size distribution and flowrate of the feed

MODSIM® is structured around a library containing several modules containing a variety of unit operations. Each unit has several models to select from guided by the data available and model appraisal. The models selected for the units incorporated in the simulations are presented below.

5.3 Semi-autogenous milling unit

The model selected in MODSIM® for modelling SAG mill was SAGM; Semi-autogenous mill modelled using the full population balance including particle attrition and wear as shown in Equation (2.33). The model assumes the mill to be perfectly mixed with post classification at the grates. The model was selected because it supports the Kansanshi sulphide ore circuit SAG mill design. The impact

fracture in this model is modelled using the standard Austin breakage and selection functions. The rate of self-breakage is modelled using the variation of particle fracture energy and the consequent breakage probability with size. The average kinetic energy on impact is determined assuming the lumps fall a fraction of the mill diameter. The load in the mill is calculated from the mill dimensions and the average residence time calculated as the ratio of the load to the throughput. The power drawn by the mill is determined using formulas of Austin and Morrell (King, 2001). Water can be added directly to the mill feed at a pre-specified rate or the simulator will calculate the water addition rate that is required to achieve a specified solid content in the mill discharge (King, 2001).

Parameters for impact, abrasion and attrition breakage were obtained from previous work on the sulphide milling circuit on a similar ore (Bepswa et al., 2015). They are presented in Table 5.1 below.

Table 5.1 Values of the impact and abrasion resistance parameters of the Kansanshi sulphide ores (Bepswa et al., 2015)

Parameter	Value
A	69.8 %
b	0.73
$A \times b$	51.0
t_a	0.36

Fracture energy parameters were left at MODSIM® default values; largest particle for fracture energy for large particles 96 J/kg, reference size d0 = 1.17 mm, and exponent phi = 1.26.

5.4 Vibrating screen

SCRN was selected in MODSIM® to model the SAG mill discharge screen. It is a simple model ideal for modelling screening. The required area of the screen is

calculated using the traditional screen capacity factors as shown in Equation (2.13). The screen dimensions can be optionally specified to compare with the required area. This model can accommodate water sprays. The model was selected because its simplicity and support the SAG discharge screen for the Kansanshi sulphide ore.

5.5 Pebble crusher

The model selected in MODSIM® for the pebble crusher was SHHD Short head crusher. This model is based on the crushing zone and internal classification behaviour described by Whiten et al. (1973). The parameters in the model were determined by Karra (1982).

The pebble crusher was not surveyed due to lack of resources and as such no particle size distribution was available for calibration and comparison. The closed side setting for the pebble crusher measured the day before the survey was applied. Other values such as proportion for fines produced during a breakage event, Alpha1 and Alpha2 were kept at MODSIM® default while impact work index = 12 and closed side setting gap = 13 mm.

5.6 Ball milling unit

GMSU was selected in MODSIM® for modelling the Kansanshi sulphide ore circuit ball mill. Mixing in the mill is modelled using three perfectly mixed regions in series with no classification between stages. This model should be used when the parameters for the selection and breakage functions have been determined from laboratory batch tests and the dimensions of the full-scale mill are known. The applicable selection and breakage functions are presented in Equations (2.25) and (2.26) respectively. Data from laboratory batch test for model is scaled up using Equations (2.27 – 2.32).

Selection function parameters determined in the test mill are specific rate of breakage at 1 mm, particle size exponent-alpha, size coefficient for maximum breakage and exponent for fall-off of selection function with size in the abnormal breakage region.

Breakage function parameters determined in the test mill are β, γ, δ and Φ at 5mm. Data required for the test and full-scale mills are diameter, length, ball load and size, powder filling and speed. Additional information for the full-scale mill includes make-up ball size and ball size distribution.

The selection function parameters were supposed to be obtained from batch laboratory milling data but the batch laboratory grinding mill was not available in the laboratory at Kansanshi mine metallurgical laboratory. The parameters were obtained by adjusting the parameter values until the simulated particle size distribution output matched the survey data for the SAG mill discharge to an acceptable extent as shown in Figure 5.5. The selection function parameters obtained from calibration of the SAG mill were α = 2.8, μ = 0.95 and Λ = 1.74.

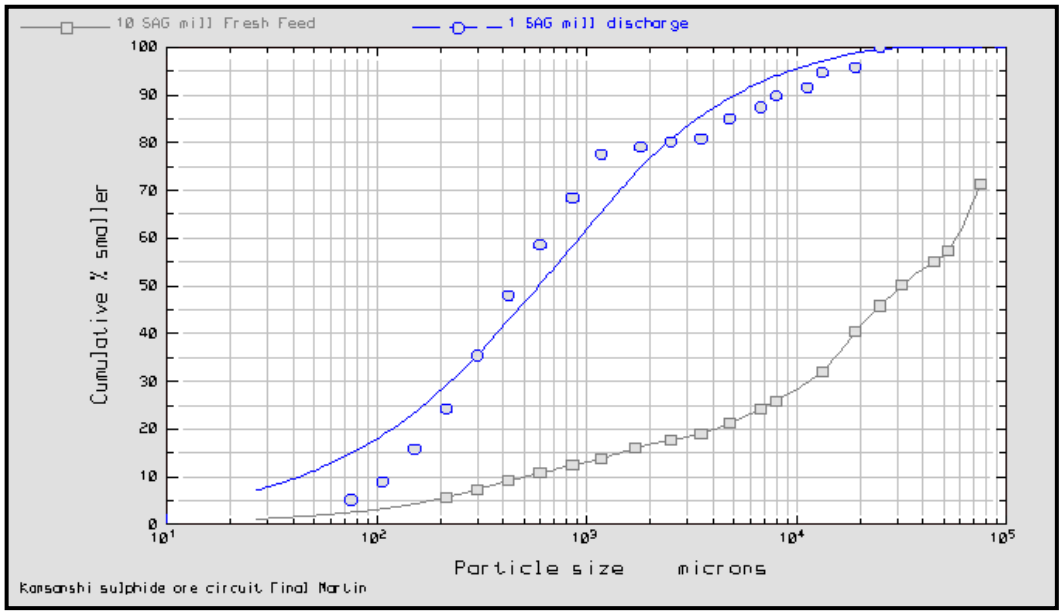

Figure 5.5 Comparison between MODSIM® predicted and surveyed particle size distributions for the feed and discharge of the SAG mill

Breakage function parameters were obtained by adjusting the parameter values until the simulated particle size distribution output matched the survey data for the feed and discharge of the ball mill to an acceptable extent as shown in Figure 5.6. Parameters obtained were $\beta = 2.5, \gamma = 1.5, \Phi = 0.2$.

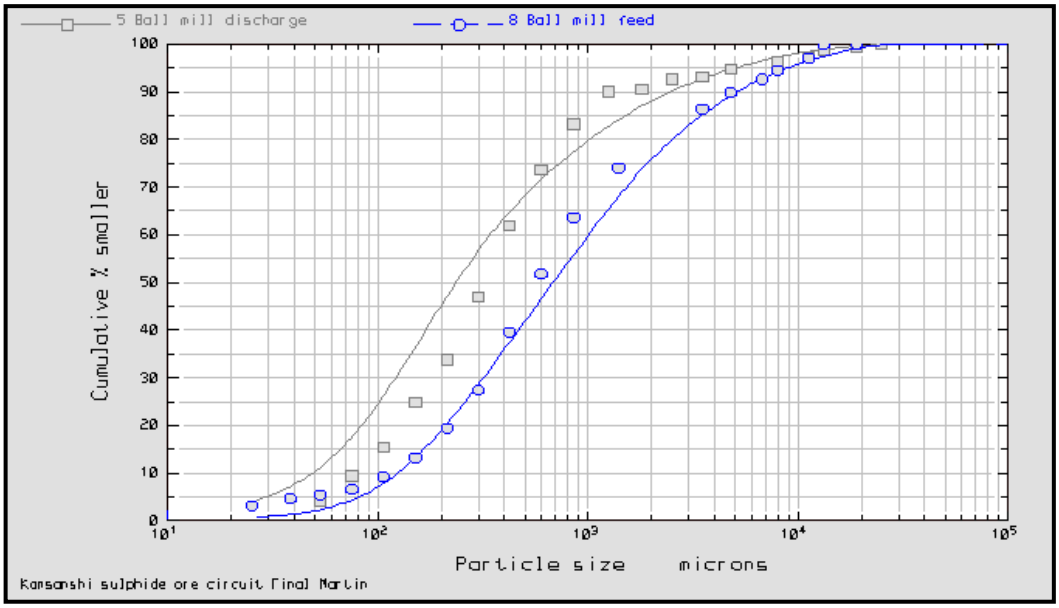

Figure 5.6 Comparison between MODSIM® predicted and surveyed particle size distribution of the feed and discharge of the ball mill

5.7 Cluster of hydrocyclones

Hydrocyclones were modelled using CYCL in MODSIM®. It is a mathematical model of the hydrocyclone classifier proposed by Plitt (1977). The geometry of the hydrocyclone can be specified as a standard configuration or each dimension can be specified individually. Roping of the cyclone is tested using the Mular-Jull and the Concha criteria (King, 2012). The exponent for the slurry density defines the variation of D50 with particle density. It reflects the flow conditions in the hydrocyclone. If Stokes law applies the exponent is 0.5 as was recommended tentatively by Plitt (1977). However, the level of turbulence in the hydrocyclone is always high and higher values of the exponent are usually required to match actual performance. The density of the slurry in the separating zone of the hydrocyclone

also has strong influence on the cut point. This density is always between the density of the carrier fluid and the density of the lightest solid component. The fraction of the difference between these two values is usually employed. The applicable models are presented in Equations (2.10 – 2.14) and (4.1 – 4.3).

The comparison between survey and MODSIM® predicted particle size distribution for hydrocyclone cluster feed, overflow and underflow are shown in Figure 5.7 below.

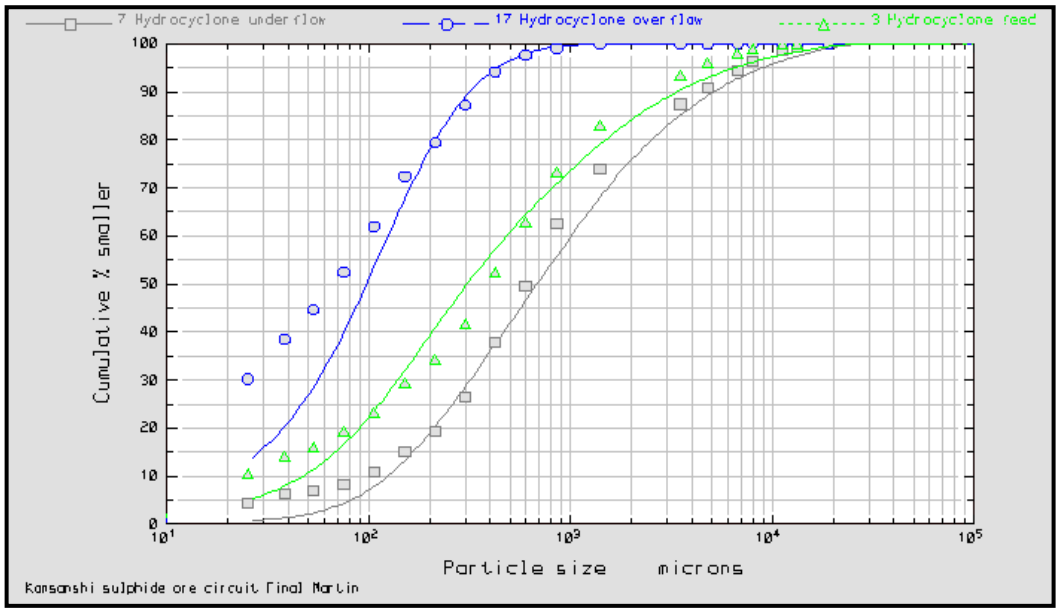

Figure 5.7 Comparison between MODSIM® predicted and surveyed particle size distributions around the hydrocyclones

5.8 Model of the flotation section

The Kansanshi sulphide ore flotation circuit comprises of the roughing, scavenging and cleaning stages. Only the rougher flotation stage was surveyed due to lack of resources hence only the rougher flotation circuit was incorporated into the simulations.

The model selected for modelling the Kansanshi sulphide ore flotation circuits in MODSIM® was FLTN. This model is based on the discrete distributed flotation

kinetic constant model. The volume of pulp in the cells in the bank must be specified and the pulp residence time is calculated to be consistent with this volume and the tailings flow from the cell. The water balance is fixed by assuming that the solids holdup per unit volume of pulp is fixed as proposed by Sutherland. The residence times of the solid and the water are assumed to be identical. The kinetic constant decreases at larger sizes. This model allows water to be added to the concentrate launder so that the solid content of the concentrate that finally leaves the bank is less than the solid content of the concentrate that leaves each cell. The water can be added at a pre-specified rate or MODSIM® will calculate the addition rate to meet a required final solid content in the concentrate. The applicable equations are presented in Equations (2.15) to (2.19).

Parameter for the flotation rate constant were obtained by adjusting the values parameters in MODSIM® until the MODSIM® predicted values for concentrate grade and recovery were very close to survey values. The rate constants for pyrites and silicates were obtained from MODSIM® tutorials. See the flotation rate constants parameters in Table 5.2.

Table 5.2 Flotation rate constants (Minerals Technology International, 2012)

Mineral	Ultimate recovery, R (%)	Kinetic constant, FRC (min^{-1})
Silicates	12	0.12 (0.0020 s^{-1})
Pyrite	53	0.8 (0.0133 s^{-1})
Chalcopyrite	83	3.5 (0.0417 s^{-1})

5.9 Calibration of the Kansanshi simulation model

MODSIM® models for SAG mill, ball mill, pebble crusher, SAG discharge screen, hydrocyclone and rougher flotation were calibrated based on the survey data, laboratory test results, plant operating as well as the design data. The accuracy of the models was controlled by altering the model parameters to ensure that model predicted particle size distributions of each stream conformed to survey particle size distribution.

The majority of streams are reflected accurate as shown in Figures 5.5 to 5.7. Note that hydrocyclone overflow and SAG mill discharge show a significant difference between predicted and measured size distributions below 100 µm and 200 µm respectively (Figures 5.5 and 5.7). Both problems can be explained by model limitations and also the quality of data. Nevertheless, it has to be kept in mind that the simulation might predict an intermediate product of the SAG mill with higher fines content as well as a final product which is finer than in reality. In overall, a good predictive capability of the models was demonstrated.

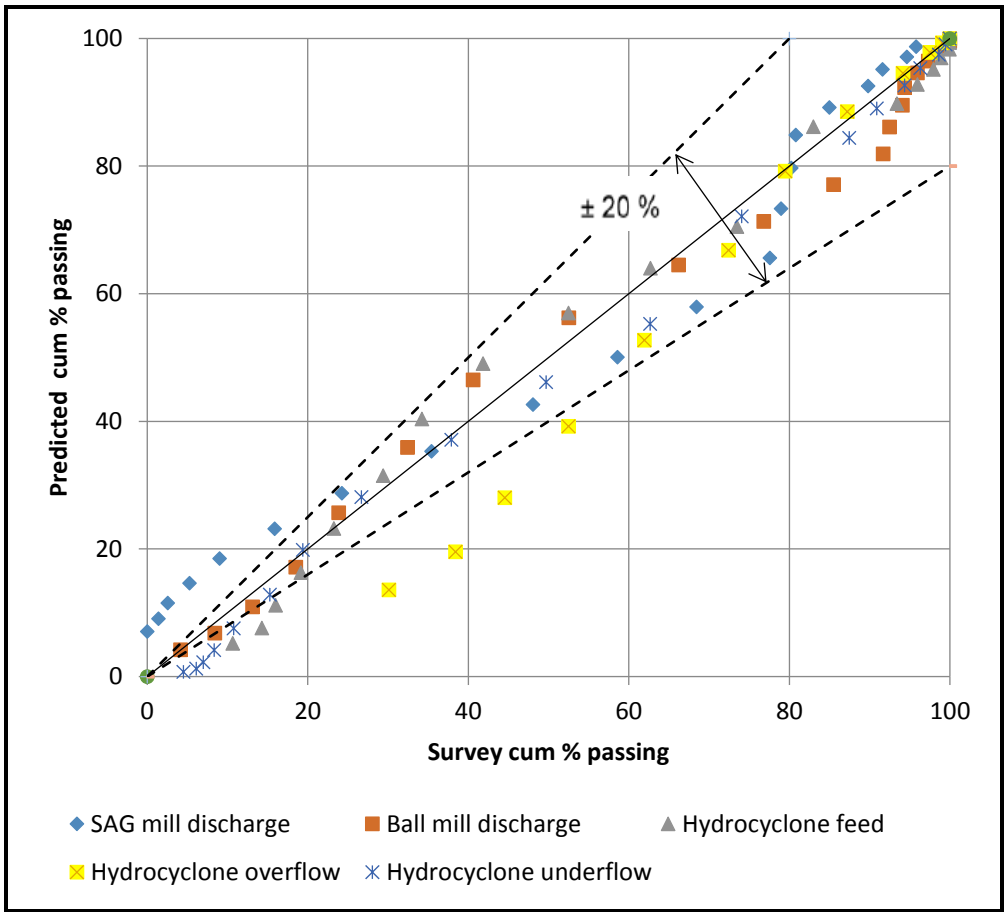

Figure 5.8 Comparison between MODSIM® predicted and survey data

A comparison between particle size distributions from the MODSIM® simulation outputs and those from the survey provided a reasonable match. As can be seen in Figure 5.8 above, most of the values are within the error boundaries of ± 20%.

5.10 Limitations of the models

The grate discharge mechanisms for SAG mills have pebble ports installed to aid the discharge of particles in the critical size range thereby preventing their build and restricting throughput (Napier-Munn et al., 1996). The model SAGM selected does not provide for inclusion of pebble ports. The recovery in flotation is impacted greatly by the rate of froth removal which is a function of air flowrate, pulp/froth level and reagents additions. The flotation models in MODSIM® have no provision for simulating these parameters. The effect of these parameters

maybe collectively accounted for in the flotation rate constant, but it would be desirable to have an insight on how they individually influence flotation recovery. Wills and Napier-Munn (2006) contended that the flotation rate constant depends on feed ore floatability, the bubble surface area flux generated in the cell and the recovery across the froth phase. It is worth noting that recovery in the froth phase is a function of froth removal rate from a flotation cell. The rate of froth removal is in turn a function of air addition rate, froth depth and frother addition rate.

Chapter 6 Optimisation of the Kansanshi sulphide ore circuit

6.1 Introduction

Optimisation of processes is key to making plant operation viable and profitable. Computer simulation of processes using commercial software to locate optimal operating conditions has gained a lot of ground in the recent past. Simulation studies were conducted to determine optimal operating parameters for the Kansanshi sulphide ore comminution circuit. The objective function was to maximize the production of material in the size range -150 +38 µm. Particles in this range have been identified at Kansanshi to yield the best flotation recovery of the sulphide ore. The calibration of MODSIM® models selected for the units incorporated into the circuit as well as the associated simulation studies are presented in this chapter. Finally, the analysis of the data generated from the simulations using attainable region techniques is discussed.

6.2 Simulation of the performance of the Kansanshi circuit

The models were used to simulate different options in order to improve the grinding efficiency and improve the quantity of material in the optimal floatable range; -150 +38 µm in the final product size for the Kansanshi sulphide ore comminution circuit.

Firstly, simulations were run using prevailing operating conditions during the survey to establish the base case and test the predictive ability of the simulation models used. The results for the base case (bc) are shown in Table 6.1.

Table 6.1 Comparison between surveyed and MODSIM® predicted data

Stream		Solids (tph)	P80 (µm)	% Solids
SAG mill discharge	Survey	1 740	2360	82
	Simulated	1 719	2390	82
Recycle scats	Survey	190	-	-
	Simulated	189	-	-
Ball mill discharge	Survey	-	692	78
	Simulated	-	729	78
Hydrocyclone overflow	Survey	1 233	217	41
	Simulated	1 290	230	34
Hydrocyclone feed pressure	Survey	126		
	Simulated	130		

Several simulations were conducted in order to evaluate if the percentage of material in the optimum floatable, -150 +38 µm could be improved. Currently material in this range is approximately 34 % of the total overflow or final product from comminution (Kaputula, 2017). For the purpose of this research, particle sizes were classified into three categories: -90000 +150 µm referred to as m1; then, -150 +38 µm referred to as m2; and finally, -38 µm referred to as m3. Because of the complexity of the circuit being investigated, a stepwise simulation approach was adopted. For each proceeding stage, the optimized parameters obtained from previous steps were used as base case/benchmark inputs for optimization of the individual next piece of equipment or circuit.

6.2.1 Effects of SAG discharge screen on circuit performance

The SAG mill discharge screen was simulated at 5, 10, 15, and 20 mm aperture sizes. Parameters for the base case at 20 mm were input to the first simulation at 15 mm. It was observed that as the screen aperture size was reduced the amount of pebbles generated increased and as a consequence the 80 % passing size (or

P80 value) of the pebble crusher, SAG feed rate as well as the P80 value of the SAG mill discharge increased as shown in Figure 6.1. The increased P80 values of the SAG mill discharge and pebble crusher product was attributed to an increase in feed rate which resulted in a reduced residence time. On the ball mill circuit, the discharge P80 decreased while no change was observed in the hydrocyclone P80. The decrease in the P80 value of the ball mill discharge was attributed to decrease in feed size to the circuit as the aperture size of the SAG discharge screen decreased. It can be seen in Figure 6.1 that at the aperture size of 5 mm, pebbles increased to 412 tph above the design capacity of 375 tph. The discharge screen aperture size of 6 mm was considered as optimum. As can be deduced from Figure 6.1 at the optimum the pebbles generated increased from 189 tph to 356 tph, SAG mill feed from 1719 tph to 1886 tph. The SAG and pebble crusher P80 increased from 2.39 mm and 3.6 mm to 2.73 mm and 9.5 mm respectively. The ball mill discharge reduced from 729 µm to 684 µm. Particle size distribution for the optimized 6 mm aperture size, P80 and throughput for key milling circuit streams are presented in Figure 6.2. Tables A.3 in the Appendices provide simulation data on SAG mill discharge screen aperture size.

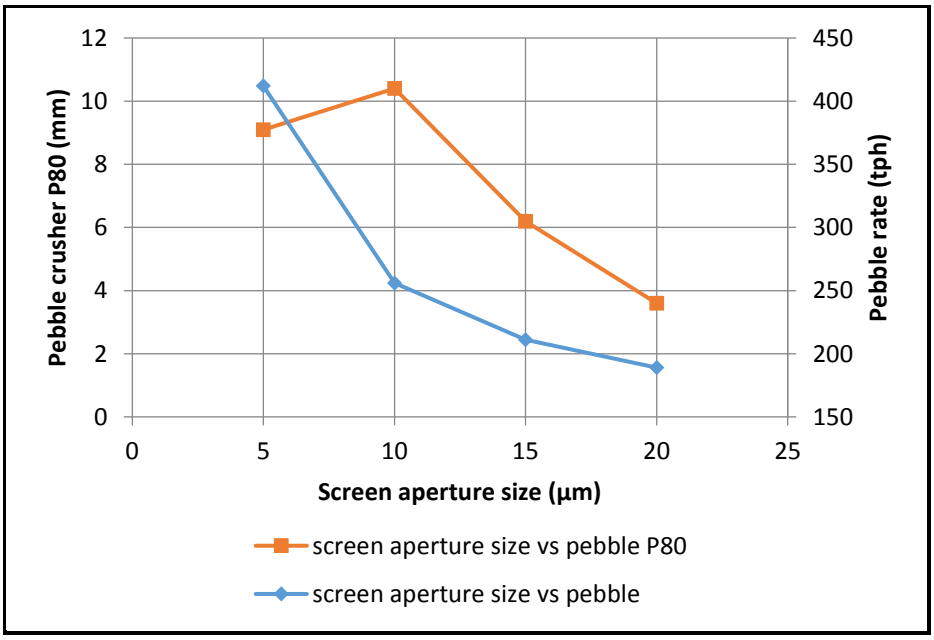

Figure 6.1 Variation of the size and rate of pebbles produced with the aperture size of the SAG mill discharge screen

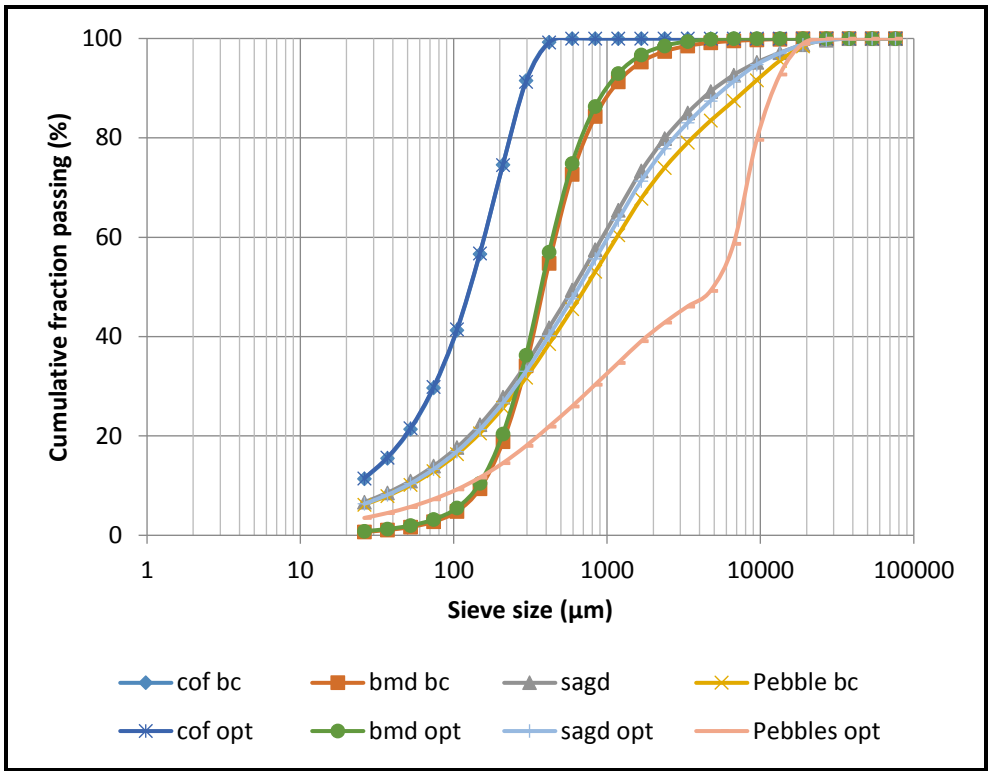

Figure 6.2 Particle size distributions of key milling streams for optimized SAG discharge screen. Legend: bc – base case, opt – optimized, cof – cyclone overflow, bmd – ball mill discharge, sagd – SAG mill discharge

6.2.2 Effects of pebble crusher on circuit performance

Optimized results from the SAG mill discharge screen aperture size simulations provided input to the pebble crusher closed side setting simulations. Simulations conducted at closed side settings CSS of 7 mm, 9 mm, 11 mm, and 13 mm. It was observed that as the crusher closed side setting was reduced the P80 value of the crusher product decreased and the quantity of pebbles generated as well as SAG mill feed reduced as shown in Figure 6.3. The pebble crusher closed side setting did not have a significant impact on the SAG and ball mill performance. The CSS of 11 mm was considered as optimal to avoid compromising the pebble crusher utilization. The optimized pebble crusher closed side setting yielded SAG mill federate of 1883 tph, pebble crusher feed rate 353 tph. Particle size distribution for key milling circuit streams for pebble crusher closed side setting simulations

are presented in Figure 6.4. The findings (see Table A.4) conform to what is contained in literature (Napier-Munn et al., 1999).

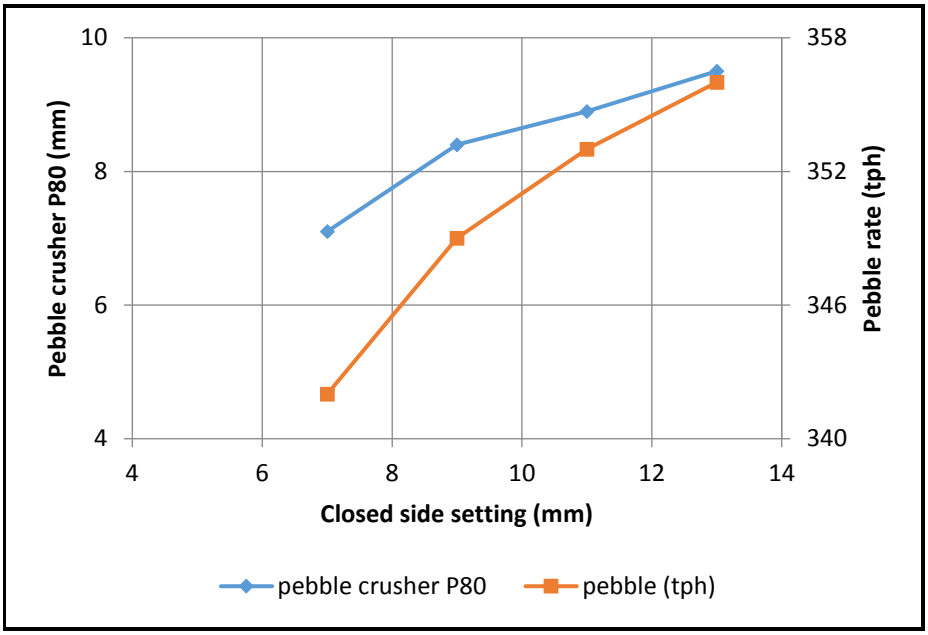

Figure 6.3 Simulated effects of the closed side setting of the pebble crusher

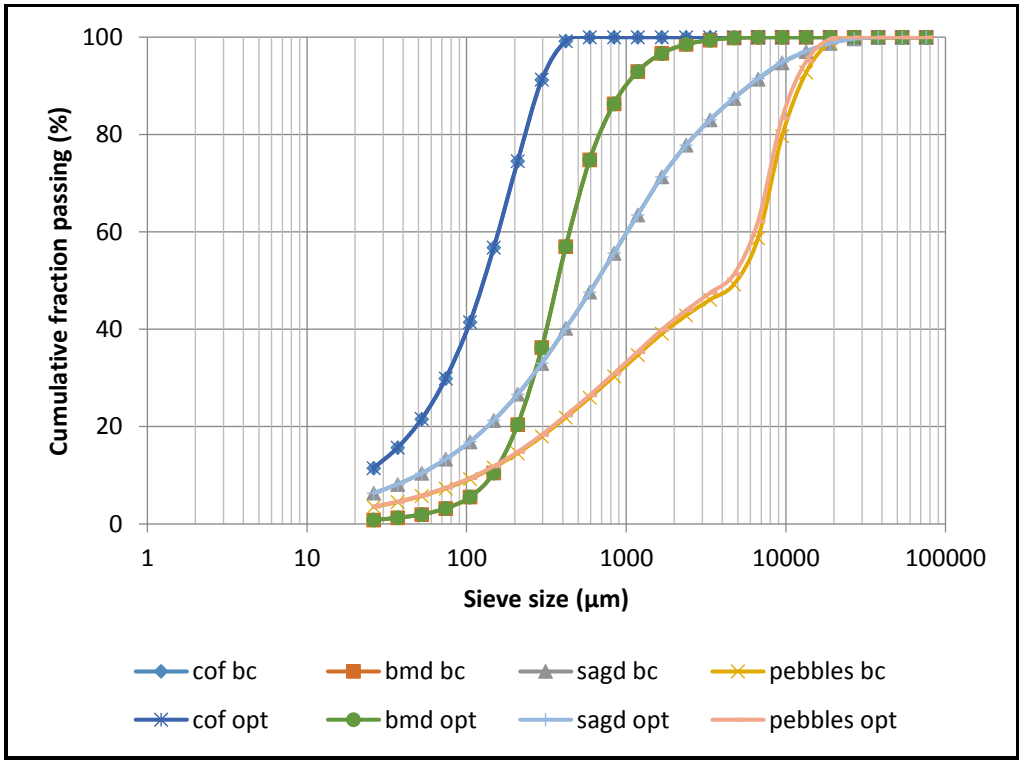

Figure 6.4 Performance of the Kansanshi milling circuit for the optimized pebble crusher

6.2.3 Effects of SAG milling on circuit performance

In the optimization of the SAG mill circuit, parameters selected for simulation were the SAG mill feed rate, the density of the slurry content of the SAG mill, ball filling and size as well as the rotational speed.

Optimized results from the effects of pebble crusher closed side setting provided input to the simulations of the effects of the ball filling of the SAG mill. Simulations were conducted at ball filling values between 12 % and 22 %. It was observed that at low ball filling, the SAG mill transfer size was high, decreasing as the ball filling increased and increasing again with further increase in ball filling as shown in Figure 6.5. The same trend was observed on the ball mill discharge product. The pebble recycle was high at low ball filling decreasing with increase in ball filling and increasing with further increase in ball filling as shown in Figure 6.5. The observed behaviour conforms to what is contained in literature. At low ball filling, cataracting motions will be predominant while cascading will predominate at a high charge volume. Cataracting motions lead to coarser product whereas cascading lead to fine product. Power draw will also increase with initial ball filling then begin to drop. High power draw will give a finer product whereas low power draw will give a coarse product (Napier-Munn et al., 1999). The ball filling of 16 % was considered optimal as it produced the smallest SAG discharge P80. Data for key milling circuit streams for SAG mill ball filling simulations are presented in TableA.5 of the Appendix section.

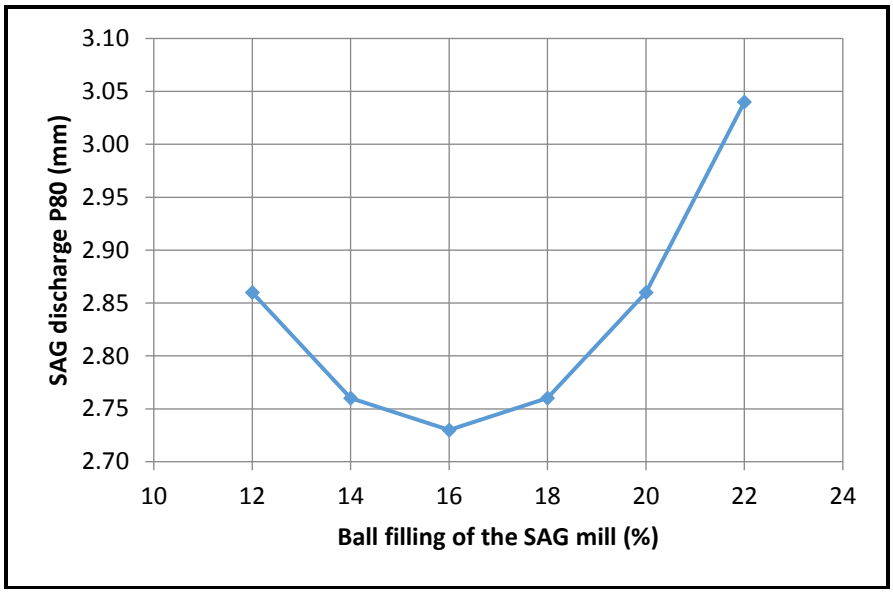

Figure 6.5 Simulated effects of the ball filling of the SAG mill

Simulation results summarised in Figure 6.5 provided information to investigate the effects of ball size making up for the SAG mill load. The simulations were conducted with ball sizes 125, 140, 160, 180, 200, 220, 240 and 260 mm. It was observed that as the ball size increased the SAG mill transfer size, ball mill P80 as well as the pebble recycle decreased as can be observed in Figure 6.6. It can also be observed in Figure 6.7 that the effect of increasing ball size is noticeable on the size range above 200 µm. This agrees with the widely accepted notion that larger balls are effective for breaking coarse particles (Austin et al., 1984; King, 2001; Napier-Munn et al., 1999). The ball size of 200 mm was adopted as optimal because too large a ball size may not be effective on breakage for smaller particles and to keep pebble crusher utilization high. The optimized ball size yielded the P80 values for the SAG and ball mill discharges of 2.17 mm and 667 µm respectively. The feed rates for the SAG mill and pebble crusher were 1736 tph and 306 tph respectively. Data for key milling circuit streams for SAG mill ball size simulation are presented in Tables A.6 the Appendix section.

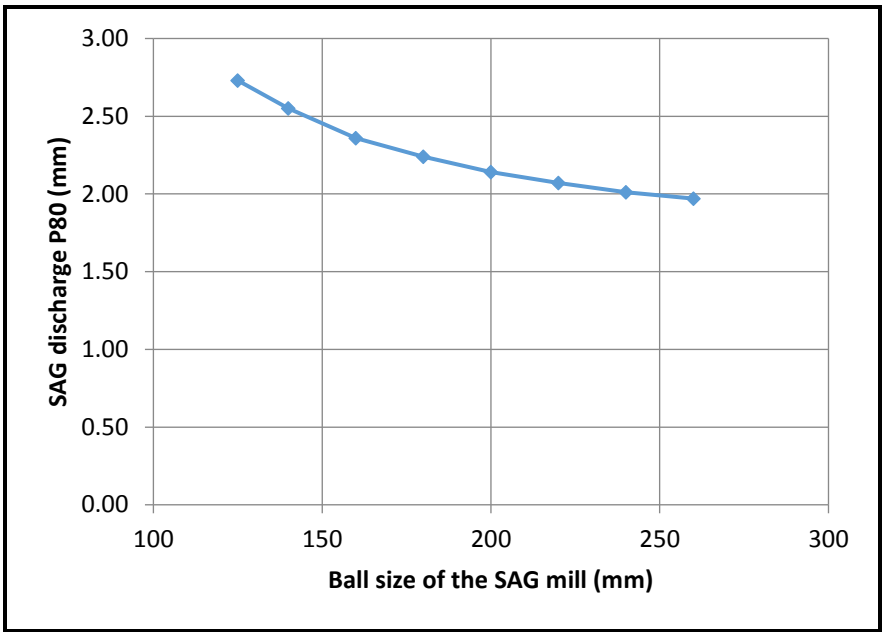

Figure 6.6 Simulated effects of ball size used in the SAG mill

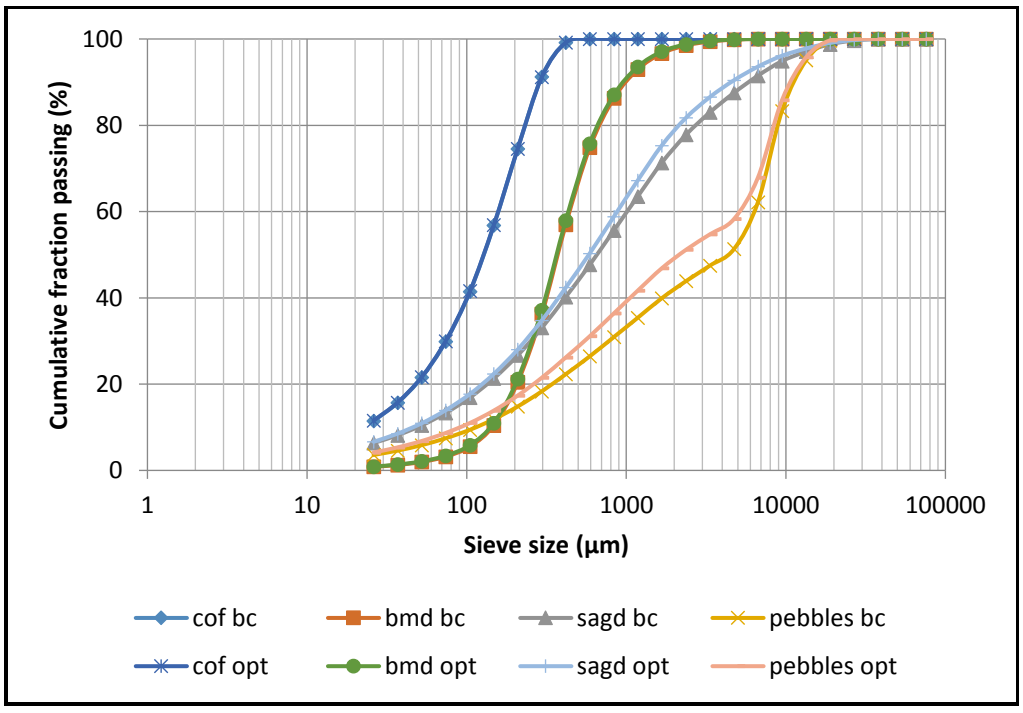

Figure 6.7 Performance of the Kansanshi milling circuit for optimized ball size of the SAG mill

Optimized results from the SAG mill ball size simulations provided input to the simulations for the effects of SAG mill speed. Simulations for SAG mill speed were conducted at 60 %, 65 %, 72 %, 75 %, 80 %, 85 % and 90 %. It was observed that

the SAG mill transfer size and pebble recycle was high at low critical speed decreasing with increase in speed and then increasing again with further increase in speed. The optimal speed was found to be 80 % as can be deduced from Figure 6.8. At the optimized speed, the P80 values for the SAG and ball mill discharges were 2.06 mm and 662 µm whereas the SAG mill and pebble crusher feed rates were 1828 tph and 299 tph respectively. Information is available in literature suggesting that mills should run around 75 – 80 % of critical to guarantee high power draw thereby ensuring that grinding is done at a faster rate (Austin et al., 1984; Wills and Napier-Munn, 2005). The optimized particle size distributions for the SAG mill speed are presented in Figure 6.9. The corresponding raw data and other key information are presented in Tables A.7 of the Appendix section.

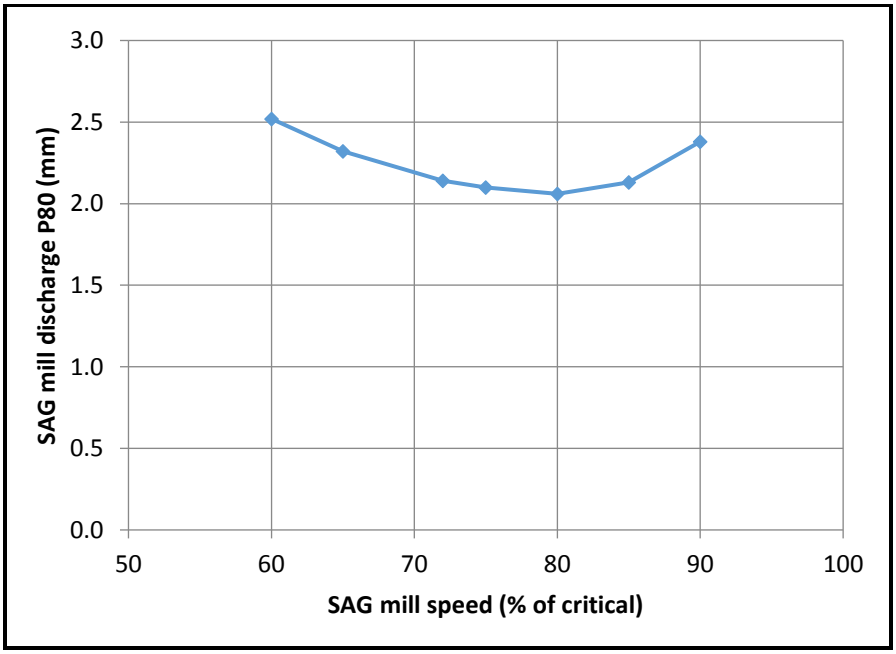

Figure 6.8 Simulated effects of SAG mill speed

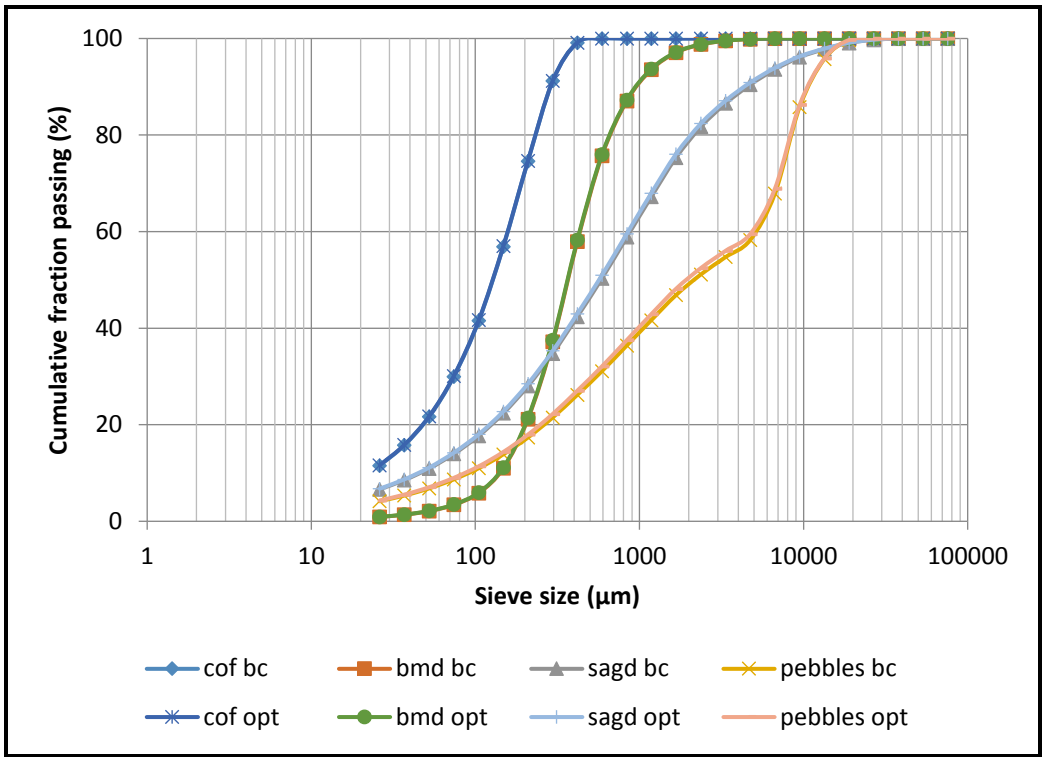

Figure 6.9 Performance of the Kansanshi milling circuit for optimized SAG mill speed

Optimized results from the SAG mill simulations in Figure 6.9 provided information for the effects of the density of the slurry content of the SAG mill. Simulations for SAG in mill density conducted between 70% and 90 % solids. The SAG in mill slurry density had no observed impact on the SAG and ball mill performance.

Optimized results from the simulation of the effects of SAG mill speed provided input to studying the effect of the SAG mill feed rate. Increase in the SAG feed rate resulted in increased P80 values of the SAG and ball mill discharges and pebble crusher. Further to this, the mass fraction of pebbles generated was increased. This was attributed to reduction in residence time (Napier-Munn et al., 1999). There was a slight decrease in the hydrocyclone P80 overflow. Increase in feed rate increased feed flowrate to the hydrocyclone which resulted in increased pressure and centrifugal forces resulting in a finer product. The results are presented in Figure 6.10. It can be observed in Table A.8 that the lowest hydrocyclone P80 was attained at a throughput of 2200 tph, but the pebbles

generated were 387 tph which was above the pebble crusher capacity. The optimal SAG mill feed rate was considered to be 2090 tph yielding P80 values of the SAG and ball mill discharges of 2.28 mm and 717 µm respectively. The hydrocyclone overflow P80 was 225 µm whereas the pebbles generated were 358 tph. The milling circuit key stream for 2090 tph and other important information are presented in Figure 6.11 and Tables A.8.

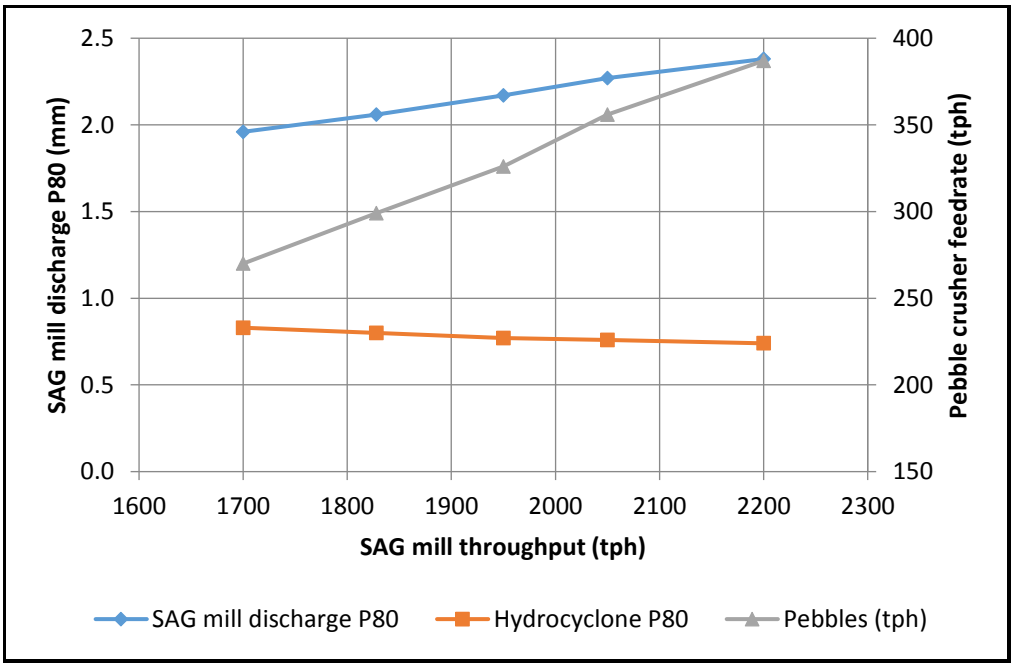

Figure 6.10 Simulated effects of SAG mill throughput

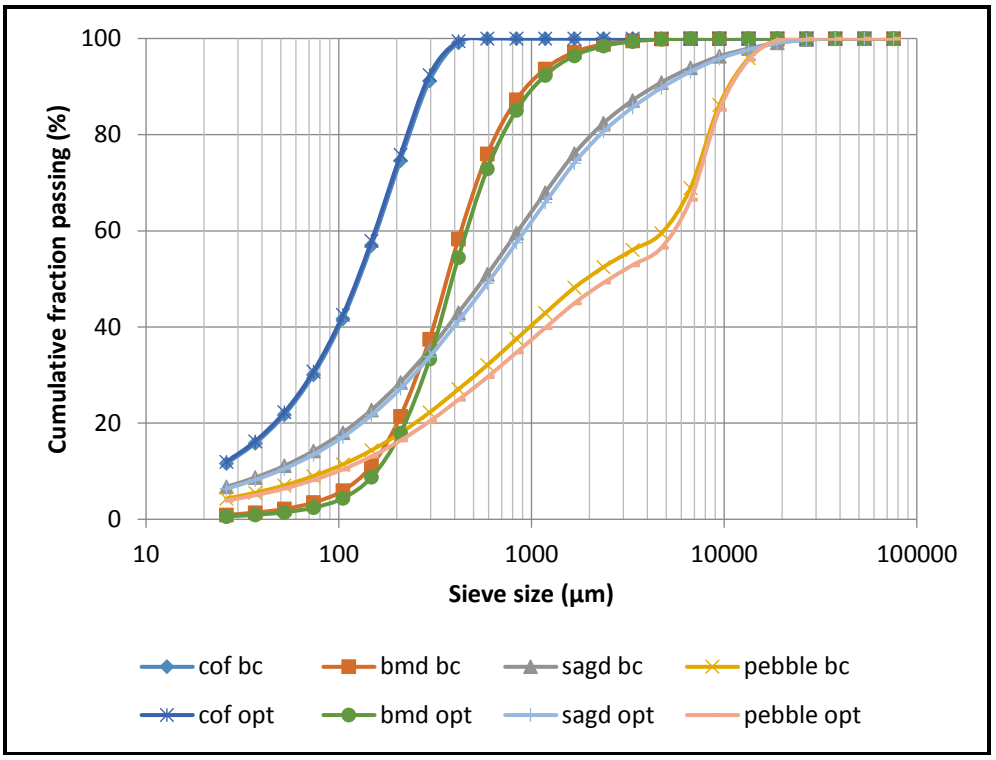

Figure 6.11 Performance of the Kansanshi milling circuit for optimized SAG mill throughput

6.2.4 Effects of ball milling on circuit performance

In the optimization of the ball milling section, the parameters selected for simulation were feed rate, slurry content, ball filling, ball size, and ball mill speed.

Optimized results from the SAG mill circuit simulations provided input to the analysis of the effects of the ball filling of the ball mill. Simulations were conducted from 22% to 40 %. It was observed that as the ball filling was increased, the P80 values of the ball mill discharge and the hydrocyclone overflow decreased as can be observed in Figure 6.12. Cataracting was responsible for coarser product whereas cascading was responsible for fine product (Napier-Munn et al., 1999). However, above 32 % ball filling, no change in the P80 value of the hydrocyclone overflow was observed; hence, the ball filling of 32 % was considered optimal. The optimized simulation results are presented in Figure 6.13. Data for key milling

streams for ball filling simulation are presented in Table A.9 of the Appendix section.

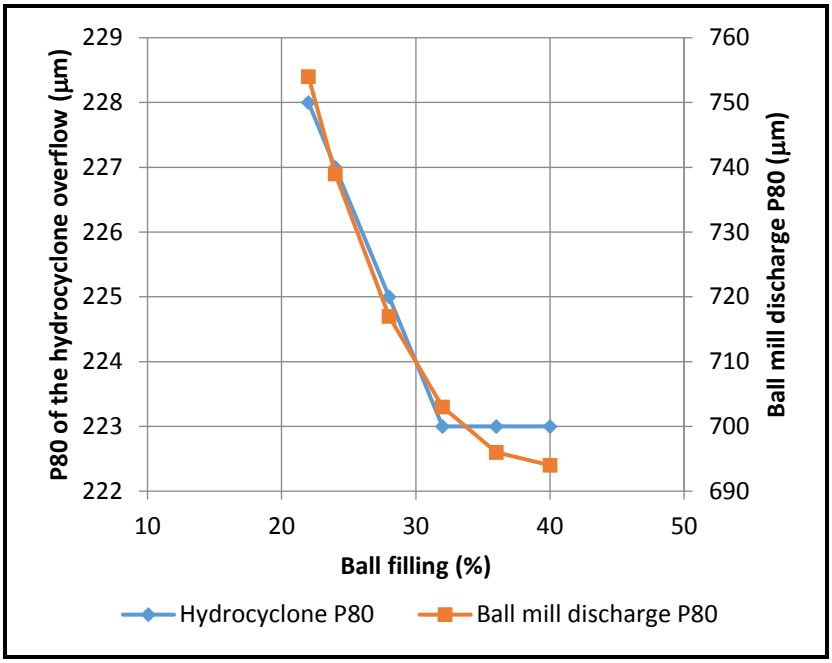

Figure 6.12 Simulated effects of the ball filling of the ball mill

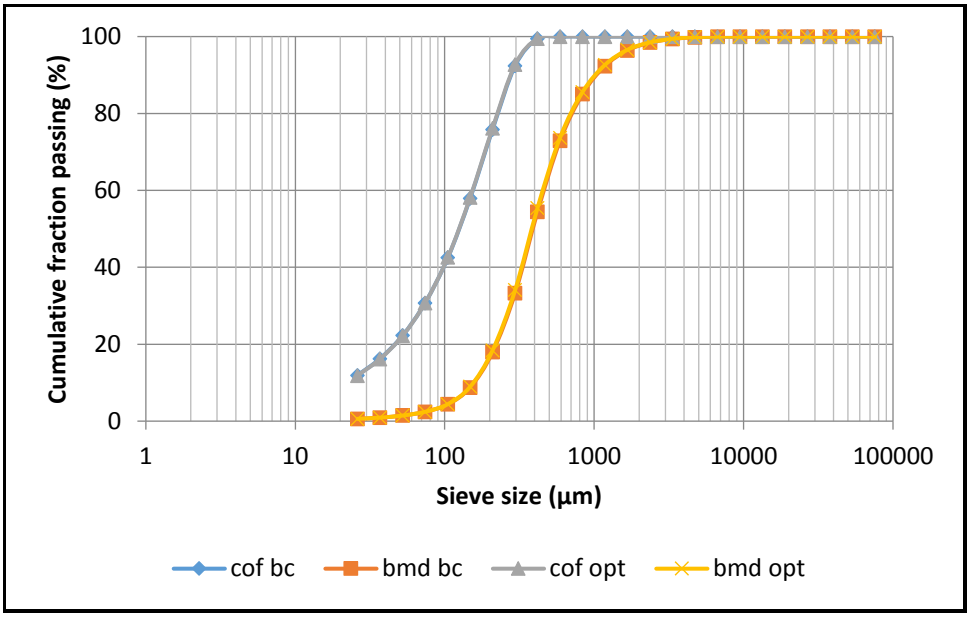

Figure 6.13 Performance of the Kansanshi milling circuit for the optimized ball filling of the ball mill

Optimized results from the simulation of the effects of the ball filling of the ball mill provided the basis for the next analysis. The simulations for the effects of ball size used in the ball mill were conducted with ball diameters between 30 mm to 70 mm. It was observed that as the ball size was increased, the P80 values of the ball mill discharge and the hydrocyclone overflow also increased (see Figure 6.14). This agrees with the widely accepted notion that smaller balls are effective for breaking fine particles (Napier-Munn et al., 1999; Wills and Napier-Munn, 2006). The ball size of 40 mm was considered optimal despite a smaller size of 30 mm yielding a finer product. This was guided by the cost implication of using smaller balls as they would require frequent replenishment (Will and Napier-Munn, 2006). The optimized ball size simulation results are presented in Figure 6.15. Data for ball mill key streams for the simulation of ball size are presented in Tables A.10 of the Appendix section.

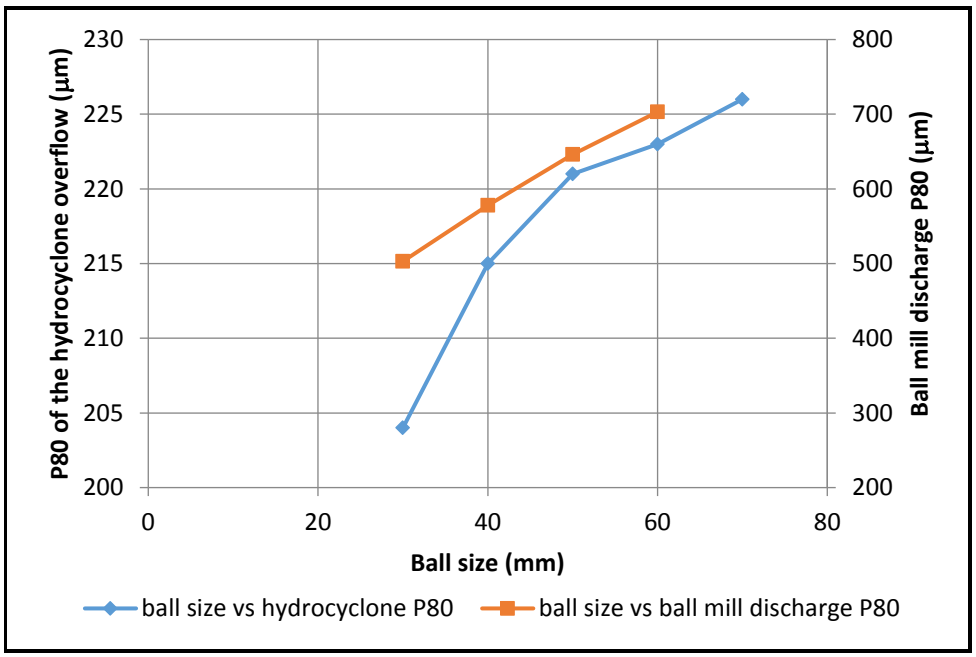

Figure 6.14 Simulated effects of the ball size used in the ball mill

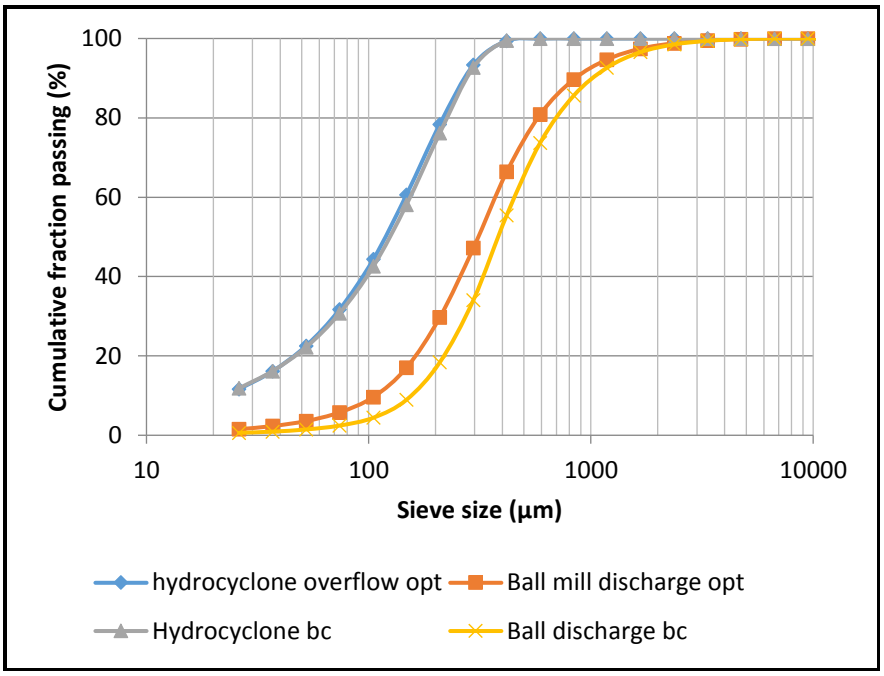

Figure 6.15 Performance of the Kansanshi milling circuit for optimized ball size of the ball mill

Optimized results from the effects of media size of the ball mill provided the basis for simulating the effects of ball mill speed. Simulations for ball mill speed were conducted between 60 % and 90 % of the critical speed. It was observed that the P80 values of the ball mill discharge and hydrocyclone overflow were high at low ball mill speed decreasing with an increase in speed before increasing again. The optimal mill speed was found to be 80 % as can be deduced from Figure 6.16. This was because of cascading and cataracting motions at low and high speeds respectively. Increase and decrease in power draw also was responsible for the noted P80 values. At the optimized speed, the P80 values of the ball mill discharge and hydrocyclone overflow were 566 µm and 213 µm respectively. The optimized particle size distributions for the ball mill speed are presented in Figure 6.17. Data of ball mill streams for mill speed simulation are presented in Tables A.11 of the Appendix section.

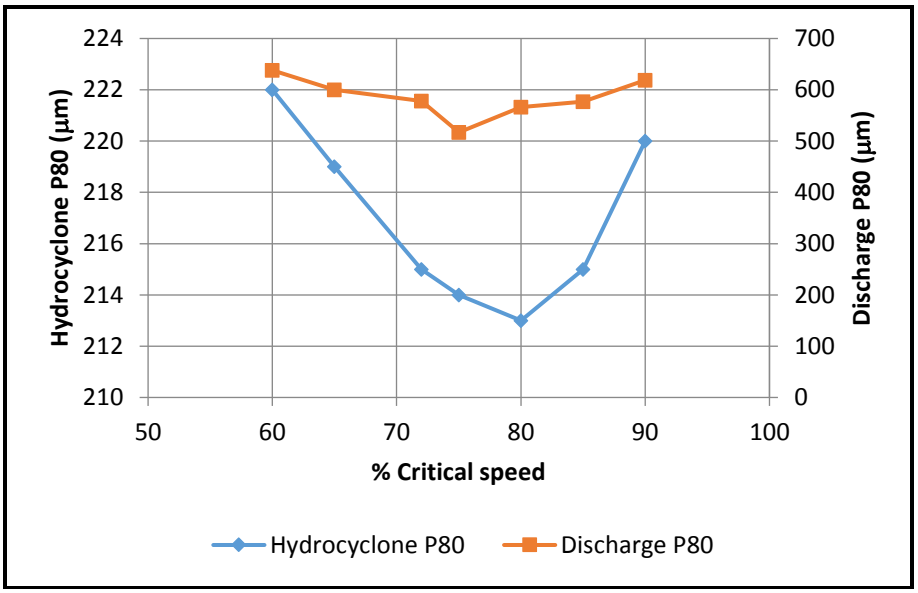

Figure 6.16 Simulated effects of ball mill speed

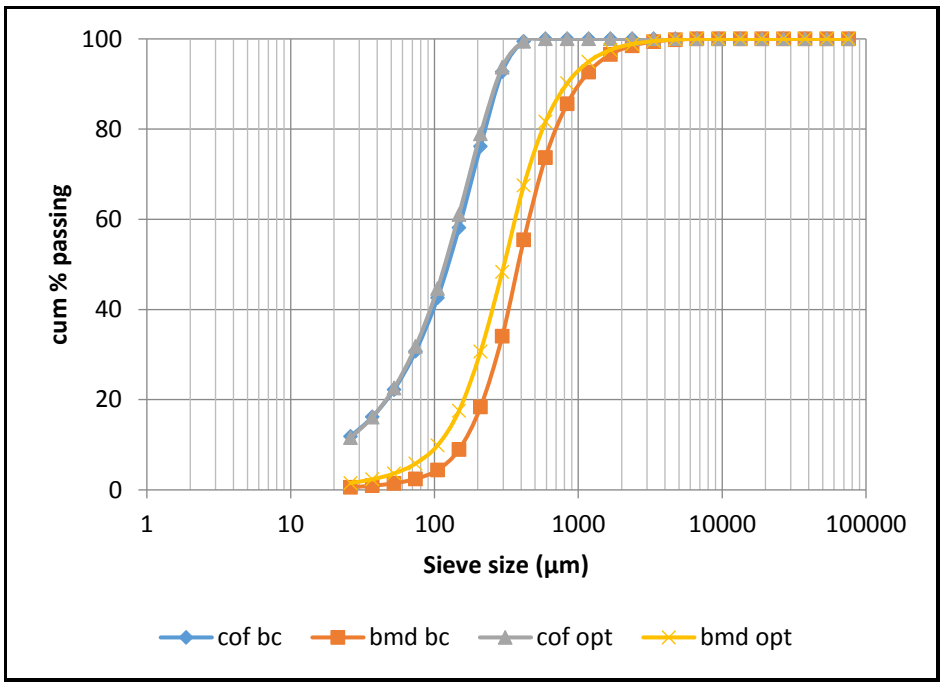

Figure 6.17 Performance of the milling circuit for optimized ball mill speed

Optimised results generated for the effects of ball mill speed were used as the starting point for simulating the effects of solid content of the ball mill feed. Simulations for the slurry concentration of the ball mill feed were conducted from 70 % to 85 % solids. The ball mill slurry concentration had no observed impact on

ball mill performance. The results for ball mill slurry concentration are summarised in Table A.12 of the Appendix section.

6.2.5 Effects of hydrocycloning on circuit performance

Optimised results from the simulation of the effects of the ball milling section provided input to studying the hydrocyclone. Only the effects of the solid content of the inlet feed to the hydrocyclone were simulated.

The feed concentrations simulated were between 62 % and 68 % solids. It was observed that the P80 values of the hydrocyclone overflow and ball mill discharge increased with increase in hydrocyclone feed slurry concentration as shown in Figure 6.18. High slurry density of the hydrocyclone feed leads to high viscosity of the carrier fluid leading to a coarser overflow (Napier-Munn et al., 1999; Wills and Napier-Munn, 2006). The slurry concentration of the feed to the hydrocyclones of 62 % by mass was considered optimal as it produced a P80 of 145 µm which was closest to the target P80 value for the circuit of 150 µm. The optimized particle size distributions for the slurry concentration of the feed to the hydrocyclones of 62 % by mass are presented in Figure 6.19. Data for ball mill streams for hydrocyclone feed slurry concentration simulations are presented in Tables A.13 of the Appendix section.

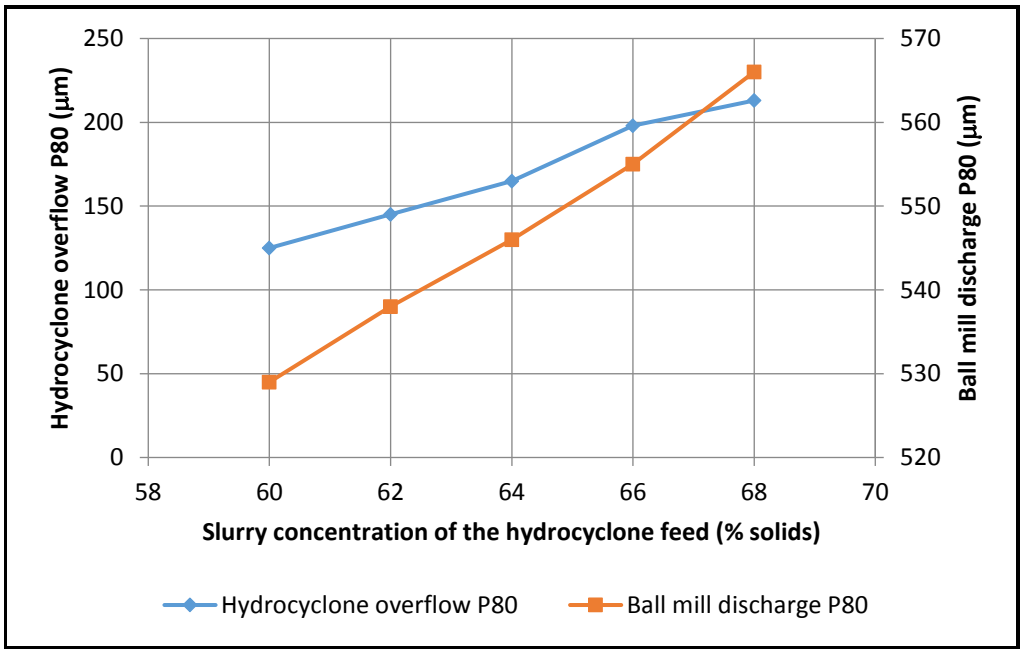

Figure 6.18 Simulated effects of the solid content of the hydrocyclone feed

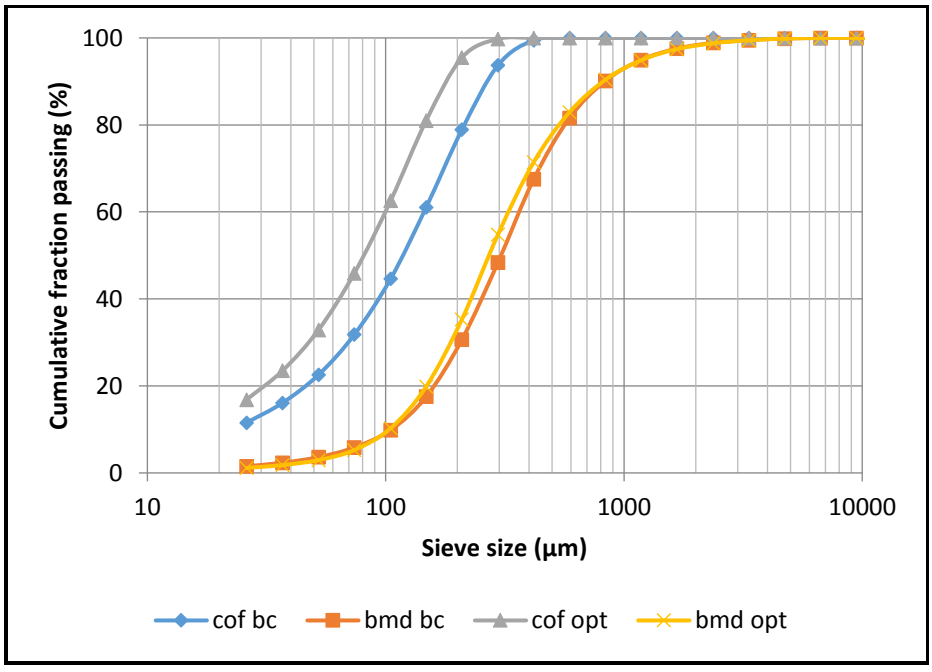

Figure 6.19 Performance of the milling circuit for optimized slurry concentration of the hydrocyclone feed

6.3 Integrated optimisation of the Kansanshi circuit

Simulations were conducted for the milling equipment to locate operating conditions which yield the best performance for individual unit and how the entire circuit was impacted. The units simulated and optimised included the SAG and ball mills, hydrocyclone, pebble crusher and SAG mill discharge screen. The optimised operating parameters of the preceding unit provided input for the next unit. The optimised circuit conditions are presented in Table 6.2.

Table 6.2 Optimised simulation parameters of the Kansanshi circuit

Parameter	**Survey**	**Base case simulation**	**Optimised simulation**
SAG throughput (tph)	1 740	1 719	2 090
Overflow P80 (µm)	217	230	145
Ball mill discharge P80 (µm)	692	717	538
SAG mill discharge P80 (µm)	2 360	2 230	2 280
Pebble crusher P80 (mm)	-	8.6	8.5
Pebble recycle (tph)	190	189	358
Slurry concentration of the hydrocyclone feed (% solids)	68	68	62
Screen aperture size at the SAG discharge (mm)	20	20	6
Pebble crusher CSS (mm)	13	13	11
Ball filling of the SAG mill (%)	16	16	16
Ball size of the SAG mill (mm)	125	125	200
SAG mill speed (% of critical)	72	72	80
Slurry concentration of the SAG mill (% solids)	82	82	82
Ball filling of the ball mill (%)	28	28	32
Ball size of the ball mill (mm)	60	60	40
Ball mill speed (% of critical)	72	72	80
Slurry concentration of the ball mill (% solids)	72	72	72
Flotation recovery (%)	79.44	79.99	82.25

6.3.1 Definition of the state variables

The focus of the optimization in this research was to maximise the conversion of feed material classified in the size range -90000 +150 µm into the range -150 +38 µm after milling. This size range has been identified as yielding the best recovery in the Kansanshi sulphide ore flotation circuit. It must be noted that the breakage process in the mills also produced material which was -38 µm. it was desirable to limit the production of material in the -38 µm range. The three size ranges were referred to as m1 for -90000 +150 µm, m2 for -150 +38 µm and m3 for -38 µm.

The attainable region analysis technique was applied to analyse and optimise the milling circuit. The analysis of how the various parameters influenced the performance of the circuit is presented below.

6.3.2 Effects of the aperture size of the SAG mill discharge screen

The change in the aperture size of the discharge screen of the SAG mill did not have a significant impact on the milling circuit production of m2. However, the AR profile showed that maximum production of m2 at 41.1 % was achieved when 43.2 % of m1 was present as shown on the AR profile in Figure 6.20.

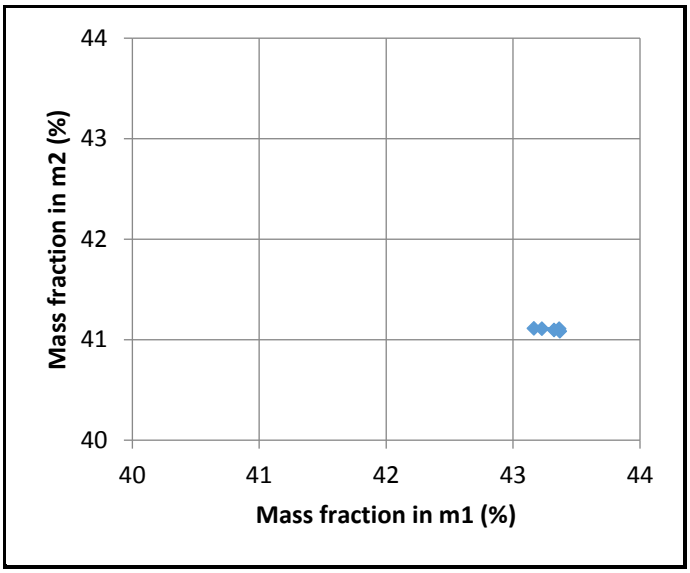

Figure 6.20 Variation of m1 and m2 with the aperture size of the SAG mill discharge screen

The aperture of the discharge screen of the SAG mill did not have a significant impact on the recovery in flotation as shown in Figure 6.21.

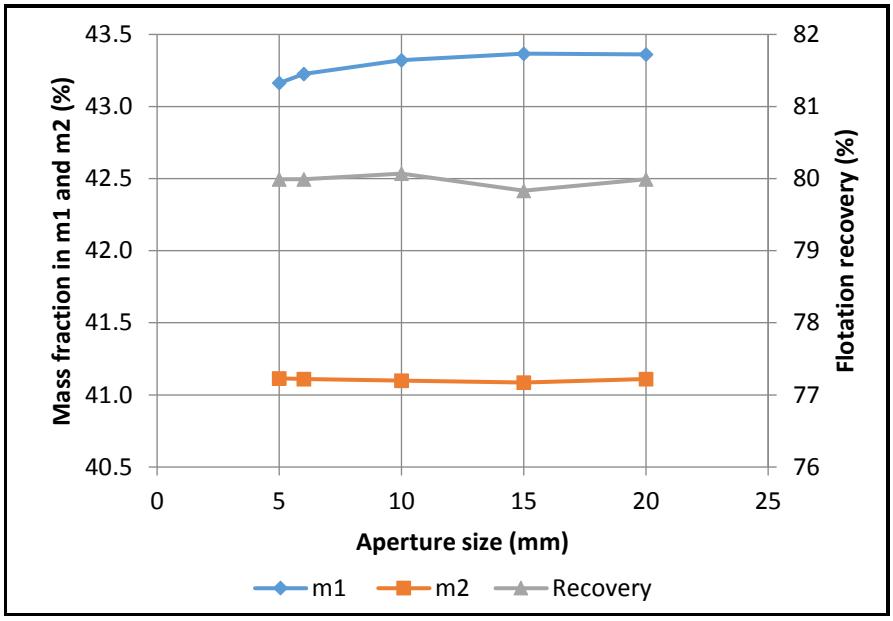

Figure 6.21 Effect of SAG mill discharge screen on flotation performance

6.3.3 Effects of the closed side setting of the pebble crusher

The closed side setting of the pebble crusher did not show any impact on the conversion of feed material from m1 to m2 of the milling circuit. The AR profile did not show any significant change in the proportions of m1 and m2 in the final product of the milling circuit as evidenced in Figure 6.22. As a direct consequence of this, the closed side setting of the pebble crusher did not also have any significant impact on the flotation recovery as in Figure 6.23.

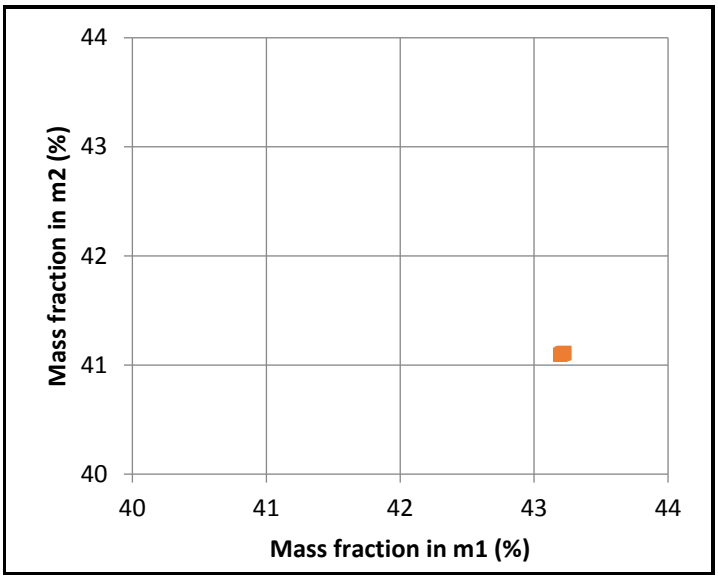

Figure 6.22 Variation of m1 and m2 with the closed side setting of the pebble crusher

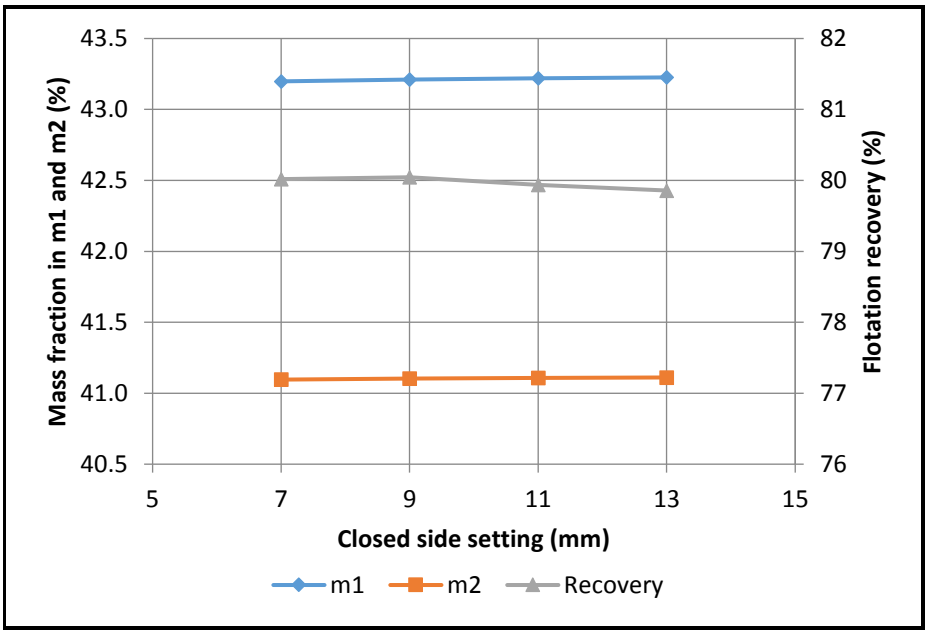

Figure 6.23 Effect of pebble crusher on flotation performance

6.3.4 Effects of the ball filling of the SAG mill

The production of m1 increased slightly with increase in ball filling then became constant. It was observed that maximum production of m2 was attained between 18 % and 22 % ball filling. The AR profile in Figure 6.24 confirmed this assertion.

Increase in ball filling promotes cascading motion which produces finer product (Napier-Munn et al., 1999; King, 2001).

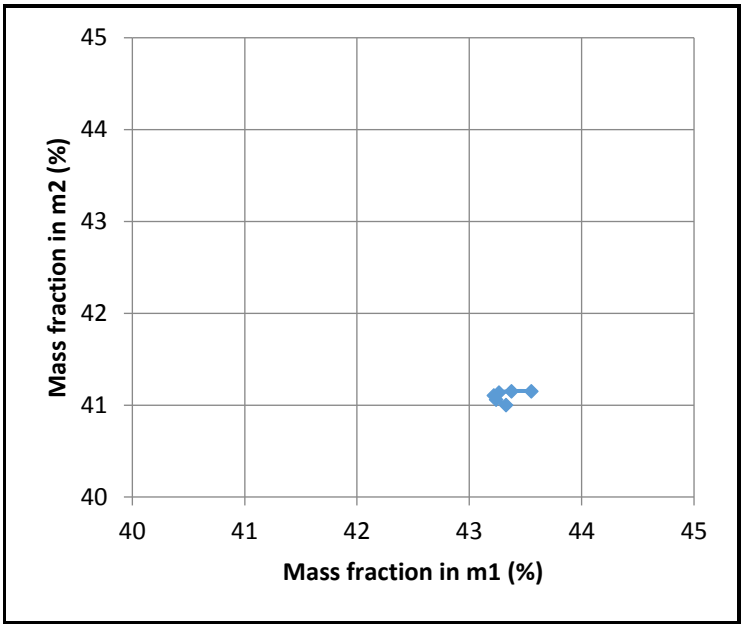

Figure 6.24 Variation of m1 and m2 with the ball filling of the SAG mill

Simulations of the effects of the ball filling of the SAG mill did not show any significant impact on flotation recovery as shown in Figure 6.25.

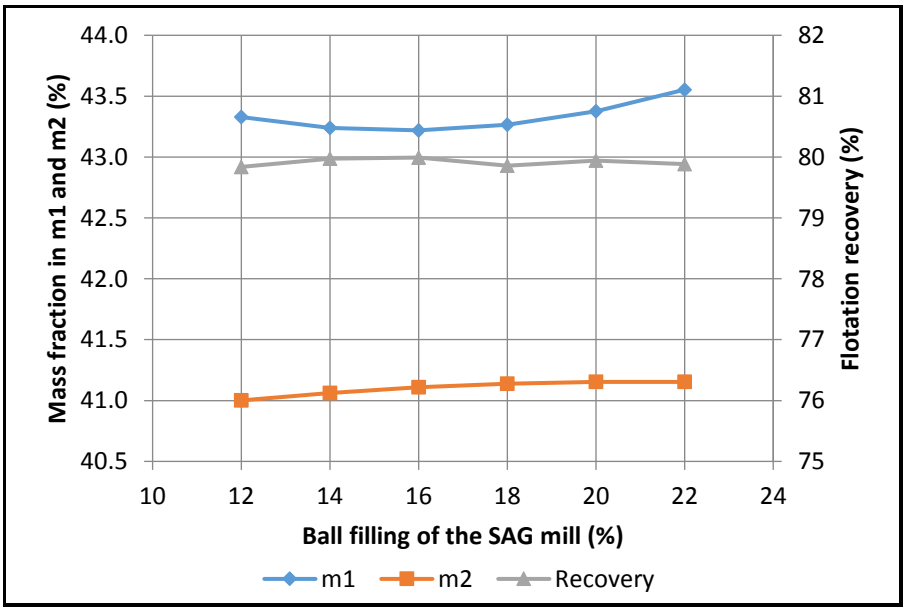

Figure 6.25 Effect of the ball filling of the SAG mill on flotation performance

6.3.5 Effects of ball size used in the SAG mill

The change in ball size did not show any significant change in production of m2. The AR profile did not exhibit any significant change as shown in Figure 6.26.

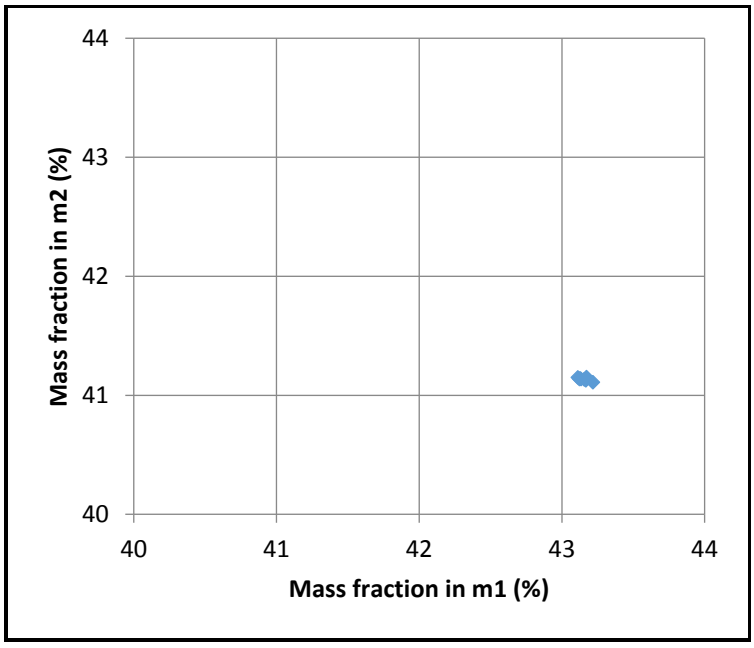

Figure 6.26 Variation of m1 and m2 with the ball size of the SAG mill

The simulation of the effects of the ball size used in the SAG mill did not show any significant impact on flotation recovery as shown in Figure 6.27.

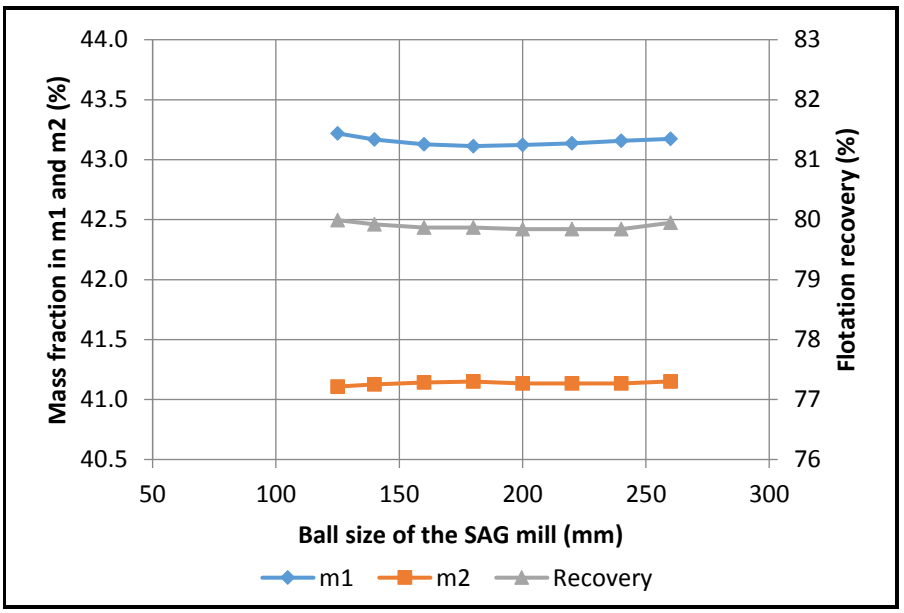

Figure 6.27 Effect of the ball size of the SAG mill on flotation performance

6.3.6 Effects of the SAG mill speed

The production of m2 increased with increase in SAG mill speed then decreased with further increase. Maximum production of m2 was observed at speed between 75 % and 85 %. The maximum amount of m2 produced was 41.16 % when 43.01 % of m1 was also present (see Figure 6.28). This agrees with what is reported in literature that mills should be operated at speeds between 75 % and 85 % of critical (Napier-Munn et al., 1999).

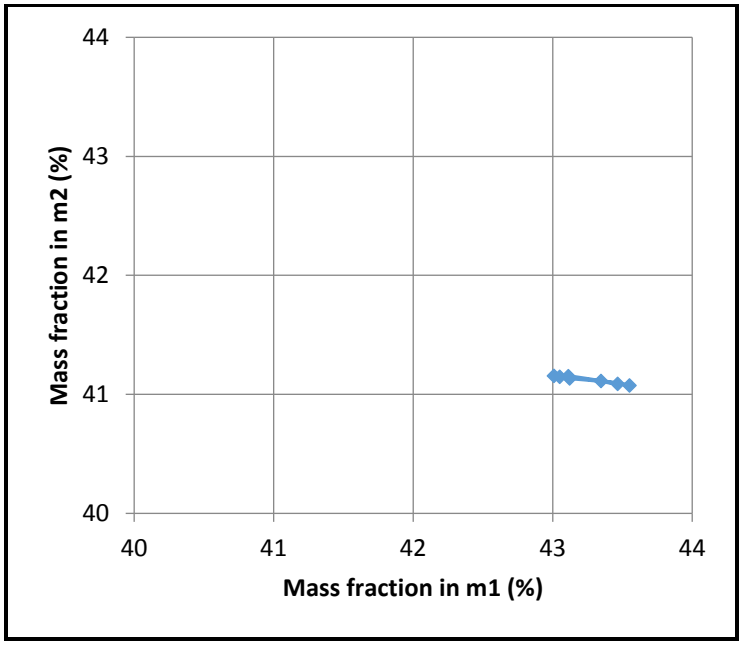

Figure 6.28 Variation of m1 and m2 with SAG mill speed

Simulations carried out on the effects of SAG mill speed did not show any significant impact on flotation recovery as shown in Figure 6.29.

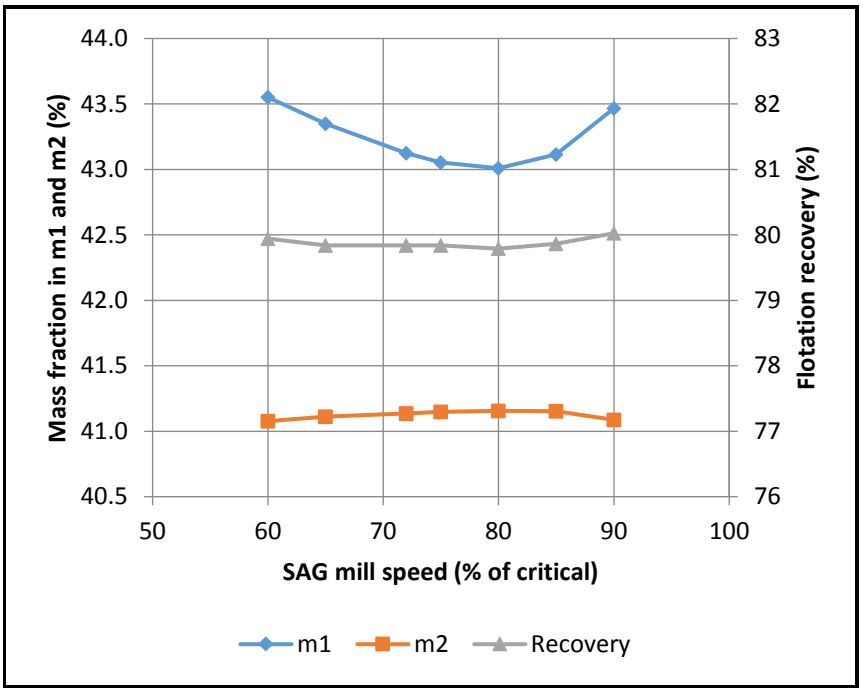

Figure 6.29 Effect of SAG mill speed on flotation performance

6.3.7 Effects of SAG mill throughput

It was observed that the production of m2 increased as the SAG mill throughput increased. However, the constraint was on the pebble crusher which could not accommodate pebbles produced at 2200 tph. The maximum quantity of m2 produced was 41.90 % at the point where m1 was 41.62 % as shown on the AR profile in Figure 6.30. Increasing throughput on the SAG mill led to increase in feed flowrate to the hydrocyclone increasing feed pressure and centrifugal forces (Wills and Napier-Munn, 2006). This translated into a finer overflow product.

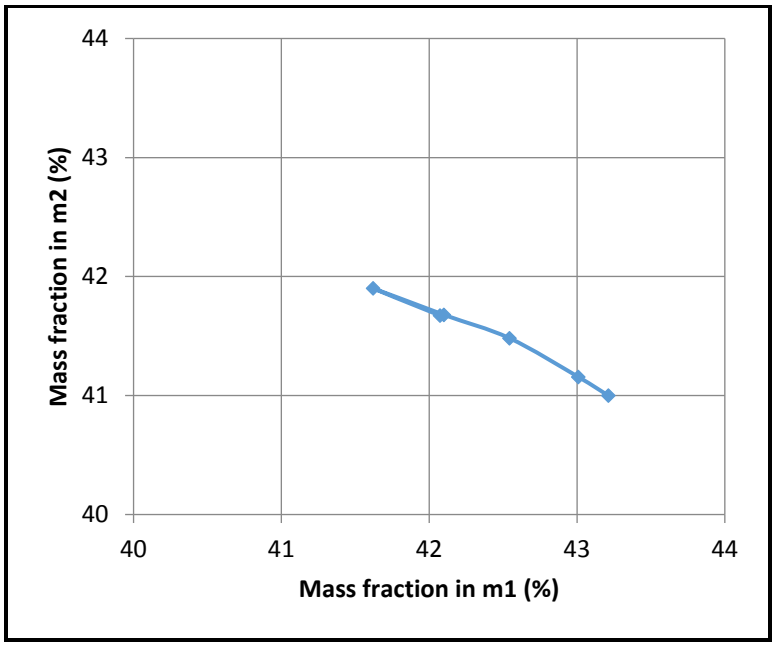

Figure 6.30 Variation of m1 and m2 with SAG mill throughput

Increase in SAG mill throughput resulted in increase in quantity material in the optimum size range m2 produced and consequently increase flotation recovery initially and then remained constant beyond 1840 tph as shown in Figure 6.31. The increase in recovery can be attributed to increase in m2.

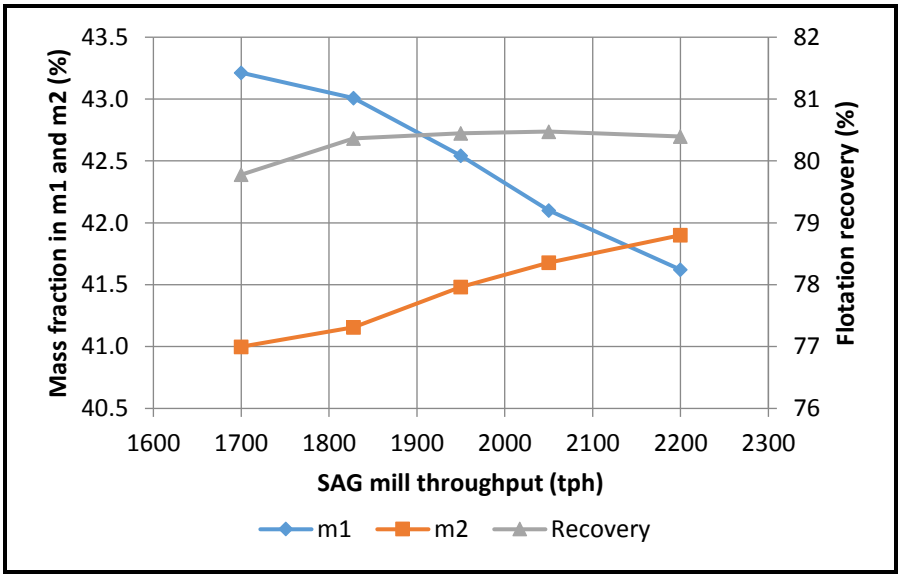

Figure 6.31 Effect of SAG mill throughput on flotation performance

6.3.8 Effects of the ball filling of the ball mill

The amount of m2 produced in the hydrocyclone overflow increased as the ball filling increased though the rate of increase slowed down beyond 32 % ball filling. The maximum quantity m2 produced was 42.09 % at the point where 41.80 % was present in the hydrocyclone overflow as can be observed on the AR profile in Figure 6.32.

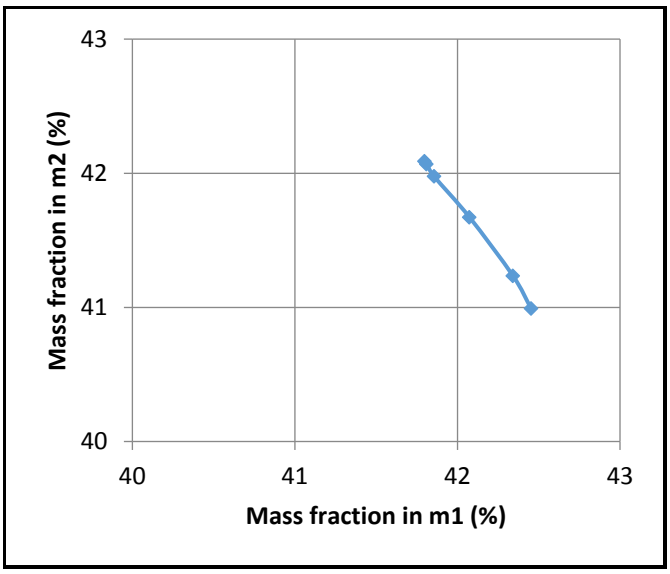

Figure 6.32 Variation of m1 and m2 with the ball filling of the ball mill

Increase in the ball filling of the ball mill resulted in increase in quantity material in the optimum size range m2 produced. Consequently, flotation recovery increased initially and then remained constant beyond 28 % ball filling as shown in Figure 6.33.

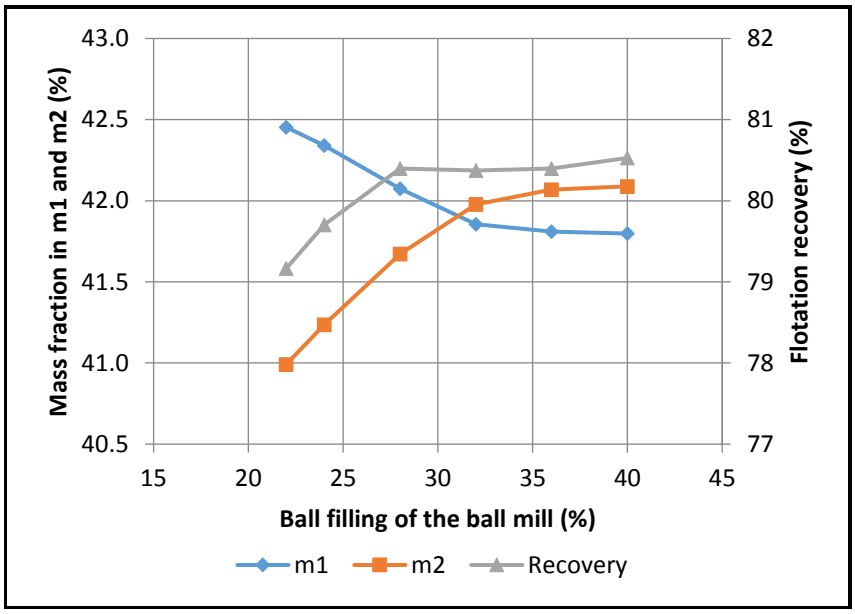

Figure 6.33 Effect of the ball filling of the ball mill on flotation performance

6.3.9 Effects of the ball size used in the ball mill

The amount of m2 produced increased as the ball size reduced. The maximum amount of m2 was 47.1 % at the point where m1 was 35.6 % as can be observed in Figure 6.34. The ball size had a huge impact on the production of m2.

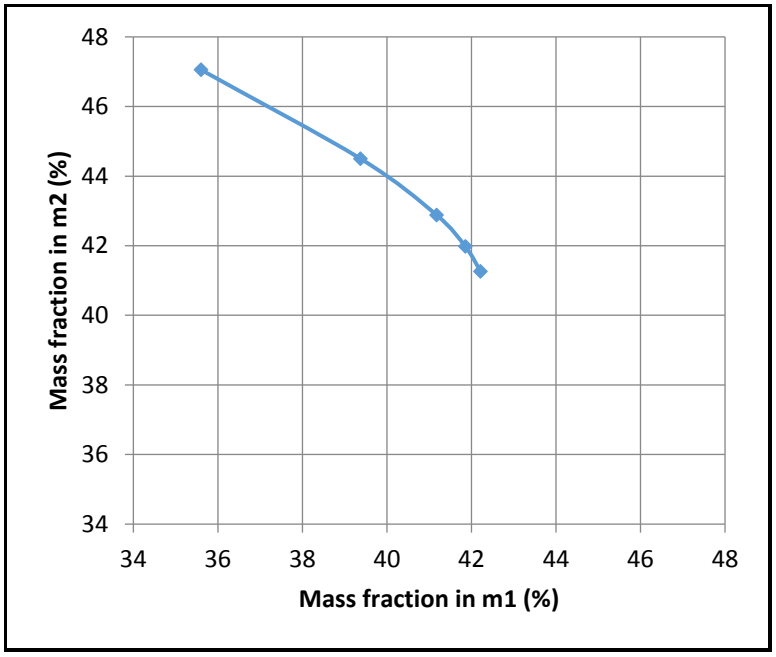

Figure 6.34 Variation of m1 and m2 with the ball size of the ball mill

Increase in the size of top-up balls used in the ball mill resulted in the reduction of material m2 produced with a gradual decrease in flotation recovery as noted in Figure 6.35.

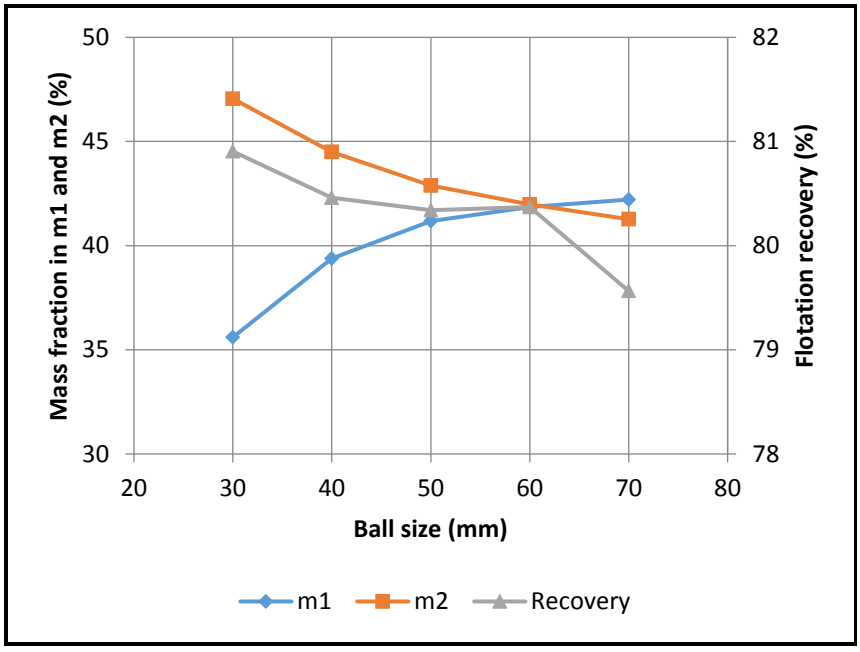

Figure 6.35 Effect of the ball size of the ball mill on flotation performance

6.3.10 Effects of ball mill speed

It was observed that the production of m2 increased with an increase in ball mill speed from 60 % to 65 %; then, declined up to 72 % of critical speed. It again increased up to 80 % of critical before decreasing beyond 80 % of critical. The maximum amount of m2 produced was 45.0 % at 80 % of critical at the point where m1 was 38.9 % in Figure 6.36.

The trends identified in Figure 6.36 are better seen in Figure 6.37 where flotation recovery tended to follow the same pattern. Variations noted in the production of m2 can be ascribed to the change in load behaviour between predominant cataracting and cascading with ball mill speed.

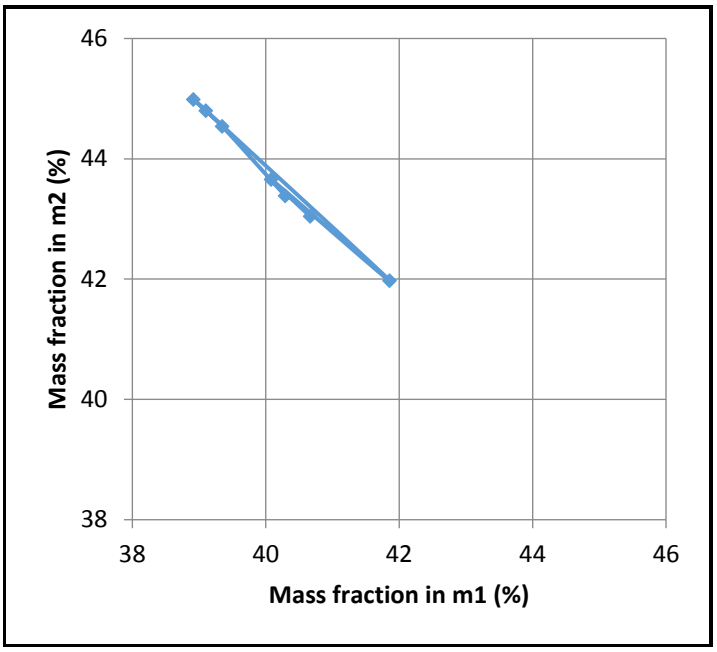

Figure 6.36 Variation of m1 and m2 with ball mill speed

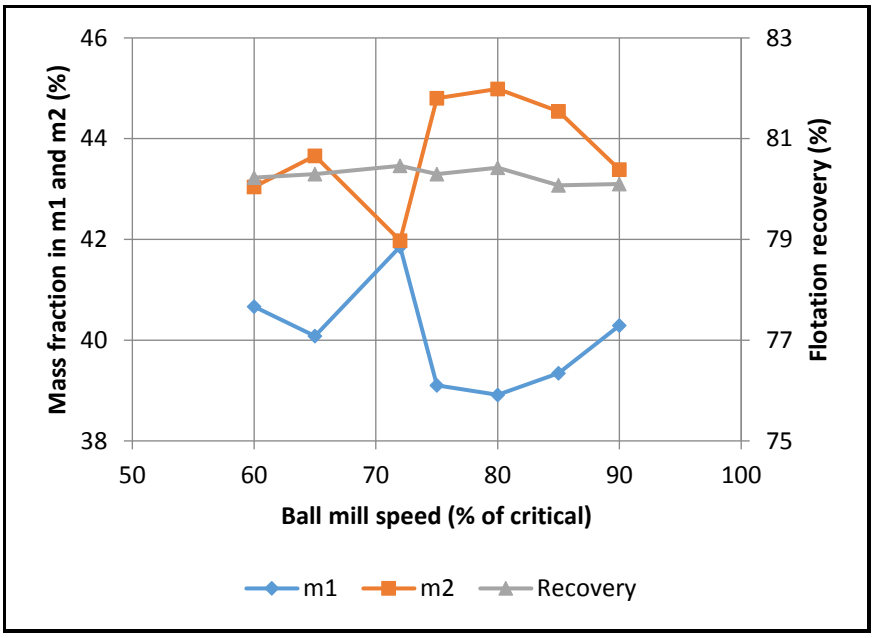

Figure 6.37 Effect of ball mill speed on flotation performance

6.3.11 Effects of the slurry concentration of the ball mill

It was observed that changes in solids content of the ball mill did not have any impact on the production of m2.

The slurry density of the ball mill content was further noted to have no significant impact on the production of m2 and flotation recovery as shown in Figure 6.38.

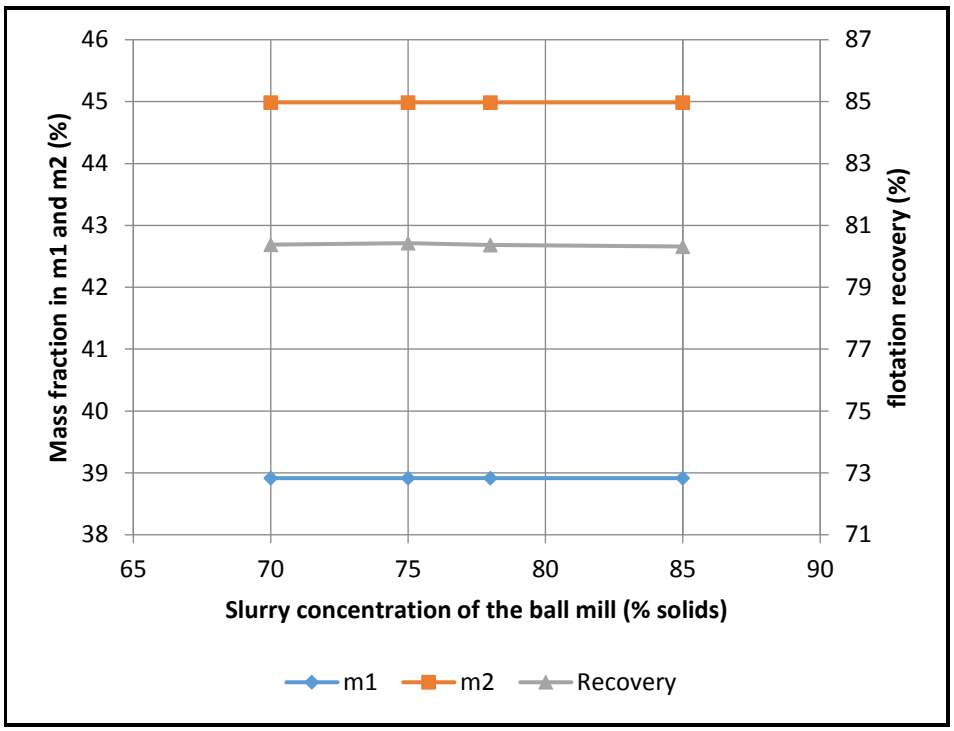

Figure 6.38 Effect of solid content of the ball mill on flotation performance

6.3.12 Effects of the slurry concentration of the hydrocyclone feed

The production of m2 increased significantly with a reduction in the solid content of the feed to the nest of hydrocyclones. The maximum mass fraction of m2 material produced was 60.9 % whereas m1 was 12.2 % as can be observed in Figure 6.39.

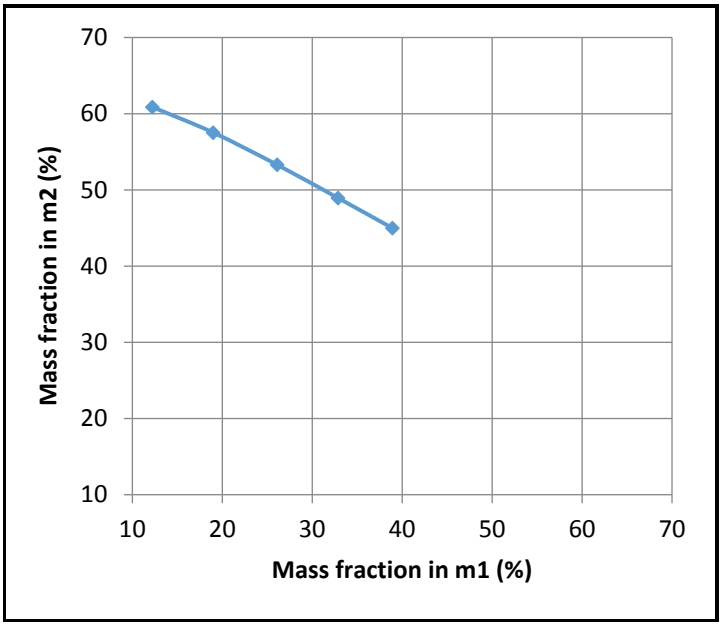

Figure 6.39 Variation of m1 and m2 with the solid content of the hydrocyclone feed

The production of m2 also decreased significantly with the increase in slurry concentration of the feed to the nest of hydrocyclones as can be observed in Figure 6.40. Flotation recovery also exhibits the same trend. This was due to a decrease in the mass fraction of material m2 readily amenable to flotation.

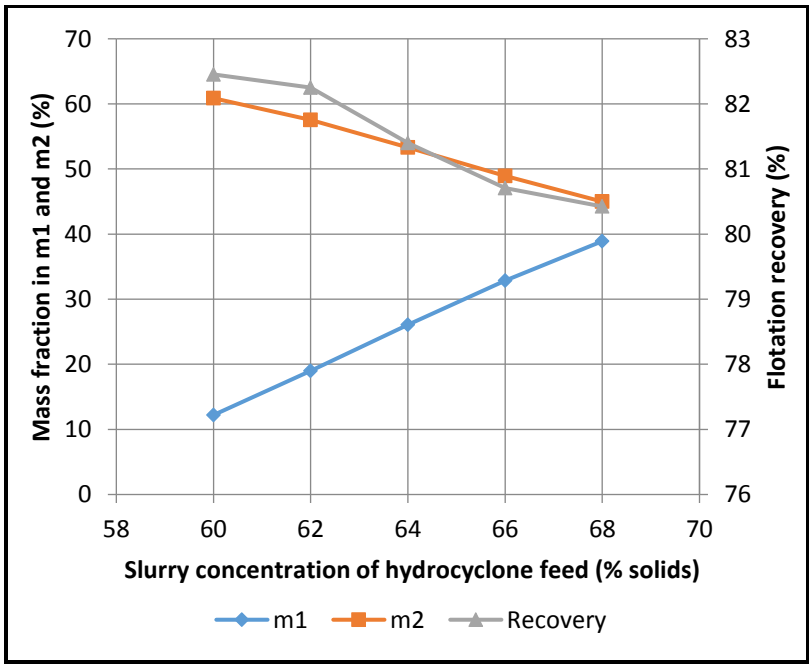

Figure 6.40 Effect of the solid content of the hydrocyclone feed on flotation

6.4 Significance of the simulation results

The simulation provided insights into the SAG and ball mills, pebble crusher operating parameters on the milling and flotation circuit performance. The impact of the operating parameters of the crusher, milling and hydrocyclones on the overall performance of the circuit were confirmed as asserted in literature. Unfortunately, the effect of in-mill slurry density could not be confirmed because the simulator did not yield any significant impact on performance. It was observed that the SAG mill circuit must be adapted to throughput optimization while ball mills are adapted to product size distribution control (Napier-Munn et al., 1999). The screen aperture size of the SAG mill discharge must be used to optimize the size of material passed to the ball mill circuit and effective utilization of the pebble crusher. The SAG mill throughput has an influence on the discharge product size distribution and performance of the hydrocyclone through feed flowrate, pressure and centrifugal force. It was observed that SAG mill throughput increase translated into a coarser SAG mill discharge product and improved production of middlings by the circuit. It was also observed that smaller steel balls yielded a fine product whereas bigger steel balls yielded a coarser product. It was also observed that big steel balls are effective for breakage of bigger particles while small steel ball are more effective for breakage of small particles. Increase in mill speed showed a decrease in product size for both SAG and ball mill initially, but the product became coarser as the speed was increased further. Low ball filling for both the SAG and ball mills produced a coarser product, which become finer as the ball filling increased, though it was observed that beyond a certain ball filling the product size for the SAG mill became coarser whereas the effect diminished for the ball mill. Hydrocyclone perform better at lower feed solid concentration. The P80 value of the hydrocyclone overflow increased as the feed solid content increased.

6.5 Conclusion

The attainable region technique was applied to evaluable the impact of operating parameters on SAG and ball mills, hydrocyclone and pebble crusher on milling circuit performance and locate the optimum operating ranges. Parameters investigated were SAG mill discharge screen aperture size, pebble crusher closed side setting, SAG mill throughput. Other parameters investigated were SAG and ball mills ball filling, ball size, mill speed, in-mill slurry density and hydrocyclone feed density. The parameters were evaluated on the impact they had on the production of material within the size range -150 +38 µm identified as yielding optimum recovery in flotation. Throughputs of SAG mill between 2000 tph and 2200 tph produced maximum quantity with the desired product size range. The optimum operating range for ball filling was found to be between 32 % and 40 % while that of ball size was between 30 mm and 40 mm. The optimum ball mill speed was between 73 % and 80 % of critical while the solid content of the hydrocyclone feed was between 60 % and 62 % by mass. The milling circuit was finally found to have the capacity to produce 60.9 % of m2 and yield a flotation recovery of 82.3 %.

Chapter 7 Conclusion and recommendations

7.1 Introduction

This section presents a summary of conclusions drawn from the research conducted on the Kansanshi mine sulphide ore milling and flotation circuit and recommendations arising from the observation. The attainable region technique was applied to evaluate the impact of milling operating parameters on the production of material within the size range -150 +38 µm identified as yielding the best recovery in Kansanshi sulphide ore flotation circuit.

The focus of the research was to optimise the Kansanshi sulphide ore milling and flotation circuits. This was achieved by building an integrated simulation model integrating milling and flotation of the Kansanshi sulphide ore circuit. Simulations were run to located the optimum SAG mill throughput, SAG and ball mills conditions of ball size, charge filling, rotational speed, and slurry concentration that would generate a final product falling predominantly in the range -150 +38 µm. Feeding the flotation circuit with material falling predominantly in the range -150 +38 µm yielded optimum recovery in flotation. Finally, the attainable region technique was used to determine a global optimum of flotation recovery across the entire milling-flotation circuit.

7.2 Modelling the sections of the Kansanshi sulphide ore circuit

The Kansanshi sulphide ore milling and flotation circuits were successfully modelled and simulated using MODSIM®. After calibration of the of the SAG and ball mills, pebble crusher, hydrocyclone and flotation cells to mimic the Kansanshi sulphide ore milling and flotation circuit simulations were run under various operating condition and data generated analysed using the attainable region

technique. On the SAG mill, parameters simulated included throughput, ball filling and size, in-mill slurry concentration, SAG mill speed and discharge screen aperture size. The ball mill, on the other hand, looked at ball filling and size, ball mill speed and in-mill slurry concentration. The feed solid content for the hydrocyclone and closed side setting of the pebble crusher were also simulated. Observations from all the parameters simulated agreed with what is reported in literature except the in-mill slurry density which did not show any significant impact on performance. This could be attributed to limitations in the models employed. Optimisation simulation improved recovery from 80.0 % to 82.3 % representing 2.26 %. It must be noted that for a plant treating 2090 tph at an average grade of 0.77 % TCu. This can translate into millions of USD per annum. The quantity of m2 in the hydrocyclone overflow improved from 41.1 % to 60.9 % and the P80 value of the hydrocyclone overflow from 230 µm to 145 µm. Other significant improvements were SAG mill throughput from 1719 tph to 2090 tph, ball mill discharge reduced from 717 µm to 538 µm and pebble crusher utilisation improved from 189 tph to 358 tph.

7.3 Attainable region analysis of the Kansanshi sulphide ore circuit

The Kansanshi milling and flotation sulphide ore was successfully simulated using the attainable region technique. The attainable region analysis proved that the circuit is capable of producing 60.9 % m2 and yield 82.3 % recovery in flotation.

7.4 Recommendations for future work

In line with insights drawn from simulation it is recommended that the SAG mill discharge screen aperture size be reduced from 20 mm to 6 mm or install a trommel screen with an aperture size of 6 mm. This will improve pebble crusher utilisation and the particle size of material being passed to the ball mill circuit. The net effect would be improved pebble crusher utilisation, increased SAG mill

throughput and ball mill performance. It must be mentioned that this recommendation has already been implemented as the SAG mill has been installed with an 8 mm trommel screen. The ball size to be topped up to the SAG mill must be increased from 125 mm to 200 mm whereas the throughput must be maintained between 2000 tph and 2100 tph. The SAG mill must be operated at a speed between 75 % and 80 % of the critical. As for the ball size for use in the ball mill, it must be reduced from 60 mm to 40 mm. The ball filling should be increased from 28 % to 32 % whereas the ball mill speed must be between 75 % and 80 % of critical. The slurry density of the feed to the cluster of hydrocyclones must be reduced from 68 % to 62 % solids. An economic analysis must also be undertaken to ascertain the financial benefits that would accrue from the improvements being proposed. The envisaged financial benefits must be communicated to Kansanshi management and permission sought to validate the simulation results on an operating sulphide ore milling and flotation circuits. Mineralogical examination of the ore to be treated should be conducted so that MODSIM® can be calibrated with actual mineralogical composition. Mineralogical examination should also include the degree of liberation and how it impacts flotation recovery. Finally, more optimisation work must be undertaken on the hydrocyclones. Here, the work must focus on optimising the diameters of the vortex finder and the spigot. The researcher was unable to subject the ore treated on Kansanshi concentrator sulphide ore circuit at the time of the survey to mineralogical examination because the mineralogical section of Kansanshi mine metallurgical laboratory had high priority tasks at hand. However, they promised that they would assist with mineralogical examination in future. In the same vain the Comminution team of Kansanshi mine metallurgical laboratory was working on other priority projects and could not be incorporated into the survey to conducted detailed investigations on the hydrocyclone, but they indicated willingness to assist in future. Lack of resources prevented the researcher from surveying the cleaner flotation and Jameson cells again this was on account of a lot of personnel at the Kansanshi mine metallurgical laboratory being committed to high priority projects.

A survey should be arranged at a time when most metallurgist and metallurgical technician are free to be incorporated into the survey.

References

Ali, S., Khan, M.M., Tufail, M., Yahya, M., 2009. Optimisation of operating process parameters of copper flotation by using statistical techniques. Journal of Chemical Society, vol. 31, no. 2, pp. 193 – 200

Austin, L.G., Barahana, C.A., Menacho, J.M., 1987. Investigation of autogenous and semi autogenous grinding in tumbling mills. Powder Technology, vol. 51, no. 3, pp. 283 – 294

Austin, L.G., Klimpel, R.R., Luckie, P.T., 1984. Process engineering of size reduction: Ball milling. Society of Mining Engineers of the AIME, New York

Barbery, G., 1972. Derivation of a formula to estimate the mass of a sample for size analysis. Transactions of the Australian Institute of Mining and Metallurgy, vol. 81, no. 784, pp. C49 – C51

Bepswa, P.A., Mainza, A.N., Powell, M., Mwansa, S., Phiri, M., Chongo, C., van der Merwe, C., Delaney, A., Mande, P., Mulenga, D., Batubenga, L., 2015. Insights into different operating philosophies – influence of a variable ore body on comminution circuit design and operation. SAG Conference, 20 – 24 September 2015, Vancouver

Bu, X., Xie, G., Peng, Y., Ge, L., Ni, C., 2016. Kinetics of flotation. order of process, rate constant distribution and ultimate recovery. Physicochemical Problems of Mineral Processing, vol. 53, no. 1, pp. 342 – 365

Chansa, K., 2018. Crusher gap setting report. Internal report, Kansanshi Mining PLC, Solwezi

Chimwani, N., 2014. An attainable region approach to optimizing product size distribution for flotation purposes. PhD Thesis, University of Witwatersrand, Johannesburg, South Africa

Compan, G., Pizarro, E., Videla, A., 2015. Geo-metallurgical model of a copper sulphide mine for long-term planning. Journal of the Southern African Institute of Mining and Metallurgy, vol. 115, no. 6, pp. 549 – 556

Danha, G., Hilderbrandt, D., Glasser, D., Bhondayi, C., 2015. A laboratory scale application of the attainable region technique on a platinum ore. Powder Technology, vol. 274, no. 1, pp. 14 – 19

Dowling, E.C., Klimpel, R.R., Aplan, F.F., 1985. Model discrimination in the flotation of a porphyry copper ore. Minerals and Metallurgical Processing, vol. 2, no. 2, pp. 87 – 101

Epstein, B., 1947. The mathematical description of certain breakage mechanisms leading to the logarithmic-normal distribution. Journal of the Franklin Institute, vol. 244, no. 6, pp. 471 – 477

Ergün, L., Ekmekçi, Z., Gülsoy, O.H., Benzer, H., 2004.The evaluation of a copper flotation plant performance by plant survey and laboratory tests. Physicochemical Problems of Mineral Processing, vol. 38, pp. 95 – 102

Faulkner, C., Mwansa, S., 2015. Step change in liner design for the Kansanshi 32FT SAG mill. SAG conference, 20 – 24 September 2015, Vancouver

Flour Australia PTY Limited, 2006. SAG Mill ML 2301 datasheet, A3BZ-24-25DS-006 datasheet, 31 August 2006

Flour Australia PTY Limited, 2011. Process design criteria, A3BZ-00-25DC-021 datasheet, 08 April 2011

Flour Australia PTY Limited, 2017. Ball Mill ML 2301 datasheet, A3BZ-23-25DS-007 datasheet, 12 January 2017

Gaudin, A.M., Groh, J.O., Henderson, H.B., 1931. Effect of particle size on flotation. American Institute of Mining and Metallurgical Engineering, vol. 414, pp. 3 – 23

Glasser, D., Hildebrandt, D., 1997. Reactor and process synthesis. Computers in Chemical Engineering, vol. 21, Suppl. 1, pp. 775 – 783

Gupta, A., Yan, D.S., 2016. Mineral processing design and operations: An Introduction. 2nd Edition, Elsevier, Amsterdam

Hanumanth, G.S., Williams, D.J.A., 1992. A three-phase model of froth flotation. International Journal of Mineral Processing, vol. 34, no. 4, pp 261 – 273

Herbst, J.A., Harris, M.C., 2007. Modeling and simulation of industrial flotation processes. A Century of Innovation, Society for Mining, Metallurgy and Exploration, Colorado, pp. 757 – 777

Hu, W., 2014. Flotation circuit optimization and design. PhD thesis, Imperial College London, United Kingdom

Jameson, G.J., 2012. The effect of surface liberation and particle size on flotation rate constants. Minerals Engineering, vol. 36, no. 38, pp. 132 – 137

Johnson, N.W., 1972. The flotation behaviour of some chalcopyrite ores. PhD Thesis, University of Queensland, Brisbane

Jovanović, I., Miljanović, I., 2015. Modelling of flotation processes by classical mathematical methods – A review. Archive Mining Science, vol. 60, no, 4, pp. 905 – 919

Kalichini, M. S., 2015. A study of the flotation characteristics of a complex ore. Master's Dissertation, University of Cape Town, South Africa

Kaputula, B., 2017. Kansanshi mine weekly mineralogical review, week 1. Internal report, Kansanshi Mining PLC, Solwezi

Karra, V.K., 1978. Development of a model for predicting the screening performance of vibrating screens. Canada Institute of Mining and Metallurgy Bulletin, no. 804, pp. 168 – 171

Karra, V.K., 1979. Development of a model for predicting the screening performance of vibrating screens. Canada Institute of Mining and Metallurgy Bulletin, no. 72, pp. 167 – 171

Karra, V.K., 1982. Process performance model for cone crushers. Proceedings of the 15th International Mineral Processing Congress, Toronto, Canada Institute of Mining and Metallurgy, Section iii, pp. 6.1 – 6.14

Katubilwa, F.M., Moys, M.H., 2009. Effect of ball size distribution on milling rate. Minerals Engineering, vol. 22, no. 15, pp. 1283 – 1288

Katubilwa, F.M., 2012. Effects of pool volume on wet milling efficiency. PhD Thesis, University of the Witwatersrand, Johannesburg

Khumalo, N., Glasser, D., Hildebrandt, D., Hausberger, B., Kauchali, S., 2006. The application of the attainable region analysis to comminution. Chemical Engineering Science, vol. 61, no. 18, pp. 5969 – 5980

King, R.P., 1972. Model for the design and control of flotation plants. Proceedings of the 10th International Symposium on Application of Computer Methods in the Mineral Industry, APCOM 10, Johannesburg, South African Institute of Mining and Metallurgy

King, R.P., 1982. Principles of Flotation. South African Institute of Mining and Metallurgy, Johannesburg

King, R.P., 2001. Modeling and simulation of mineral processing systems. Butterworth-Heinemann, Oxford, United Kingdom

King, R.P., 2012. Modeling and simulation of mineral processing systems – 2nd Edition. Schneider C.L. and King E.A. (Eds.), Society for Mining, Metallurgy, and Exploration, Colorado

Latchireddi, S., Morrell, S., 2003. Slurry flow in mills: grate-only discharge mechanism (Part 1). Minerals Engineering, vol. 16, no. 7, pp. 625 – 633

Lynch, A.J., Johnson, N.W., McKee, D.J., Thorne, G.C., 1974. The behaviour of minerals in sulphide flotation processes, with reference to simulation and control. Journal of the South African Institute of Mining and Metallurgy, vol. 74, no. 9, pp. 349 – 362

Lynch, A., Johnson, N., Manlapig, E., Thorne, C., 1981. Mineral and coal flotation circuits: their simulation and control. Developments in Mineral Processing, Elsevier Scientific Publishing Co., Amsterdam, Netherlands

Makokha, A.B., Moys, M.H., Bwalya, M.M., 2011. Modelling the residence time distribution of an industrial overflow ball mill as a function of load volume and slurry concentration. Minerals Engineering, vol. 24, no. 3 – 4, pp 335 – 340

Makokha, A.B., Madala, D.S., Namago, S.S., 2014. Effect of slurry solid concentration and ball loading on mill residence time distribution. International Journal of Mining Engineering and Mineral Processing, vol. 3, no. 2, pp. 21 – 27

Maldonado, M., Araya, R., Finch, J., 2011. Optimising flotation circuit by considering recovery profiling. Minerals Engineering, vol. 24, pp. 939 – 943

Maldonado, M., Araya, R., Finch, J., 2012. An overview of optimising strategies for flotation banks. Minerals Engineering, vol. 2, pp. 258 – 271

Marchand, J.C, Hodouin, D., Everell, M.D., 1980. Residence time distribution and mass transport characteristics of large industrial grinding mill. Proceedings of the 3rd International Federation of Automatic Control symposium, Pergamon Press, pp. 295 – 302

Metso Minerals, 2010. Basics in Minerals Processing, Metso Corporation. URL: https://www.metso.com/contentassets/0efc5d1a7c5a4357baecc5e990dc1fe7/basics-in-mineral-processing-handbook-18-lr.pdf (Accessed 30 October 2019)

Metzger, M.J., Glasser, B.J., Glasser, D., Hausberger, B., Hildebrandt, D., 2007. Teaching reaction engineering using the attainable region. Chemical Engineering Education, vol. 41, no. 4, pp. 258 – 264

Minerals Technology International, 2012. Modular simulator for mineral processing plants, South Salt Lake City, Minerals Technology International Inc.

Morar, S.H., Bradshaw, D.J., Harris, M., 2012. The use of froth surface lamellae burst rate as a flotation froth measurement. Minerals Engineering, vol. 36, no. 38, pp. 152 – 159

Morris, T.M., 1952. Measurement and evaluate of the rate of flotation as a function of particle size. Transactions of the American Institute of Mining, Metallurgical, and Petroleum Engineers, no. 187, pp. 91 – 95

Mphanza, V., 2016. Production summary tables – December 2016. Internal report, Kansanshi Mining PLC, Solwezi

Mphanza, V., 2018. Production summary tables – December 2018. Internal report, Kansanshi Mining PLC, Solwezi

Mulenga, F.K., M.M. Bwalya, M.M., 2015. Application of the attainable region technique to the analysis of a full-scale mill in open circuit. Journal of the Southern African Institute of Mining and Metallurgy, vol. 115, no. 8, pp. 729 – 740

Murthy, N., Basavaraj, K., 2012. Assessing the performance of a floatex density separator for the recovery of iron from low-grade Australian iron ore fines – a case study. XXVI International Mineral Processing Congress, 24 – 28 September 2012, New Delhi, pp. 3612 – 3621

Nageswararao, K., Wiseman, D.M., and Napier-Munn, T.J., 2004. Two empirical hydrocyclone models revisited. Minerals Engineering, vol. 17, no. 5, pp. 671 – 687

Naik, S., van Drunick, W., 2007. Anglo research (AR) experiences with integrated comminution and flotation plant modelling. 4th Southern African Conference on Base Metals, 23 – 25 July 2007, Swakopmund, The Southern African Institute of Mining and Metallurgy, pp. 273 – 292

National Geographical Society, 2013. Cited in Paquot, F.X., 2013. Kansanshi mixed ore treatment: Development and optimization. Master of Science Dissertation, University of Exeter

Napier-Munn, T.J., Morrell, S., Morrison, R.D., Kojovic, T., 1996. Mineral comminution circuits – Their operation and optimization. JKMRC Monograph Series, University of Queensland

Napier-Munn, T.J., Morrell, S., Morrison, R.D., Kojovic, T., 1999. Mineral comminution circuits – Their operation and optimization 2. JKMRC Monograph Series, University of Queensland

Narayanan, S.S., Hess, F.W., Burns, R.S., 1987. Optimisation of comminution stages at Bougainville Copper Limited. Copper '87, Barcelona, Chile, pp. 43 – 57

Newall, C., 2017. First Quantum Minerals Reports Fourth Quarter 2017 Results (Press release). 12 February 2018. Available at: https://www.first-quantum.com/Media-Centre/Press-Releases/Press-Release-Details/2018/First-Quantum-Minerals-Reports-Fourth-Quarter-2017-Results/default.aspx
(Accessed: 09 April 2018)

Neethling, S.J., Cilliers, J.J., 2008. Predicting air recovery in flotation cells. Minerals Engineering, vol. 21, no. 12 – 14, pp. 937 – 943

Plitt, L.R., 1976. A mathematical model of the hydrocyclone classifier. Canadian Institute of Mining, vol. 69, pp. 114 – 123

Rahman, R.M., Graeme, S.A., Jameson, J., 2012. The effect of flotation variables on the recovery of different particle size fractions in the froth and the pulp. International Journal of Mineral Processing, vol. 106, no. 109, pp. 70 – 77

Schlanz, J.W., 1987. Grinding: An overview of operations and design. Mill Operator's Symposium, October 1987, Spruce Pine, North Carolina

Shoji, K., Austin, L.G., Smaila, F., Brame, K., Luckie, P.T., 1982. Further studies of ball and powder filling effects in ball milling. Powder Technology, vol. 31, no. 1, pp. 121 – 126

Stanley, G.G., 1974. Mechanisms in the autogenous mill and their mathematical representation. Journal of the South African Institute Mining and Metallurgy, vol. 75, no. 4, pp. 77 – 98

Tangsathitkulchai, C., 2003. Effects of slurry concentration and powder filling on the net mill power of a laboratory ball mill. Powder Technology, vol. 137, no. 3, pp. 131 – 138

Weller, K.R., 1980. Hold-up and residence time characteristics of full-scale grinding circuits. Proceedings of the 3rd International Federation of Automatic Control symposium, Pergamon Press, pp. 303 – 309

Wills, B.A., Napier-Munn, T.J., 2006. Wills' mineral processing technology: an introduction to the practical aspects of ore treatment and mineral recovery. 7th Edition, Elsevier, London

Yahyaei, M., Vos, F., Powell, M.S., Siliezar, J., Perkins, P. (2014), Challenges in developing integrated process models based on industrial survey data. 12th AUSIMM Mill Operators Conference. Australian Institute of Mining and Metallurgy, Victoria. pp. 437–446.

Yekeler, M., 2007. Breakage and morphological parameters determined by laboratory tests (Chapter 9). in Handbook of Powder Technology, vol. 12, pp. 437 – 486

Yianatos, J.B., 1989. Column flotation: modelling and technology. Proceedings of the International Colloquium: Developments in Froth Flotation, 3 – 4 August 1989, Cape Town, South Africa, vol. 2, pp. 1 – 30

Whiten, W.J., Walter, G.W., White, M.E., 1973. A breakage function suitable for crusher models. 4th Tewkesbury Symposium, Melbourne, pp. 19.1 – 19.3

Wikedzi, W., 2018. Optimization and performance of grinding circuits: The case study of Buzwagi gold mine. Doctor of Engineering Thesis, Technical University Bergakademie Freiberg, Germany

Woodburn, E.T., 1970. Mathematical modelling of flotation processes. Mineral Science Engineering, vol. 2, no. 2, pp. 3 – 17

Zuniga, H.G., 1935. Flotation recovery is an exponential function of its rate. National Mining Society Bulletin, vol. 47, pp 83 – 86

Appendices

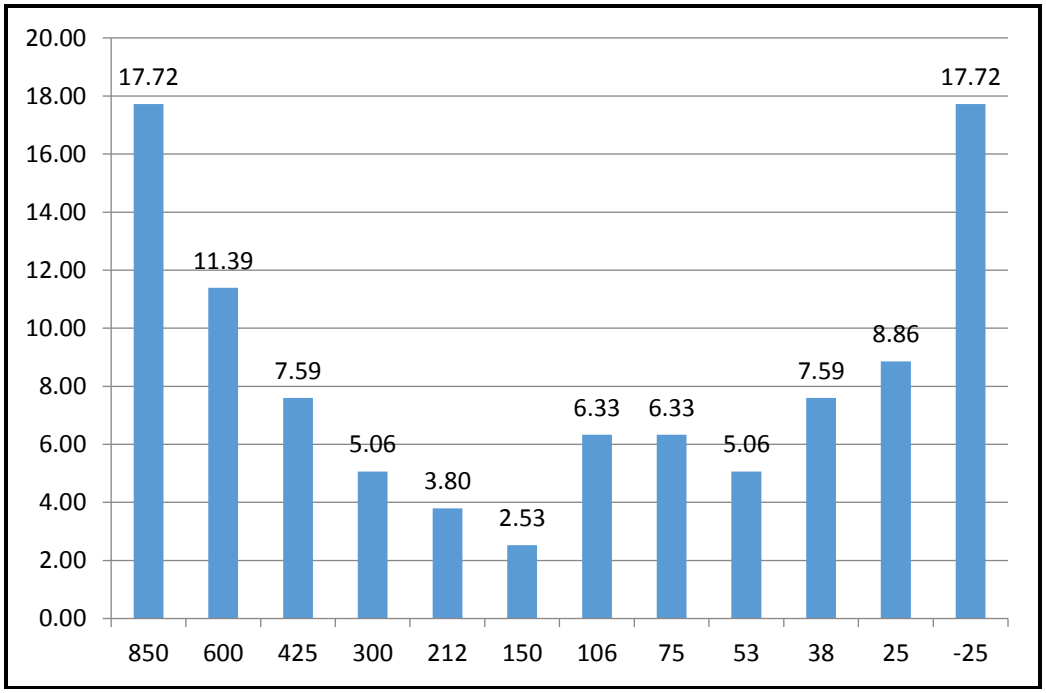

Figure A.1: Copper loses to the taillings by size

Table A.1: Particle size analysis of cyclone overflow

Sieve Size (µm)	Wt Retained	% Wt Retained	Cum % Retained	Cum % Passing
13200	0.00	0.00	0.00	100.00
11200	0.00	0.00	0.00	100.00
8000	0.00	0.00	0.00	100.00
6700	0.00	0.00	0.00	100.00
4750	0.00	0.00	0.00	100.00
3500	0.00	0.00	0.00	100.00
1400	0.00	0.00	0.00	100.00
850	0.01	0.94	0.94	99.06
600	0.02	1.55	2.49	97.51
425	0.03	3.35	5.84	94.16
300	0.07	6.95	12.79	87.21
212	0.08	7.73	20.52	79.48
150	0.07	7.07	27.58	72.42
106	0.10	10.48	38.06	61.94
75	0.09	9.46	47.52	52.48
53	0.08	7.93	55.45	44.55
38	0.06	6.14	61.59	38.41
25	0.08	8.29	69.89	30.11
-25	0.30	30.11	100.00	
Total	1.00	100		

Table A.2 Comparison between surveyed and MODSIM® predicted PSD's of feed, underflow and overflow to the hydrocyclones

Sieve size (µm)	Cyclone Feed survey	Cyclone Feed Pred	Cyclone Underflow survey	Cyclone Underflow Pred	Cyclone Overflow survey	Cyclone Overflow Pred
19000	100	100	100	100	100	100
13200	100	99.39	99.48	99.06	100	100
11200	99.94	98.34	98.61	97.46	100	100
8000	98.90	96.99	96.32	95.40	100	100
6700	97.96	95.19	94.38	92.64	100	100
4750	95.96	92.83	90.88	89.03	100	100
3500	93.40	89.82	87.46	84.44	100	100
1400	83.00	86.21	74.07	72.12	100	100
850	73.47	70.52	62.66	55.28	99.06	99.33
600	62.71	64.02	49.68	46.14	97.51	97.81
425	52.50	56.98	37.88	37.10	94.16	94.55
300	41.86	49.05	26.69	28.15	87.21	88.56
212	34.21	40.40	19.39	19.86	79.48	79.23
150	29.40	31.53	15.27	12.85	72.42	66.82
106	23.27	23.22	10.77	7.59	61.94	52.75
75	19.14	16.32	8.35	4.18	52.48	39.25
53	16.02	11.17	6.99	2.25	44.55	28.02
38	14.28	7.60	6.12	1.26	38.41	19.58

Table A.3 Simulation of the effects of SAG discharge screen

Screen size	Pebble (tph)	Pebble P80	SAGD P80	BMD P80	SAG Feed (tph)	COF P80
20	189	3.60	2.39	729	1719	230
15	211	6.20	2.42	721	1741	230
10	256	10.40	2.50	708	1786	230
5	412	9.10	2.89	672	1942	231
6	356	9.50	2.73	684	1886	230

Table A.4 Simulation of the effects of the CSS of the pebble crusher

CSS	Pebble P80	Pebble (tph)	SAG Feed tph	SAGD P80	BMD P80
13	9.50	356	1886	2.73	684
11	8.90	353	1883	2.73	685
9	8.40	349	1879	2.72	686
7	7.10	342	1872	2.70	687

Table A.5 Simulation of ball filling of SAG mill

% Ball filling	SAGD P80	SAG Feed tph	Pebble (tph)	BMD P80
12	2.86	1891	360	693
14	2.76	1885	355	687
16	2.73	1883	353	685
18	2.76	1886	357	685
20	2.86	1894	364	689
22	3.04	1908	376	695

Table A.6 Simulation for ball size of SAG mill

Ball size (mm)	SAGD P80	BMD P80	Pebble (tph)	SAG Feed tph
125	2.73	685	353	1883
140	2.55	679	340	1870
160	2.36	674	326	1857
180	2.24	670	315	1845
200	2.14	667	306	1736
220	2.07	665	296	1828
240	2.01	664	291	1821
260	1.97	664	286	1815

Table A.7 Simulation of the effects of SAG mill speed

% Critical speed	SAGD P80	BMD P80	Pebble (tph)	SAG Feed (tph)
60	2.52	688	336	1866
65	2.32	678	321	1850
72	2.14	667	306	1736
75	2.10	664	301	1832
80	2.06	662	299	1828
85	2.13	668	304	1833
90	2.38	686	323	1853

Table A.8 Simulation of the effects of SAG mill feed rate

Throughput (tph)	SAGD P80	BMD P80	COF P80	Pebble (tph)	Pebble P80
1700	1.96	629	233	270	8.10
1828	2.06	662	230	299	8.30
1950	2.17	671	227	326	8.40
2050	2.27	681	226	356	8.50
2200	2.38	694	224	387	8.60
2090	2.28	717	225	358	8.50

Table A.9 Simulation of the effects of ball filling of SAG mill

Ball filling (%)	COF P80	BMD P80
22	228	754
24	227	739
28	225	717
32	223	703
36	223	696
40	223	694

Table A.10 Simulation of effects of ball size of ball mill

Ball size (mm)	COF P80	BMD P80
30	204	503
40	215	578
50	221	646
60	223	703
70	226	748

Table A.11 Simulation of effects of ball mill speed

% critical speed	COF P80	BMD P80
60	222	638
65	219	600
72	215	578
75	214	517
80	213	566
85	215	577
90	220	619

Table A.12 Simulation of the effects of slurry concentration of the ball mill

% solids	COF P80	BMD P80
70	213	566
75	213	566
78	213	566
85	213	566

Table A.13 Simulation of the effects of the slurry concentration of the hydrocyclone feed

% solids	COF P80	BMD P80
60	125	529
62	145	538
64	165	546
66	198	555
68	213	566

Table A.14 Simulation of variation in size classes for aperture size of SAG screen discharge

Aperture size (mm)	m1	m2	m3
5	43.16	41.12	15.72
6	43.23	41.11	15.66
10	43.32	41.10	15.58
15	43.37	41.09	15.55
20	43.36	41.11	15.53

Table A.15 Simulation of variation in size classes for closed side setting of pebble crusher

CSS (mm)	m1	m2	m3
13	43.23	41.11	15.66
11	43.22	41.11	15.67
9	43.21	41.10	15.69
7	43.20	41.10	15.71

Table A.16 Simulation of variation in size classes for ball filling of SAG mill

Ball filling (%)	m1	m2	m3
12	43.33	41.00	15.67
14	43.24	41.06	15.70
16	43.22	41.11	15.67
18	43.27	41.14	15.60
20	43.38	41.15	15.47
22	43.55	41.15	15.29

Table A.17 Simulation of variation in size classes for ball size of SAG mill

Ball size (mm)	m1	m2	m3
125	43.22	41.11	15.67
140	43.17	41.13	15.71
160	43.13	41.14	15.73
180	43.11	41.15	15.74
200	43.12	41.14	15.74
220	43.14	41.14	15.74
240	43.16	41.13	15.71
260	43.17	41.15	15.68

Table A.18 Simulation of variation in size classes for SAG mill speed

% critical speed	m1	m2	m3
60	43.55	41.08	15.37
65	43.35	41.11	15.54
72	43.12	41.14	15.74
75	43.05	41.15	15.80
80	43.01	41.16	15.84
85	43.11	41.15	15.73
90	43.47	41.09	15.45

Table A.19 Simulation of variation in size classes for SAG mill throughput

Throughput	m1	m2	m3
1700	43.21	41.00	15.79
1828	43.01	41.16	15.84
1950	42.54	41.48	15.98
2050	42.10	41.68	16.22
2200	41.62	41.90	16.48

Table A.20 Simulation of variation in size classes for ball filling of ball mill

Ball filling	m1	m2	m3
22	42.45	40.99	16.56
24	42.34	41.24	16.42
28	42.07	41.67	16.25
32	41.86	41.98	16.17
36	41.81	42.07	16.12
40	41.80	42.09	16.11

Table A.21 Simulation of variation in size classes for ball size of ball mill

Ball size	m1	m2	m3
30	35.60	47.06	17.35
40	39.37	44.50	16.13
50	41.18	42.88	15.94
60	41.86	41.98	16.17
70	42.22	41.27	16.52

Table A.22 Simulation of variation in size classes for ball mill speed

% critical speed	m1	m2	m3
60	40.67	43.04	16.29
65	40.08	43.66	16.26
72	41.86	41.98	16.17
75	39.10	44.80	16.10
80	38.92	44.99	16.10
85	39.35	44.54	16.11
90	40.29	43.39	16.32

Table A.23 Simulation of variation in size classes for solid content of ball mill

% solids	m1	m2	m3
70	38.92	44.99	36.90
75	38.92	44.99	16.10
78	38.92	44.99	16.10
85	38.92	44.99	16.10

Table A.24 Simulation of variation in size classes for solid content of hydrocyclone feed

% solids	m1	m2	m3
60	12.21	60.88	26.91
62	18.97	57.53	23.50
64	26.09	53.30	20.61
66	32.87	48.94	18.19
68	38.92	44.99	16.10

Table A.25 Variation of flotation recovery with ball filling of ball mill

Ball filling	Concentrate	Tail	Recovery
22	12.80	0.401	79.17
24	12.80	0.391	79.70
28	12.80	0.378	80.40
32	12.80	0.376	80.37
36	12.80	0.378	80.40
40	12.80	0.378	80.53

Table A.26 Variation of flotation recovery with ball size of ball mill

Ball size (mm)	Float Feed	Conc	Tail	Recovery (%)
30	1.74	12.10	0.38	80.90
40	1.73	12.60	0.38	80.46
50	1.74	12.80	0.38	80.34
60	1.71	12.80	0.38	80.37
70	1.63	12.40	0.37	79.56

Table A.27 Variation of flotation recovery with ball mill speed

% critical speed	Concentrate	Tail	Recovery (%)
60	13.00	0.383	80.22
65	13.20	0.381	80.29
72	12.60	0.380	80.46
75	13.50	0.380	80.29
80	13.50	0.380	80.42
85	13.40	0.382	80.07
90	13.10	0.385	80.10

Table A.28 Variation of flotation recovery with the solid content of the hydrocyclone feed

% solids	Float Feed	Conc	Tail	Recovery (%)
60	1.72	10.30	0.350	82.45
62	1.74	11.00	0.355	82.25
64	1.72	11.80	0.363	81.40
66	1.73	12.70	0.375	80.71
68	1.74	13.50	0.380	80.42